

# Minimum Amount of Text Overlapping in Document Separation

Antonio Boccuto, Ivan Gerace and Valentina Giorgetti

Laboratorio di Matematica Computazionale “Sauro Tulipani”  
Dipartimento di Matematica e Informatica  
Università degli Studi di Perugia  
Via Vanvitelli, 1  
I-06123 Perugia (Italy)



September 24, 2018

## Abstract

We consider a **Blind Source Separation** problem. In particular we focus on reconstruction of digital documents degraded by **bleed-through** and **show-through** effects. In this case, since the mixing matrix, the source and data images are nonnegative, the solution is given by a Nonnegative Factorization. As the problem is ill-posed, further assumptions are necessary to estimate the solution. In this paper we propose an iterative algorithm in order to estimate the correct overlapping level from the verso to the recto of the involved document. Thus, the proposed method is a Correlated Component Analysis technique. This method has low computational costs and is fully unsupervised. Moreover, we give an extension of the proposed algorithm in order to deal with a not translation invariant model. Our experimental results confirm the goodness of the method.

**Key words:** Blind Source Separation, Digital Document Restoration, Nonnegative Factorization, Correlated Component Analysis.

**2010 A. M. S. Subject Classification:** 65D18, 68U10.

## 1 Introduction

In this paper we deal with a *Blind Source Separation* (BSS) problem. This problem has been an active research topic in signal processing since the end of the last century and

has several applications in different fields, for example, in the cocktail party problem, in which the single signal separation is extracted from a number of speech signals which form a single observed mixture; in image classification and change detection (see also [7]); in determining the structure of the buildings in thermographic images for seismic engineering (see also [14, 15, 16]); in the problem of estimating the *Cosmic Microwave Background* (CMB) from galactic and extragalactic emissions (see also [20, 39]).

In particular we study the reconstruction of digital documents. There are several causes which lead a document to be degraded. Some of them are, for instance, weathering, seeping, humidity, powder, mold, light transmission, which cause a progressive degradation and decay of the paper and the ink of the analyzed documents. Some of the consequences in damaged documents are, for instance, stains, noise, transparency of writing on the reverse side and on the close pages, unfocused or overlapping characters, and so on. Historically, the first techniques of restoration for degraded documents were manual, and they led to a material restoration. Recently, thanks to the diffusion of scanners and software for reconstruction of images, videos, texts, photographs and films, several new techniques were used in the recovery and restoration of deteriorated material, like for instance digital or virtual restoration. Digital imaging for documents is very important, because it allows to have digital achieves, to make always possible the accessibility and the readability. Indeed, documents are often difficult to be read with the naked eye. Moreover sometimes, in the study of documents, some further informations can be achieved from images taken at the infrared or ultraviolet wavelenghts. Since the classical manual techniques of restoration are more expensive, irreversible, often ineffective or even inapplicable, then digital restoration is very successful. The process of acquisition of a digital document, if necessary, can be preceded by a manual intervention to remove physical elements like, for example, dust, mud or other impurities. The acquired document is modified by a set of processes which will give a restored copy, sufficiently close to the original document. The *Digital Document Restoration* consists of a set of processes finalized to the visual and aesthetic improvement of a virtual reconstruction of a corrupted document, without risk of deterioration. Another field in which these techniques are very important is to include digital documents into a suitable database. To search into it, some machine readable versions of the original text are required. When the database is large, it is suitable that the machine readable documents are read quickly and independently of human interventions. This is usually done by the *Optical Character Recognition* (OCR) system (see also [5, 10, 47]), whose performance, however, depends also on the quality of the data. Since ancient documents are often very degraded, before applying OCR, image processing techniques can be viewed as a preprocessing method. When degraded original documents are managed, different kinds of digital image restoration algorithms can be useful both to improve human readability and to get acceptable OCR performances.

Here we deal with *bleed-through* and *show-through* effects. The bleed-through is an intrinsic front-back physical deterioration of the document. It occurs, for example, because of humidity, or particular environmental condition during storage, or simply due to the passage of time. In the case of handmade documents, it consists in the seeping and the absorption of the ink from part of the fibers of the paper. The result is a document with an overlay of the main contents of the involved front and back pages. The show-through is a front-back interference, mainly due to the scanning process and the paper transparency. This effect occurs when the paper of the document is not completely opaque and the scan-

ner uses a white background. In the case of the just described degradation phenomena, it is advisable to have a model that includes availability of the front and the back of the involved document, and that the data are combinations of the source ideals (see also [52]). To remove the bleed-through (or the show-through) patterns from a digital document scan is in general not an easy task, especially in the case of ancient documents, where the interferences are often very wide. Indeed, to deal with strong bleed-through by a simple threshold technique is practically impossible, since the intensities of the unwanted ink filtered from the back can be very close to the intensity of the ones of the main text. For instance, in [40] several threshold techniques are compared for separating the text in degraded historical documents, and in general neither global nor local thresholds have satisfactory results.

Here initially we deal with the linear and translation invariant model (see also [12, 25, 26, 27, 28, 31, 32, 53, 54, 56]) in the problem of estimating both the two source images corresponding to the ideal front and the ideal back of the document and the mixture matrix related to the linear model from two observed data images which are the mixtures of these sources, produced by the bleed-through or the show-through effect. This problem is ill-posed in the sense of Hadamard (see also [24]). In fact, as the estimated mixture matrix varies, the corresponding estimated sources are in general different, and so we have infinitely many solutions.

So far, many techniques were proposed to solve this ill-posed inverse problem. Among them, the *Independent Component Analysis* (ICA) methods are based on the assumption of mutual independence of the sources (see also [17, 29, 30, 48]). The most known of the ICA techniques is the so-called FastICA (see also [25, 26, 27, 28, 31, 32, 36, 37, 41, 42, 49]), which by means of a fixed point iteration argument looks for an orthogonal rotation of prewhitened data, which maximizes a measure of non-Gaussianity of the rotated components. FastICA algorithm is a parameter free and extremely fast procedure. However, the ICA solution to BSS problem presents some drawbacks. Indeed, the independence condition can be satisfied in some BSS problems, but in our analyzed problem there is clearly a correlation among the sources.

On the other hand, several of the ill-posed inverse problem techniques impose that the estimated sources are just mutually uncorrelated. By means of the technique of *Principal Component Analysis* (PCA) (see also [12, 52, 53, 54]), the estimated sources are determined through a linear transformation of the data by imposing the condition of orthogonality between them, while in the *Whitening* (W) and *Symmetric Whitening* (SW) techniques (see also [12, 52, 53, 54, 56]) an orthonormality constraint is imposed. The PCA, W and SW algorithms require only a single very fast processing step. In [12, 53] it is observed that the results obtained by means of the SW method are substantially equivalent to those got by an ICA technique in the symmetric mixing case.

In this paper we assume that the mixture matrix is *stochastic*, because we suppose that the means of the light intensities of the sources and of those of the data coincide. In our setting, we do a change of variables of data, in order that high and low light intensity correspond to presence and absence of that text in the document, respectively. We define the *overlapping matrix* both of the observed data and of the ideal sources, from which we deduce the *overlapping level*, which yields a measure of how the front coincides with the back. The PCA, W and SW techniques give an estimate of the mixture matrix as a symmetric factorization of the data covariance matrix, while in our setting we estimate

the mixture matrix as the best symmetric factorization of data overlapping matrix, which allows to have the text as disjoint as possible. In particular, we propose an iterating procedure, in which in every iteration we obtain an estimate of the source overlapping level. During this estimation we impose, by means of an orthogonal projection operator, a non-negativity constraint on the estimated source (see also [11, 13, 22, 43, 45]). We repeat this procedure until we reach a fixed point. By means of this technique, we obtain an estimate not only of the ideal sources of the mixture matrix, but also of the source overlapping level. Such a value indicates the correlation between the ideal sources. In this way, our method can be classified as a *Correlated Component Analysis (CCA) technique* (see also [6, 18, 46, 50, 51, 55]). We refer to the proposed algorithm as *Minimum Amount of Text Overlapping in Document Separation (MATODS)*. Similarly to the FastICA technique, the MATODS algorithm is a parameter free and extremely fast procedure.

In many ancient documents the infiltration of the ink is not spatially uniform, thus the fully translation invariant linear model is not always realistic. To overcome this problem, we propose a locally linear new model, where the mixture matrix varies smoothly. So we present an extension of the MATODS algorithm that fits this model. We call such an extension as the *Not Invariant for Translation MATODS (NIT-MATODS)* algorithm.

In Section 2 we present the initial translation invariant linear model of the problem. In Section 3 we develop the proposed algorithm MATODS. In Section 4 we analyze how to choose the algorithm used in MATODS for minimizing the related objective function. In Section 5 we present the not translation invariant model and give the NIT-MATODS algorithm. In Section 6 we illustrate the experimental results, comparing the MATODS algorithm with other fast and unsupervised methods existing in literature and showing how the NIT-MATODS algorithm works in restoring real ancient documents.

## 2 Formulation of the problem

A  $n \times n$  color image is usually encoded in the *RGB* space, where  $R, G, B$  indicate the red, green and blue color, respectively, and can be represented as a matrix belonging to  $\mathbb{R}^{n^2 \times 3}$ , whose elements are the channel light intensity (which varies between 0 and 255) of the pixels, ordered in the lexicographic sense. We consider a document as a pair of images, which represent its sides, the front (*recto*) and the back (*verso*), respectively. In particular, we denote by

$$\hat{x}_r = [\hat{x}_{rR} \quad \hat{x}_{rG} \quad \hat{x}_{rB}] \quad (1)$$

the RGB color front image of the observed document, where  $\hat{x}_{rR}, \hat{x}_{rG}, \hat{x}_{rB} \in [0, 255]^{n^2 \times 1}$ , and by

$$\hat{x}_v = [\hat{x}_{vR} \quad \hat{x}_{vG} \quad \hat{x}_{vB}], \quad (2)$$

with  $\hat{x}_{vR}, \hat{x}_{vG}, \hat{x}_{vB} \in [0, 255]^{n^2 \times 1}$ , the associated RGB color back image. Here, we assume that the data recto  $\hat{x}_r$  in (1) and the data verso  $\hat{x}_v$  in (2) are spatially registered by a horizontal flip of the verso. The red, green and blue data components are

$$\hat{x}_R = [\hat{x}_{rR} \quad \hat{x}_{vR}], \quad \hat{x}_G = [\hat{x}_{rG} \quad \hat{x}_{vG}], \quad \hat{x}_B = [\hat{x}_{rB} \quad \hat{x}_{vB}],$$

respectively, and finally we write the observed document as

$$\hat{x} = [\hat{x}_{rR} \quad \hat{x}_{vR} \quad \hat{x}_{rG} \quad \hat{x}_{vG} \quad \hat{x}_{rB} \quad \hat{x}_{vB}],$$

which belongs to  $[0, 255]^{n^2 \times 6}$ . The source ideal document is given by the matrix

$$\hat{s} = [\hat{s}_{rR} \ \hat{s}_{vR} \ \hat{s}_{rG} \ \hat{s}_{vG} \ \hat{s}_{rB} \ \hat{s}_{vB}]^T,$$

where  $\hat{s} \in [0, 255]^{n^2 \times 6}$ , and we set

$$\hat{s}_R = [\hat{s}_{rR} \ \hat{s}_{vR}]^T, \quad \hat{s}_G = [\hat{s}_{rG} \ \hat{s}_{vG}]^T, \quad \hat{s}_B = [\hat{s}_{rB} \ \hat{s}_{vB}]^T.$$

In this paper we initially consider a linear and translation invariant model

$$\hat{x}^T = A \hat{s}^T \quad (3)$$

(see also [12, 25, 26, 27, 28, 31, 32, 53, 54, 56]), where the symbol  $\cdot^T$  denotes the transpose operation of a matrix, and  $A \in \mathbb{R}^{6 \times 6}$ , which is called *mixture matrix*, is the following block matrix:

$$A = \begin{bmatrix} A_R & 0 & 0 \\ 0 & A_G & 0 \\ 0 & 0 & A_B \end{bmatrix},$$

with

$$A_R = \begin{bmatrix} a_{11}^R & a_{12}^R \\ a_{21}^R & a_{22}^R \end{bmatrix}, \quad A_G = \begin{bmatrix} a_{11}^G & a_{12}^G \\ a_{21}^G & a_{22}^G \end{bmatrix}, \quad A_B = \begin{bmatrix} a_{11}^B & a_{12}^B \\ a_{21}^B & a_{22}^B \end{bmatrix}.$$

Note that, according to our model, every single observed channel is formed by a linear combination of components related to the same channel of the front and the back of the ideal source document.

In this paper we assume that the mean of the light intensities of the sources are similar to that of the data, so we suppose that  $A_R, A_G, A_B$  are *stochastic matrices*, that is they are nonnegative matrices and

$$a_{11}^R + a_{12}^R = a_{21}^R + a_{22}^R = a_{11}^G + a_{12}^G = a_{21}^G + a_{22}^G = a_{11}^B + a_{12}^B = a_{21}^B + a_{22}^B = 1. \quad (4)$$

Thus,  $A_R, A_G, A_B \in [0, 1]^{2 \times 2}$ . Moreover we assume that the mixing matrix  $A$  is a diagonally dominant matrix.

In our approach it is useful that a high light intensity indicates a presence of meaningful data (for example, a letter or a figure), and a low light intensity corresponds to an absence of data. Since the background usually has bright colors while text or figures contain dark colors, we apply the following change of variables:

$$\begin{aligned} x_R &= m_R e - \hat{x}_R, \quad x_G = m_G e - \hat{x}_G, \quad x_B = m_B e - \hat{x}_B, \\ s_R &= m_R e - \hat{s}_R, \quad s_G = m_G e - \hat{s}_G, \quad s_B = m_B e - \hat{s}_B, \end{aligned} \quad (5)$$

where  $e \in \mathbb{R}^{n^2 \times 2}$  be that matrix such that

$$e_{i,j} = 1 \text{ for each } i = 1, 2, \dots, n^2 \text{ and } j = 1, 2, \quad (6)$$

and  $m_R, m_G, m_B$  are the maximum of the light intensity of both sides of the red, green and blue components, respectively, of the data document. Note that, since we deal with paper documents, we assume that the involved maximum is achieved on the background.

Thanks to (5), the values of the light intensity corresponding to the background are equal to 0, while the other pixels containing the informations have positive light intensity values, whose maximum is given by  $m_R$ . Since  $A_R$  is stochastic, for the red channel we get

$$e^T = A_R e^T, \quad (7)$$

and hence from (3) and (7) we obtain

$$\begin{aligned} x_R^T &= (m_R e)^T - A_R \tilde{s}_R^T = A_R (m_R e)^T - A_R \tilde{s}_R^T = A_R ((m_R e)^T - \tilde{s}_R^T) \\ &= A_R s_R^T. \end{aligned} \quad (8)$$

Similarly it is possible to verify the analogous relations involving the channels green and blue. From now on, we refer only to the red channel, because similar arguments can be done also in green and blue channel.

Now we show that the request that the mixture matrix is stochastic is not restrictive.

**Proposition 2.1.** *Let  $(\tilde{A}_R, \tilde{s}_R)$  be a solution of the linear model in equation (8), where  $\tilde{A}_R$  is non-singular with  $\tilde{a}_{22}^R \neq \tilde{a}_{12}^R$  and  $\tilde{a}_{11}^R \neq \tilde{a}_{21}^R$ , then there exist  $t_1, t_2 \neq 0$  and  $\bar{A}^R$  satisfies the condition (4) and such that  $(\bar{A}_R, \bar{s}_R)$  is a solution of (8) with  $\bar{s}_R = [\frac{1}{t_1} \tilde{s}_r R \quad \frac{1}{t_2} \tilde{s}_v R]$ .*

*Proof.* Since  $(\tilde{A}_R, \tilde{s}_R)$  is a solution of the linear model in equation (8), then

$$\tilde{x}_R^T = \tilde{A}_R \tilde{s}_R^T = \begin{bmatrix} \tilde{a}_{11}^R & \tilde{a}_{12}^R \\ \tilde{a}_{21}^R & \tilde{a}_{22}^R \end{bmatrix} \begin{bmatrix} \tilde{s}_r R^T \\ \tilde{s}_v R^T \end{bmatrix}.$$

Let  $\bar{s} = [\bar{s}_r R \quad \bar{s}_v R]$  be a document such that

$$\tilde{s}_r R = t_1 \bar{s}_r R, \quad \tilde{s}_v R = t_2 \bar{s}_v R,$$

with  $t_1, t_2 \in \mathbb{R}$ . We have

$$\hat{x}_R^T = \tilde{A}_R \begin{bmatrix} t_1 \bar{s}_r R^T \\ t_2 \bar{s}_v R^T \end{bmatrix} = \tilde{A}_R \begin{bmatrix} t_1 & 0 \\ 0 & t_2 \end{bmatrix} \begin{bmatrix} \bar{s}_r R^T \\ \bar{s}_v R^T \end{bmatrix}.$$

Set

$$\bar{A}_R = \tilde{A}_R \begin{bmatrix} t_1 & 0 \\ 0 & t_2 \end{bmatrix} = \begin{bmatrix} t_1 \tilde{a}_{11}^R & t_2 \tilde{a}_{12}^R \\ t_1 \tilde{a}_{21}^R & t_2 \tilde{a}_{22}^R \end{bmatrix}, \quad (9)$$

then  $(\bar{A}_R, \bar{s}_R)$  is a solution of (8). If we impose that

$$\begin{aligned} t_1 \tilde{a}_{11}^R + t_2 \tilde{a}_{12}^R &= 1, \\ t_1 \tilde{a}_{21}^R + t_2 \tilde{a}_{22}^R &= 1, \end{aligned}$$

as  $\det \tilde{A}_R \neq 0$ , then such a system in the unknowns  $t_1$  and  $t_2$  has solution

$$\begin{bmatrix} t_1 \\ t_2 \end{bmatrix} = \frac{1}{\det A_R} \begin{bmatrix} \tilde{a}_{22}^R - \tilde{a}_{12}^R \\ \tilde{a}_{11}^R - \tilde{a}_{21}^R \end{bmatrix}. \quad (10)$$

By hypothesis, it turns out that all involved quantities on the right hand in (10) are different from zero.  $\square$

**Proposition 2.2.** Let  $(\tilde{A}_R, \tilde{s}_R)$  be a solution of the linear model in equation (8), with  $\tilde{A}_R$  non-singular, nonnegative and column strictly diagonally dominant matrix, then there exist  $t_1, t_2 > 0$  and  $\bar{A}_R$  stochastic matrix, such that  $(\bar{A}_R, \bar{s}_R)$  is a solution of (8) with  $\bar{s}_R = \begin{bmatrix} \frac{1}{t_1} \tilde{s}_{rR} & \frac{1}{t_2} \tilde{s}_{vR} \end{bmatrix}$ .

*Proof.* As  $\tilde{A}_R$  is nonnegative and column strictly diagonally dominant matrix, then from (10) we obtain  $t_1, t_2 > 0$ . Thus,  $(\bar{A}_R, \bar{s}_R)$  is a solution of (8), where the mixture matrix  $\bar{A}_R$  satisfies the condition (4). Moreover,  $\bar{A}_R$  turns to be nonnegative by (9), and thus  $\bar{A}_R$  is a stochastic matrix.  $\square$

**Proposition 2.3.** Let  $(\tilde{A}_R, \tilde{s}_R)$  be a solution of the linear model in equation (8), where  $\tilde{A}_R$  is a singular matrix. Then there exists  $t \in \mathbb{R}$  such that  $x_{vR} = tx_{rR}$ .

*Proof.* If  $\tilde{A}_R$  is a singular matrix, then there exists  $t \in \mathbb{R}$  such that  $\tilde{a}_{11}^R = t \tilde{a}_{21}^R$  and  $\tilde{a}_{12}^R = t \tilde{a}_{22}^R$ . Thus,  $x_{rR} = \tilde{a}_{11}^R \tilde{s}_{rR} + \tilde{a}_{12}^R \tilde{s}_{vR}$  and  $x_{vR} = \tilde{a}_{21}^R \tilde{s}_{rR} + \tilde{a}_{22}^R \tilde{s}_{vR} = t \tilde{a}_{11}^R \tilde{s}_{rR} + t \tilde{a}_{12}^R \tilde{s}_{vR} = tx_{rR}$ .  $\square$

In the case  $x_v = t x_r$ , in the next section we show how to find a more realistic solution with a stochastic mixing matrix.

**Proposition 2.4.** Let  $(\tilde{A}_R, \tilde{s}_R)$  be a solution of the linear model in equation (8), where  $\tilde{a}_{11}^R = \tilde{a}_{21}^R$ . Then an alternative solution is given by

$$\bar{s}_R = \begin{bmatrix} \tilde{a}_{11}^R \tilde{s}_{rR} + \tilde{s}_{vR} & \tilde{a}_{11}^R \tilde{s}_{rR} \end{bmatrix}, \quad \bar{A}_R = \begin{bmatrix} \tilde{a}_{12}^R & 1 - \tilde{a}_{12}^R \\ \tilde{a}_{22}^R & 1 - \tilde{a}_{22}^R \end{bmatrix}.$$

*Proof.* If  $\tilde{a}_{11}^R = \tilde{a}_{21}^R$ , then  $x_{rR} = \tilde{a}_{11}^R \tilde{s}_{rR} + \tilde{a}_{12}^R \tilde{s}_{vR}$  and  $x_{vR} = \tilde{a}_{11}^R \tilde{s}_{rR} + \tilde{a}_{22}^R \tilde{s}_{vR}$ . The same result is obtained if we calculate  $x_R$  as  $x_R^T = \bar{A}_R \bar{s}_R^T$ .  $\square$

**Proposition 2.5.** Let  $(\tilde{A}_R, \tilde{s}_R)$  be a solution of the linear model in equation (8), where  $\tilde{a}_{22}^R = \tilde{a}_{12}^R$  then an alternative solution is given by

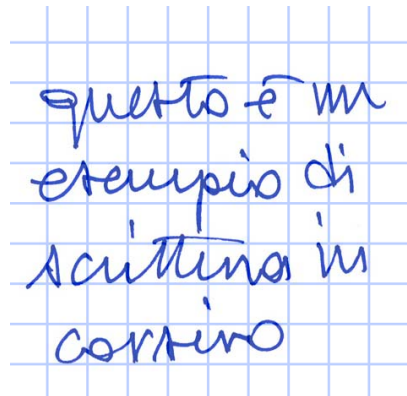
$$\bar{s}_R = \begin{bmatrix} \tilde{s}_{rR} + \tilde{a}_{12}^R \tilde{s}_{vR} & \tilde{a}_{12}^R \tilde{s}_{vR} \end{bmatrix}, \quad \bar{A}_R = \begin{bmatrix} \tilde{a}_{11}^R & 1 - \tilde{a}_{11}^R \\ \tilde{a}_{21}^R & 1 - \tilde{a}_{21}^R \end{bmatrix}.$$

*Proof.* If  $\tilde{a}_{22}^R \tilde{a}_{12}^R$ , then  $x_{rR} = \tilde{a}_{11}^R \tilde{s}_{rR} + \tilde{a}_{12}^R \tilde{s}_{vR}$  and  $x_{vR} = \tilde{a}_{21}^R \tilde{s}_{rR} + \tilde{a}_{12}^R \tilde{s}_{vR}$ . The same result is obtained if we calculate  $x_R$  as  $x_R^T = \bar{A}_R \bar{s}_R^T$ .  $\square$

When  $\tilde{a}_{11}^R = \tilde{a}_{21}^R$  or  $\tilde{a}_{12}^R = \tilde{a}_{22}^R$ , usually one of the estimated sources corresponds to the common background of the recto and the verso, that is a pattern which is equally present on both sides of the document. An example with

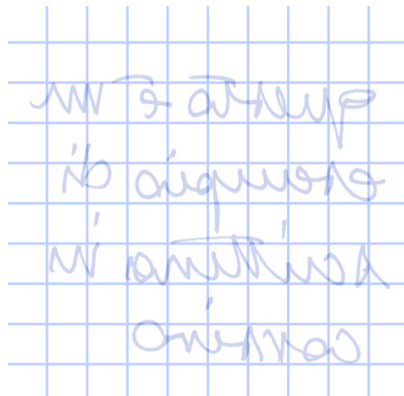
$$\tilde{A}_R = \tilde{A}_G = \tilde{A}_B = \begin{bmatrix} 1 & 0.8 \\ 1 & 0.2 \end{bmatrix} \quad \text{and} \quad \bar{A}_R = \bar{A}_G = \bar{A}_B = \begin{bmatrix} 0.8 & 0.2 \\ 0.2 & 0.8 \end{bmatrix}$$

is shown in Figure 1.



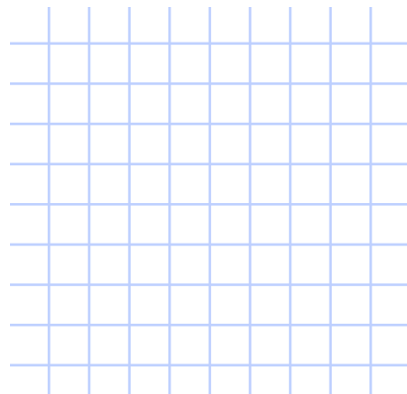
questo è un  
esempio di  
scrittura in  
corsivo

(a) Observed recto of the document.



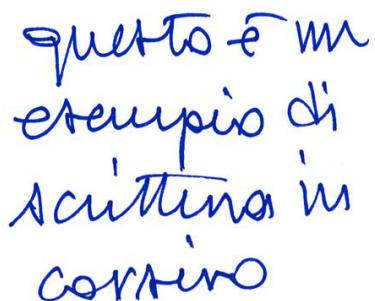
non so cosa scrivere  
ho dimenticato  
mi manca la  
matita

(b) Observed verso of the document.



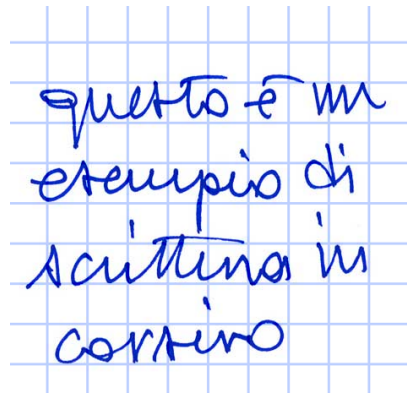
questo è un  
esempio di  
scrittura in  
corsivo

(c) Recto restored with  $\tilde{a}_{11} = \tilde{a}_{21}$ .



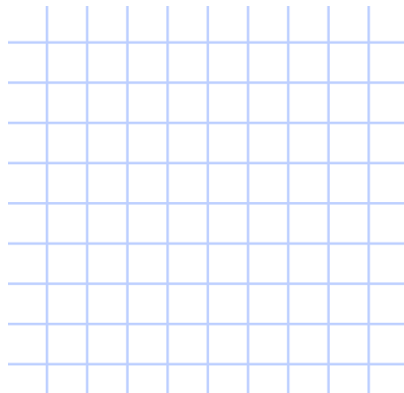
questo è un  
esempio di  
scrittura in  
corsivo

(d) Verso restored with  $\tilde{a}_{11} = \tilde{a}_{21}$ .



questo è un  
esempio di  
scrittura in  
corsivo

(e) Recto restored with a stochastic  
matrix.



questo è un  
esempio di  
scrittura in  
corsivo

(f) Verso restored with a stochastic  
mixture matrix.

Figure 1: Stochastic mixture matrix reconstruction.

Here we define the following  $2 \times 2$  *data overlapping matrix* of the observed data.

$$C_R = \begin{bmatrix} c_{11}^R & c_{12}^R \\ c_{21}^R & c_{22}^R \end{bmatrix} = x_R^T x_R = \begin{bmatrix} x_{rR}^T \cdot x_{rR} & x_{rR}^T \cdot x_{vR} \\ x_{vR}^T \cdot x_{rR} & x_{vR}^T \cdot x_{vR} \end{bmatrix}. \quad (11)$$

This matrix, when  $x_{rR}$  and  $x_{vR}$  have zero mean, is denoted by *data covariance matrix* (see also [42, 53, 54, 56]). The matrix  $C_R$  gives an information about how much the text of the front overlaps with the one of the back. In fact in our case, since  $x_R$  is a nonnegative matrix, the data overlapping matrix is always a nonnegative matrix, and it is diagonal if and only if there is no overlapping text from the recto to the verso of the document. In particular we refer to the entries  $d_R = c_{12}^R = c_{21}^R$  as the *data overlapping level*.

Similarly as above, it is possible to define the *source overlapping matrix* as follows:

$$P_R = \begin{bmatrix} p_{11}^R & p_{12}^R \\ p_{21}^R & p_{22}^R \end{bmatrix} = s_R^T s_R = \begin{bmatrix} s_{rR}^T \cdot s_{rR} & s_{rR}^T \cdot s_{vR} \\ s_{vR}^T \cdot s_{rR} & s_{vR}^T \cdot s_{vR} \end{bmatrix}.$$

We refer to the entries  $k_R = p_{12}^R = p_{21}^R$  as the *source overlapping level*.

Moreover, it is easy to see that the matrices  $C_R$  and  $P_R$  are symmetric and positive semidefinite. Indeed,

$$x_{rR}^T \cdot x_{vR}^T = x_{vR}^T \cdot x_{rR}^T, \quad \text{and} \quad s_{rR}^T \cdot s_{vR}^T = s_{vR}^T \cdot s_{rR}^T$$

for the symmetry of the scalar product. Moreover, for every  $y \in \mathbb{R}^2$  we get

$$y^T C_R y = y^T x_R^T x_R y = (x_R y)^T \cdot (x_R y) = \|x_R y\|^2 \geq 0,$$

and similarly for the matrix  $P_R$ .

### 3 The estimates of the sources

In this paper we deal with the problem of estimating both the ideal sources and the mixture matrix from the observed data, which in the literature is called *Blind Source Separation* (BSS) (see also [2, 12, 30, 52]). If we have an invertible estimate  $\tilde{A}_R$  of  $A_R$ , then an estimate of  $s_R$  is

$$\tilde{s}_R^T = \tilde{A}_R^{-1} x_R^T. \quad (12)$$

Since there are infinitely many choices of  $\tilde{A}_R$ , our problem admits infinitely many solutions. Thus we are dealing with an ill-posed problem in the sense of Hadamard (see also [24]). Even if we assume that  $\tilde{A}_R$  and  $\tilde{s}_R$  are nonnegative matrices, the problem is NP-hard (see [57]) and ill-posed (see [23]). To overcome this fact, it is necessary to impose some constraints on the solutions.

Existing techniques in the literature, like the *Principal Component Analysis* (PCA), the *Whitening* (W) and *Symmetric Whitening* (SW), by considering data images with zero mean in each component, deal with the data covariance matrices instead of the data overlapping matrices. In our context we extend the use of overlapping matrices to these techniques. In particular, let us consider a spectral decomposition of the red data overlapping matrix  $C_R = \Pi_R \Lambda_R \Pi_R^T$ , where  $\Pi_R$  is orthogonal, the columns of  $\Pi_R$  are the eigenvectors

of  $C_R$ , and  $\Lambda_R$  is a diagonal matrix, whose diagonal entries are the eigenvalues of  $C_R$ . An assumption used in these techniques is that the source overlapping matrix (source covariance matrix, in the case of red data images with zero mean)  $P_R$  is diagonal. In particular in the PCA technique it is supposed that  $P_R = \Lambda_R$ , while in the W and SW techniques it is assumed that  $P_R = I$ , where  $I$  is the identity  $2 \times 2$  matrix (see also [52, 53, 54]). By (8), we obtain

$$C_R = x_R^T x_R = A_R s_R^T s_R A_R^T = A_R P_R A_R^T. \quad (13)$$

The estimates of the mixture matrices by means of the PCA, W and SW techniques are given by  $\tilde{A}_R = \Pi_R$ ,  $\tilde{A}_R = \Pi_R \Lambda_R^{1/2}$  and  $\tilde{A}_R = \Pi_R \Lambda_R^{1/2} \Pi_R^T = C_R^{1/2}$ , respectively. Moreover, in the *Optimal Whitening* (OW) technique it is assumed that  $P_R = c^2 I$  for some  $c \in \mathbb{R} \setminus \{0\}$ . This technique imposes that  $\|\tilde{s}_R - x_R\|_F$  is minimal, where  $\|\cdot\|_F$  is the Frobenius norm. Thus, we get  $\tilde{A}_R = \frac{2}{\sqrt{\lambda_1^R} + \sqrt{\lambda_2^R}} C_R^{1/2}$ , where  $\lambda_1^R$  and  $\lambda_2^R$  are the eigenvalues of  $C_R$  (see also [19]).

In the proposed technique, we distinguish two cases,  $\det C_R = 0$  and  $\det C_R \neq 0$ . We first assume  $\det C_R = 0$ . From (11), since  $x_{rR}$  and  $x_{vR}$  are nonnegative vectors, and from the Cauchy-Schwartz inequality it follows that there exists  $\zeta > 0$  with  $x_{rR} = \zeta x_{vR}$ . An example can be shown in Figure 2 (a) and (b).

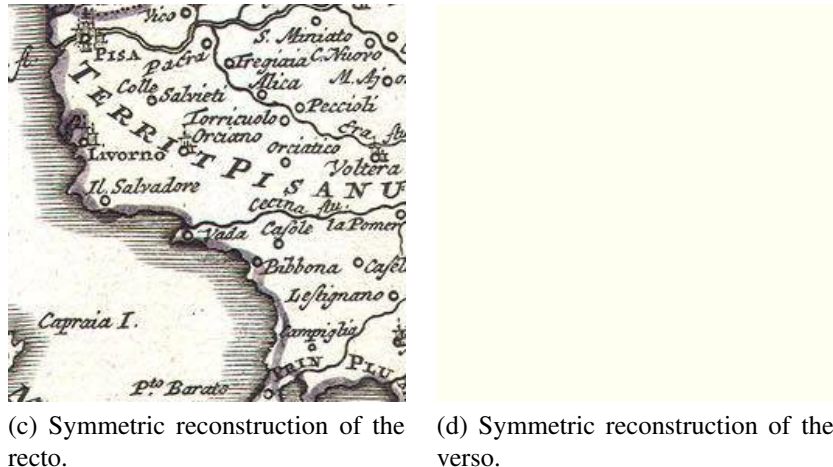
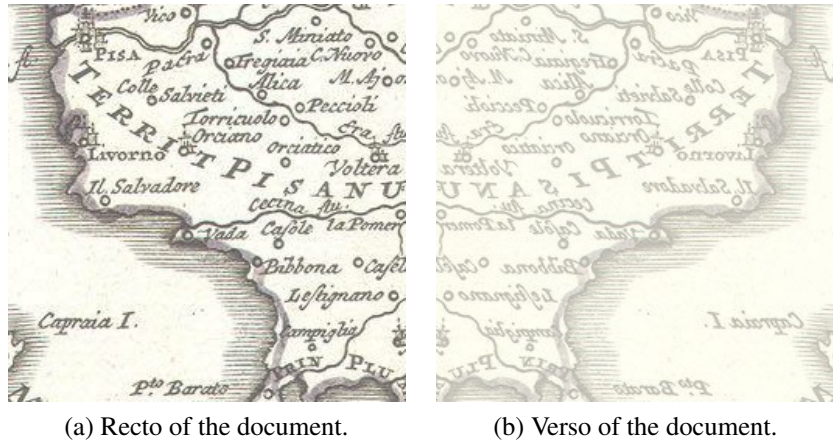


Figure 2: Document whose recto is a multiple of the verso.

In this case, it is natural to assume that  $\tilde{s}_{rR} = 0 e$  or  $\tilde{s}_{vR} = 0 e$ , where  $e$  is as in (6),

and  $\tilde{s}_{rR}, \tilde{s}_{vR}$  are the estimates of the ideal sources  $s_{rR}, s_{vR}$ , respectively, that is the recto or the verso of the ideal source document is an empty page. When  $\zeta \geq 1$ , we assume that  $\tilde{s}_{vR} = 0 e$ , and so we get  $x_{rR} = \tilde{a}_{11}^R \tilde{s}_{rR}$ ,  $x_{vR} = \tilde{a}_{21}^R \tilde{s}_{rR}$  and  $\zeta = \frac{\tilde{a}_{11}^R}{\tilde{a}_{21}^R}$ , where  $\tilde{a}_{11}^R$  and  $\tilde{a}_{21}^R$  are estimates of  $a_{11}^R$  and  $a_{21}^R$ , respectively. Therefore we obtain

$$\tilde{s}_{rR} = \frac{1}{\tilde{a}_{11}^R} x_{rR}, \quad \tilde{s}_{vR} = 0 e, \quad \tilde{A}_R = \begin{bmatrix} \tilde{a}_{11}^R & 1 - \tilde{a}_{11}^R \\ \frac{1}{\zeta} \tilde{a}_{11}^R & 1 - \frac{1}{\zeta} \tilde{a}_{11}^R \end{bmatrix},$$

where  $\tilde{a}_{11}^R$  is arbitrarily chosen in  $]0, 1]$  and  $\tilde{A}_R$  is an estimate of the mixing matrix  $A_R$ . If we impose that the matrix  $\tilde{A}_R$  is symmetric, then we have  $\tilde{a}_{11}^R = \frac{\zeta}{\zeta + 1}$ . In Figure 2 (c) and (d) we present a symmetric reconstruction of the document shown in Figure 2 (a) and (b).

If  $0 < \zeta < 1$ , then we put  $\tilde{s}_{rR} = 0 e$ , and so we get  $x_{vR} = \tilde{a}_{12}^R \tilde{s}_{vR}$ ,  $x_{rR} = \tilde{a}_{22}^R \tilde{s}_{vR}$  and  $\zeta = \frac{\tilde{a}_{12}^R}{\tilde{a}_{22}^R}$ , where  $\tilde{a}_{12}^R$  and  $\tilde{a}_{22}^R$  are estimates of  $a_{12}^R$  and  $a_{22}^R$ , respectively. Therefore we obtain

$$\tilde{s}_{vR} = 0 e, \quad \tilde{s}_{vR} = \frac{1}{\tilde{a}_{22}^R} x_{vR}, \quad \tilde{A}_R = \begin{bmatrix} 1 - \zeta \tilde{a}_{22}^R & \zeta \tilde{a}_{22}^R \\ 1 - \tilde{a}_{22}^R & \tilde{a}_{22}^R \end{bmatrix},$$

where  $\tilde{a}_{22}^R$  is arbitrarily chosen in  $]0, 1]$ . If we require the symmetry of the estimated mixing matrix  $\tilde{A}_R$ , then we get  $\tilde{a}_{22}^R = \frac{1}{\zeta + 1}$ .

Now we deal with the more frequent case  $\det C_R \neq 0$ . We would like to estimate not only the ideal sources  $s_{rR}$  and  $s_{vR}$  and the mixture matrix  $A_R$ , but also the source overlapping matrix  $P_R$ . In particular we would like to estimate the source overlapping level  $k_R$ . Since in our algorithm we impose the non-negativity of the estimated sources  $\tilde{s}_{rR}$  and  $\tilde{s}_{vR}$ , the value of the estimate of  $k_R$  represents the level of overlapping of the recto of the source document with its verso, that is, how much the text of the estimated front source is disjoint from the one of the estimated back source. Since the value of  $k_R$  is in general different from zero, the proposed method can be classified as a *Correlated Component Analysis* (CCA) technique (see also [6, 18, 46, 50, 51, 55]).

Now we define a *symmetric factorization* of a symmetric and positive definite matrix  $Y \in \mathbb{R}^{n \times n}$  as an equality of the type  $Y = ZZ^T$ , where  $Z \in \mathbb{R}^{n \times n}$  is a nonsingular matrix. Observe that, given any orthogonal matrix  $Q \in \mathbb{R}^{n \times n}$  and a symmetric factorization of the type  $Y = ZZ^T$ , then the equality  $Y = ZQ(ZQ)^T$  is also a symmetric factorization of  $Y$ . Indeed, if  $Y = ZZ^T$ , then

$$ZQ(ZQ)^T = ZQQ^TZ^T = ZZ^T = Y,$$

since  $Q$  is orthogonal. Moreover, if we consider any two symmetric factorizations of the type

$$Y = Z_1 Z_1^T = Z_2 Z_2^T, \tag{14}$$

then there is an orthogonal matrix  $Q \in \mathbb{R}^{n \times n}$  with

$$Z_1 = Z_2 Q. \tag{15}$$

Indeed, first of all observe that, thanks to the Binet theorem, the matrices  $Z_1$  and  $Z_2$  are nonsingular. Let  $Y, Z_1$  and  $Z_2$  be as in (14), then it is

$$Z_1 = Z_2 Z_2^T Z_1^{-T} = Z_2 Q, \quad (16)$$

where the symbol  $\cdot^{-T}$  denotes the transposed of the inverse matrix, and

$$Q = Z_2^T Z_1^{-T}. \quad (17)$$

We get

$$\begin{aligned} QQ^T &= Z_2^T Z_1^{-T} Z_1^{-1} Z_2 = Z_2^T (Z_1 Z_1^T)^{-1} Z_2 \\ &= Z_2^T (Z_2 Z_2^T)^{-1} Z_2 = Z_2^T Z_2^{-T} Z_2^{-1} Z_2 = I. \end{aligned}$$

In the particular case  $2 \times 2$ , the set of the orthogonal matrices is the union of all rotations and reflections in  $\mathbb{R}^2$ , which are expressed as

$$Q_1(\theta) = \begin{bmatrix} \sin \theta & -\cos \theta \\ \cos \theta & \sin \theta \end{bmatrix} \quad \text{and} \quad Q_{-1}(\theta) = \begin{bmatrix} \cos \theta & \sin \theta \\ \sin \theta & -\cos \theta \end{bmatrix}, \quad (18)$$

respectively, as  $\theta$  varies in  $[0, 2\pi[$ . Note that  $C_R = C_R^{1/2} (C_R^{1/2})^T = C_R^{1/2} C_R^{1/2}$  is a symmetric factorization of  $C_R$ , and thus all possible factorizations of  $C_R$  are given by

$$Z_{R,\iota}(\theta) = C_R^{1/2} Q_\iota(\theta) = \begin{bmatrix} z_{11}^{R,\iota}(\theta) & z_{12}^{R,\iota}(\theta) \\ z_{21}^{R,\iota}(\theta) & z_{22}^{R,\iota}(\theta) \end{bmatrix}, \quad (19)$$

where  $\theta \in [0, 2\pi[$  and  $\iota \in \{-1, 1\}$ .

To have a joint estimation of the mixture, the source matrices and the source overlapping level, we use an iterative algorithm. At the  $l$ -th step, given  $\theta \in [0, 2\pi[$  and  $\iota \in \{-1, 1\}$ , by using (13) we get

$$C_R = A_R \tilde{P}_{R,\iota}^{(l)}(\theta) A_R^T,$$

where the matrix

$$\tilde{P}_{R,\iota}^{(l)}(\theta) = \begin{bmatrix} \tilde{p}_{11}^{R,\iota,(l)}(\theta) & k_R^{(l)} \\ k_R^{(l)} & \tilde{p}_{22}^{R,\iota,(l)}(\theta) \end{bmatrix} \quad (20)$$

is a symmetric and positive definite estimate of the source overlapping matrix  $P_R$ , and  $k_R^{(l)}$  is the estimate of the red source overlapping level obtained at the  $(l-1)$ -th step (we assume  $k_R^{(0)} = 0$ ), while  $\tilde{p}_{11}^{R,\iota,(l)}(\theta)$  and  $\tilde{p}_{22}^{R,\iota,(l)}(\theta)$  will be chosen in order that the estimated mixture matrix is stochastic. Given a factorization

$$\tilde{P}_{R,\iota}^{(l)}(\theta) = W_{R,\iota}^{(l)}(\theta) (W_{R,\iota}^{(l)}(\theta))^T, \quad (21)$$

where

$$W_{R,\iota}^{(l)}(\theta) = \begin{bmatrix} w_{11}^{R,\iota,(l)}(\theta) & w_{12}^{R,\iota,(l)}(\theta) \\ w_{21}^{R,\iota,(l)}(\theta) & w_{22}^{R,\iota,(l)}(\theta) \end{bmatrix} \quad (22)$$

is a suitable nonsingular matrix, from (20) and (21) we deduce

$$w_{11}^{R,\iota,(l)}(\theta) w_{21}^{R,\iota,(l)}(\theta) + w_{12}^{R,\iota,(l)}(\theta) w_{22}^{R,\iota,(l)}(\theta) = k_R^{(l)}. \quad (23)$$

Moreover, by virtue of (13) and (21), it is

$$C_R = A_R W_{R,\iota}^{(l)}(\theta) (W_{R,\iota}^{(l)}(\theta))^T A_R^T = A_R W_{R,\iota}^{(l)}(\theta) (A_R W_{R,\iota}^{(l)}(\theta))^T,$$

and so  $A_R W_{R,\iota}^{(l)}(\theta)$  realizes a factorization of  $C_R$ . Thus we define an estimation

$$\tilde{A}_{R,\iota}^{(l)}(\theta) = \begin{bmatrix} a_{11}^{R,\iota,(l)}(\theta) & a_{12}^{R,\iota,(l)}(\theta) \\ a_{21}^{R,\iota,(l)}(\theta) & a_{22}^{R,\iota,(l)}(\theta) \end{bmatrix} \quad (24)$$

of the mixture matrix  $A_R$  as a matrix such that

$$\tilde{A}_{R,\iota}^{(l)}(\theta) W_{R,\iota}^{(l)}(\theta) = Z_{R,\iota}(\theta),$$

where  $Z_{R,\iota}(\theta)$  is as in (19) and  $W_{R,\iota}^{(l)}(\theta)$  is chosen in order that the matrix  $\tilde{A}_{R,\iota}^{(l)}(\theta)$  satisfies the stochastic condition in equation (4), that is

$$\begin{cases} z_{11}^{R,\iota}(\theta) w_{22}^{R,\iota,(l)}(\theta) - z_{12}^{R,\iota}(\theta) w_{21}^{R,\iota,(l)}(\theta) + z_{12}^{R,\iota}(\theta) w_{11}^{R,\iota,(l)}(\theta) \\ - z_{11}^{R,\iota}(\theta) w_{12}^{R,\iota,(l)}(\theta) = w_{11}^{R,\iota,(l)}(\theta) w_{22}^{R,\iota,(l)}(\theta) - w_{21}^{R,\iota,(l)}(\theta) w_{12}^{R,\iota,(l)}(\theta), \\ z_{21}^{R,\iota}(\theta) w_{22}^{R,\iota,(l)}(\theta) - z_{22}^{R,\iota}(\theta) w_{21}^{R,\iota,(l)}(\theta) + z_{22}^{R,\iota}(\theta) w_{11}^{R,\iota,(l)}(\theta) \\ - z_{21}^{R,\iota}(\theta) w_{12}^{R,\iota,(l)}(\theta) = w_{11}^{R,\iota,(l)}(\theta) w_{22}^{R,\iota,(l)}(\theta) - w_{21}^{R,\iota,(l)}(\theta) w_{12}^{R,\iota,(l)}(\theta). \end{cases} \quad (25)$$

If we assume that  $z_{11}^{R,\iota}(\theta) \neq z_{21}^{R,\iota}(\theta)$  and  $z_{12}^{R,\iota}(\theta) \neq z_{22}^{R,\iota}(\theta)$ , then a possible choice of  $w_{ij}^{(l)}(\theta)$ ,  $i, j = 1, 2$ , taking into account (23) and (25), is given by

$$\begin{cases} w_{11}^{R,\iota,(l)}(\theta) = \frac{\det(Z_{R,\iota}(\theta))}{z_{22}^{R,\iota}(\theta) - z_{12}^{R,\iota}(\theta)} - k_R^{(l)} \frac{(z_{11}^{R,\iota}(\theta) - z_{21}^{R,\iota}(\theta))^2}{(z_{22}^{R,\iota}(\theta) - z_{12}^{R,\iota}(\theta)) \det(Z_{R,\iota}(\theta))}, \\ w_{12}^{R,\iota,(l)}(\theta) = k_R^{(l)} \frac{z_{11}^{R,\iota}(\theta) - z_{21}^{R,\iota}(\theta)}{\det(Z_{R,\iota}(\theta))}, \\ w_{21}^{R,\iota,(l)}(\theta) = 0, \\ w_{22}^{R,\iota,(l)}(\theta) = \frac{\det(Z_{R,\iota}(\theta))}{z_{11}^{R,\iota}(\theta) - z_{21}^{R,\iota}(\theta)}. \end{cases} \quad (26)$$

This choice is arbitrary, since the nonlinear system given by the equations (23) and (25) has other infinitely many solutions. Moreover, recall that the matrix  $W_{R,\iota}^{(l)}(\theta)$  must be necessarily be non-singular. From equation (26), as  $\det(Z_{R,\iota}(\theta)) \neq 0$ , we have that  $W_{R,\iota}^{(l)}(\theta)$  is not singular if and only if  $w_{11}^{R,\iota,(l)}(\theta) \neq 0$ . Let us examine the case  $w_{11}^{R,\iota,(l)}(\theta) = 0$ . This holds if and only if

$$\frac{\det(Z_{R,\iota}(\theta))}{z_{22}^{R,\iota}(\theta) - z_{12}^{R,\iota}(\theta)} - k_R^{(l)} \frac{(z_{11}^{R,\iota}(\theta) - z_{21}^{R,\iota}(\theta))^2}{(z_{22}^{R,\iota}(\theta) - z_{12}^{R,\iota}(\theta)) \det(Z_{R,\iota}(\theta))} = 0,$$

namely

$$k_R^{(l)} = \frac{(\det(Z_{R,\iota}(\theta)))^2}{(z_{11}^{R,\iota}(\theta) - z_{21}^{R,\iota}(\theta))^2} = \frac{\det(C_R)}{(z_{11}^{R,\iota}(\theta) - z_{21}^{R,\iota}(\theta))^2}.$$

Indeed,  $\det(Q_1(\theta)) = 1$  and  $\det(Q_2(\theta)) = -1$  for each  $\theta \in \mathbb{R}$ , so we get  $(\det(Z_{R,\iota}(\theta)))^2 = \det(C_R)$ . Note that  $\det(C_R) > 0$ , because  $C_R$  is symmetric and positive definite. As  $k_R^{(l)} > 0$ , we obtain

$$(z_{11}^{R,\iota}(\theta) - z_{21}^{R,\iota}(\theta))^2 = \frac{\det(C_R)}{k_R^{(l)}},$$

and hence

$$z_{11}^{R,\iota}(\theta) - z_{21}^{R,\iota}(\theta) = \frac{(\det(C_R))^{1/2}}{(k_R^{(l)})^{1/2}} \quad (27)$$

or

$$z_{21}^{R,\iota}(\theta) - z_{11}^{R,\iota}(\theta) = \frac{(\det(C_R))^{1/2}}{(k_R^{(l)})^{1/2}}. \quad (28)$$

Given

$$C_R^{1/2} = \begin{bmatrix} \bar{c}_{11}^R & \bar{c}_{12}^R \\ \bar{c}_{21}^R & \bar{c}_{22}^R \end{bmatrix}, \quad (29)$$

then  $\iota = 1$ , the relations (27) and (28) become

$$(\bar{c}_{11}^R - \bar{c}_{21}^R) \sin \theta + (\bar{c}_{12}^R - \bar{c}_{22}^R) \cos \theta = \frac{(\det(C_R))^{1/2}}{(k_R^{(l)})^{1/2}} \quad (30)$$

and

$$(\bar{c}_{21}^R - \bar{c}_{11}^R) \sin \theta + (\bar{c}_{22}^R - \bar{c}_{12}^R) \cos \theta = \frac{(\det(C_R))^{1/2}}{(k_R^{(l)})^{1/2}}, \quad (31)$$

respectively. When  $\iota = -1$ , the relations (27) and (28) assume the expressions

$$(\bar{c}_{12}^R - \bar{c}_{22}^R) \sin \theta + (\bar{c}_{11}^R - \bar{c}_{21}^R) \cos \theta = \frac{(\det(C_R))^{1/2}}{(k_R^{(l)})^{1/2}} \quad (32)$$

and

$$(\bar{c}_{22}^R - \bar{c}_{12}^R) \sin \theta + (\bar{c}_{21}^R - \bar{c}_{11}^R) \cos \theta = \frac{(\det(C_R))^{1/2}}{(k_R^{(l)})^{1/2}}, \quad (33)$$

respectively.

Now we solve the equation

$$\hat{a} \sin \theta + \hat{b} \cos \theta = \hat{c}. \quad (34)$$

By setting  $\xi = \tan \frac{\theta}{2}$ , the equation (34) becomes

$$(\hat{b} + \hat{c})\xi^2 - 2\hat{a}\xi + \hat{c} - \hat{b} = 0, \quad (35)$$

which has no solutions when  $\hat{a}^2 + \hat{b}^2 < \hat{c}^2$ , and admits the solutions

$$\xi_{\pm} = \frac{\hat{a} \pm \sqrt{\hat{a}^2 + \hat{b}^2 - \hat{c}^2}}{\hat{b} + \hat{c}} \quad (36)$$

when  $\hat{a}^2 + \hat{b}^2 \geq \hat{c}^2$ , provided that  $\hat{b} + \hat{c} \neq 0$ , while

$$\xi_0 = -\frac{\hat{b}}{\hat{a}} \quad (37)$$

when  $\hat{b} = -\hat{c}$  and  $\hat{a} \neq 0$ . Moreover, it is readily seen that, when  $\hat{b} = -\hat{c}$ , (34) has the solution  $\theta = \pi$ .

When  $\hat{b} = -\hat{c}$  and  $\hat{a} = 0$ , (35) is satisfied for every  $\xi \in \mathbb{R}$  if and only if  $\hat{b} = \hat{c} = 0$ , while if  $\hat{b} \neq 0$  (or equivalently  $\hat{c} \neq 0$ ), (35) has no solutions. From (36) and (37) we obtain that (34) admits the solutions  $\varphi_R^{(9)} = 2 \arctan \xi_+$ ,  $\varphi_R^{(10)} = 2 \arctan \xi_-$ ,  $\varphi_R^{(11)} = 2 \arctan \xi_0$ . First, observe that, in all cases (30), (31), (32), (33), it is  $\hat{a}^2 + \hat{b}^2 \geq \hat{c}^2$  if and only if

$$(\bar{c}_{11}^R - \bar{c}_{21}^R)^2 + (\bar{c}_{12}^R - \bar{c}_{22}^R)^2 \geq \frac{\det(C_R)}{k_R^{(l)}},$$

if and only if

$$(\bar{c}_{11}^R - \bar{c}_{21}^R)^2 + (\bar{c}_{12}^R - \bar{c}_{22}^R)^2 < \frac{\det(C_R)}{k_R^{(l)}},$$

that is

$$k_R^{(l)} < k_{sup}^R = \frac{\det(C_R)}{(\bar{c}_{11}^R - \bar{c}_{21}^R)^2 + (\bar{c}_{12}^R - \bar{c}_{22}^R)^2}. \quad (38)$$

Note that the expression in (38) makes sense. Indeed, if

$$(\bar{c}_{11}^R - \bar{c}_{21}^R)^2 + (\bar{c}_{12}^R - \bar{c}_{22}^R)^2 = 0,$$

then we should get  $\bar{c}_{11}^R = \bar{c}_{21}^R$ ,  $\bar{c}_{12}^R = \bar{c}_{22}^R$ , and hence  $\det(C_R) = 0$ , which is impossible. We refer to  $k_{sup}^R$  in the equation (38) as the *red source overlapping level upper bound*. We show in Section 4.2 how the proposed algorithm, in general, avoids the case in which the source overlapping levels are larger than their upper bounds. Thus, during the computation, the matrix  $W_{R,\ell}^{(l)}(\theta)$  is always not singular.

Therefore, (38) is a necessary condition to have  $w_{11}^{R,\ell,(l)}(\theta) = 0$ . For such values of  $k_R^{(l)}$ , equation (30) has the solutions

$$\xi_{\pm} = \frac{\bar{c}_{11}^R - \bar{c}_{21}^R \pm \sqrt{(\bar{c}_{11}^R - \bar{c}_{21}^R)^2 + (\bar{c}_{12}^R - \bar{c}_{22}^R)^2 + \frac{\det(C_R)}{k_R^{(l)}}}}{\bar{c}_{12}^R - \bar{c}_{22}^R + \frac{(\det(C_R))^{1/2}}{(k_R^{(l)})^{1/2}}}, \quad \text{when } \bar{c}_{12}^R + \frac{(\det(C_R))^{1/2}}{(k_R^{(l)})^{1/2}} \neq \bar{c}_{22}^R,$$

$$\pi, \quad \text{when } \bar{c}_{12}^R + \frac{(\det(C_R))^{1/2}}{(k_R^{(l)})^{1/2}} = \bar{c}_{22}^R,$$

$$\xi_0 = \frac{\bar{c}_{22}^R - \bar{c}_{12}^R}{\bar{c}_{11}^R - \bar{c}_{21}^R}, \quad \begin{aligned} &\text{when } \bar{c}_{12}^R + \frac{(\det(C_R))^{1/2}}{(k_R^{(l)})^{1/2}} = \bar{c}_{22}^R \\ &\text{and } \bar{c}_{11}^R \neq \bar{c}_{21}^R. \end{aligned}$$

Equation (31) admits the solutions

$$\xi_{\pm} = \frac{\bar{c}_{21}^R - \bar{c}_{11}^R \pm \sqrt{(\bar{c}_{11}^R - \bar{c}_{21}^R)^2 + (\bar{c}_{12}^R - \bar{c}_{22}^R)^2 + \frac{\det(C_R)}{k_R^{(l)}}}}{\bar{c}_{22}^R - \bar{c}_{12}^R + \frac{(\det(C_R))^{1/2}}{(k_R^{(l)})^{1/2}}}, \quad \text{when } \bar{c}_{22}^R + \frac{(\det(C_R))^{1/2}}{(k_R^{(l)})^{1/2}} \neq \bar{c}_{12}^R,$$

$$\pi, \quad \text{when } \bar{c}_{22}^R + \frac{(\det(C_R))^{1/2}}{(k_R^{(l)})^{1/2}} = \bar{c}_{12}^R,$$

$$\xi_0 = \frac{\bar{c}_{22}^R - \bar{c}_{12}^R}{\bar{c}_{11}^R - \bar{c}_{21}^R}, \quad \begin{aligned} &\text{when } \bar{c}_{22}^R + \frac{(\det(C_R))^{1/2}}{(k_R^{(l)})^{1/2}} = \bar{c}_{12}^R \\ &\text{and } \bar{c}_{11}^R \neq \bar{c}_{21}^R. \end{aligned}$$

The solutions of Equation (32) are

$$\xi_{\pm} = \frac{\bar{c}_{12}^R - \bar{c}_{22}^R \pm \sqrt{(\bar{c}_{11}^R - \bar{c}_{21}^R)^2 + (\bar{c}_{12}^R - \bar{c}_{22}^R)^2 + \frac{\det(C_R)}{k_R^{(l)}}}}{\bar{c}_{11}^R - \bar{c}_{21}^R + \frac{(\det(C_R))^{1/2}}{(k_R^{(l)})^{1/2}}}, \quad \text{when } \bar{c}_{11}^R + \frac{(\det(C_R))^{1/2}}{(k_R^{(l)})^{1/2}} \neq \bar{c}_{21}^R,$$

$$\pi, \quad \text{when } \bar{c}_{11}^R + \frac{(\det(C_R))^{1/2}}{(k_R^{(l)})^{1/2}} = \bar{c}_{21}^R,$$

$$\xi_0 = \frac{\bar{c}_{11}^R - \bar{c}_{21}^R}{\bar{c}_{22}^R - \bar{c}_{12}^R}, \quad \begin{aligned} &\text{when } \bar{c}_{11}^R + \frac{(\det(C_R))^{1/2}}{(k_R^{(l)})^{1/2}} = \bar{c}_{21}^R \\ &\text{and } \bar{c}_{12}^R \neq \bar{c}_{22}^R. \end{aligned}$$

Finally, Equation (33) has the solutions

$$\xi_{\pm} = \frac{\bar{c}_{22}^R - \bar{c}_{12}^R \pm \sqrt{(\bar{c}_{11}^R - \bar{c}_{21}^R)^2 + (\bar{c}_{12}^R - \bar{c}_{22}^R)^2 + \frac{\det(C_R)}{k_R^{(l)}}}}{\bar{c}_{21}^R - \bar{c}_{11}^R + \frac{(\det(C_R))^{1/2}}{(k_R^{(l)})^{1/2}}}, \quad \text{when } \bar{c}_{21}^R + \frac{(\det(C_R))^{1/2}}{(k_R^{(l)})^{1/2}} \neq \bar{c}_{11}^R,$$

$$\pi, \quad \text{when } \bar{c}_{21}^R + \frac{(\det(C_R))^{1/2}}{(k_R^{(l)})^{1/2}} = \bar{c}_{11}^R,$$

$$\xi_0 = \frac{\bar{c}_{11}^R - \bar{c}_{21}^R}{\bar{c}_{22}^R - \bar{c}_{12}^R}, \quad \begin{aligned} &\text{when } \bar{c}_{21}^R + \frac{(\det(C_R))^{1/2}}{(k_R^{(l)})^{1/2}} = \bar{c}_{11}^R \\ &\text{and } \bar{c}_{12}^R \neq \bar{c}_{22}^R. \end{aligned}$$

Now, we consider the case  $z_{11}^{R,\iota}(\theta) = z_{21}^{R,\iota}(\theta)$  when the equation (23) is not defined. When  $\iota = 1$ , we get  $z_{11}^{R,1}(\theta) = \bar{c}_{11}^R \sin \theta + \bar{c}_{12}^R \cos \theta$  and  $z_{21}^{R,1}(\theta) = \bar{c}_{21}^R \sin \theta + \bar{c}_{22}^R \cos \theta$ . Thus,  $z_{11}^{R,1}(\theta) = z_{21}^{R,1}(\theta)$  if and only if  $\theta$  assumes the values  $\varphi_R^{(1)}$  or  $\varphi_R^{(2)}$ , where

$$\varphi_R^{(1)} = \begin{cases} \arctan \left( \frac{\bar{c}_{22}^R - \bar{c}_{12}^R}{\bar{c}_{11}^R - \bar{c}_{21}^R} \right), & \text{if } \bar{c}_{11}^R \neq \bar{c}_{21}^R, \\ \frac{\pi}{2}, & \text{if } \bar{c}_{11}^R = \bar{c}_{21}^R \end{cases}, \quad \varphi_R^{(2)} = \varphi_R^{(1)} + \pi. \quad (39)$$

When  $\iota = -1$ , it is  $z_{11}^{R,-1}(\theta) = \bar{c}_{11} \cos \theta + \bar{c}_{12} \sin \theta$  and  $z_{21}^{R,-1}(\theta) = \bar{c}_{21} \cos \theta + \bar{c}_{22} \sin \theta$ , and hence  $z_{11}^{R,-1}(\theta) = z_{21}^{R,-1}(\theta)$  if and only if  $\theta$  assumes the values  $\varphi_R^{(3)}$  or  $\varphi_R^{(4)}$ , where

$$\varphi_R^{(3)} = \begin{cases} \arctan\left(\frac{\bar{c}_{21} - \bar{c}_{11}}{\bar{c}_{12} - \bar{c}_{22}}\right), & \text{if } \bar{c}_{12} \neq \bar{c}_{22}, \\ \frac{\pi}{2}, & \text{if } \bar{c}_{12} = \bar{c}_{22} \end{cases}, \quad \varphi_R^{(4)} = \varphi_R^{(3)} + \pi. \quad (40)$$

Now we turn to the case  $z_{12}^{R,\iota}(\theta) = z_{22}^{R,\iota}(\theta)$ , that is the last case in which the equation (23) is not defined. When  $\iota = 1$ , we get  $z_{12}^{R,1}(\theta) = \bar{c}_{12} \sin \theta - \bar{c}_{11} \cos \theta$  and  $z_{22}^{R,1}(\theta) = \bar{c}_{22} \sin \theta - \bar{c}_{21} \cos \theta$ . We have that  $z_{12}^{R,1}(\theta) = z_{22}^{R,1}(\theta)$  if and only if  $\theta$  has the values  $\varphi_R^{(5)}$  or  $\varphi_R^{(6)}$ , where

$$\varphi_R^{(5)} = \begin{cases} \arctan\left(\frac{\bar{c}_{11} - \bar{c}_{21}}{\bar{c}_{12} - \bar{c}_{22}}\right), & \text{if } \bar{c}_{12} \neq \bar{c}_{22}, \\ \frac{\pi}{2}, & \text{if } \bar{c}_{12} = \bar{c}_{22} \end{cases}, \quad \varphi_R^{(6)} = \varphi_R^{(5)} + \pi. \quad (41)$$

When  $\iota = -1$ , it is  $z_{12}^{R,-1}(\theta) = \bar{c}_{11} \sin \theta - \bar{c}_{12} \cos \theta$  and  $z_{22}^{R,-1}(\theta) = \bar{c}_{21} \sin \theta - \bar{c}_{22} \cos \theta$ , and hence  $z_{12}^{R,-1}(\theta) = z_{22}^{R,-1}(\theta)$  if and only if  $\theta$  assumes the values  $\varphi_R^{(7)}$  or  $\varphi_R^{(8)}$ , where

$$\varphi_R^{(7)} = \begin{cases} \arctan\left(\frac{\bar{c}_{12} - \bar{c}_{22}}{\bar{c}_{11} - \bar{c}_{21}}\right), & \text{if } \bar{c}_{11} \neq \bar{c}_{21}, \\ \frac{\pi}{2}, & \text{if } \bar{c}_{11} = \bar{c}_{21} \end{cases}, \quad \varphi_R^{(8)} = \varphi_R^{(7)} + \pi. \quad (42)$$

In the next section, in formulating the minimization algorithm, we will show how to avoid these cases.

We have

$$(\tilde{A}_{R,\iota}^{(l)}(\theta))^{-1} = Y_{R,\iota}^{(l)}(\theta) = \begin{bmatrix} y_{11}^{R,\iota,(l)}(\theta) & y_{12}^{R,\iota,(l)}(\theta) \\ y_{21}^{R,\iota,(l)}(\theta) & y_{22}^{R,\iota,(l)}(\theta) \end{bmatrix},$$

where

$$\begin{aligned} y_{11}^{R,\iota,(l)}(\theta) &= \frac{z_{22}^{R,\iota}(\theta)((\det(Z_{R,\iota}(\theta)))^2 - k_R^{(l)}(z_{11}^{R,\iota}(\theta) - z_{21}^{R,\iota}(\theta))^2)}{(z_{22}^{R,\iota}(\theta) - z_{12}^{R,\iota}(\theta))(\det(Z_{R,\iota}(\theta)))^2} - z_{21}^{R,\iota}(\theta) \frac{k_R^{(l)}(z_{11}^{R,\iota}(\theta) - z_{21}^{R,\iota}(\theta))}{(\det(Z_{R,\iota}(\theta)))^2} \\ &= \frac{z_{22}^{R,\iota}(\theta)(\det(C_R) - k_R^{(l)}(z_{11}^{R,\iota}(\theta) - z_{21}^{R,\iota}(\theta))^2)}{(z_{22}^{R,\iota}(\theta) - z_{12}^{R,\iota}(\theta))\det(C_R)} - z_{21}^{R,\iota}(\theta) \frac{k_R^{(l)}(z_{11}^{R,\iota}(\theta) - z_{21}^{R,\iota}(\theta))}{\det(C_R)}, \\ y_{12}^{R,\iota,(l)}(\theta) &= -\frac{z_{12}^{R,\iota}(\theta)((\det(Z_{R,\iota}(\theta)))^2 - k_R^{(l)}(z_{11}^{R,\iota}(\theta) - z_{21}^{R,\iota}(\theta))^2)}{(z_{22}^{R,\iota}(\theta) - z_{12}^{R,\iota}(\theta))(\det(Z_{R,\iota}(\theta)))^2} + z_{11}^{R,\iota}(\theta) \frac{k_R^{(l)}(z_{11}^{R,\iota}(\theta) - z_{21}^{R,\iota}(\theta))}{(\det(Z_{R,\iota}(\theta)))^2} \\ &= -\frac{z_{12}^{R,\iota}(\theta)(\det(C_R) - k_R^{(l)}(z_{11}^{R,\iota}(\theta) - z_{21}^{R,\iota}(\theta))^2)}{(z_{22}^{R,\iota}(\theta) - z_{12}^{R,\iota}(\theta))\det(C_R)} + z_{11}^{R,\iota}(\theta) \frac{k_R^{(l)}(z_{11}^{R,\iota}(\theta) - z_{21}^{R,\iota}(\theta))}{\det(C_R)}, \\ y_{21}^{R,\iota,(l)}(\theta) &= -\frac{z_{21}^{R,\iota}(\theta)}{z_{11}^{R,\iota}(\theta) - z_{21}^{R,\iota}(\theta)}, \\ y_{22}^{R,\iota,(l)}(\theta) &= \frac{z_{11}^{R,\iota}(\theta)}{z_{11}^{R,\iota}(\theta) - z_{21}^{R,\iota}(\theta)}. \end{aligned}$$

Hence, by the equation (12), the estimated sources are given by

$$\begin{aligned}\tilde{s}_{rR,\iota}^{(l)}(\theta) &= \left( \frac{z_{22}^{R,\iota}(\theta)(\det(C_R) - k_R^{(l)}(z_{11}^{R,\iota}(\theta) - z_{21}^{R,\iota}(\theta))^2)}{(z_{22}^{R,\iota}(\theta) - z_{12}^{R,\iota}(\theta))\det(C_R)} \right. \\ &\quad \left. - z_{21}^{R,\iota}(\theta) \frac{k_R^{(l)}(z_{11}^{R,\iota}(\theta) - z_{21}^{R,\iota}(\theta))}{\det(C_R)} \right) x_{rR} + \\ &\quad \left( - \frac{z_{12}^{R,\iota}(\theta)(\det(C_R) - k_R^{(l)}(z_{11}^{R,\iota}(\theta) - z_{21}^{R,\iota}(\theta))^2)}{(z_{22}^{R,\iota}(\theta) - z_{12}^{R,\iota}(\theta))\det(C_R)} \right. \\ &\quad \left. + z_{11}^{R,\iota}(\theta) \frac{k_R^{(l)}(z_{11}^{R,\iota}(\theta) - z_{21}^{R,\iota}(\theta))}{\det(C_R)} \right) x_{vR}, \\ \tilde{s}_{vR,\iota}^{(l)}(\theta) &= - \frac{z_{21}^{R,\iota}(\theta)}{z_{11}^{R,\iota}(\theta) - z_{21}^{R,\iota}(\theta)} x_{rR} + \frac{z_{11}^{R,\iota}(\theta)}{z_{11}^{R,\iota}(\theta) - z_{21}^{R,\iota}(\theta)} x_{vR}.\end{aligned}\tag{43}$$

As we assumed that the mixing matrix  $A_R$  is diagonally predominant, if the estimated matrix  $\tilde{A}_{R,\iota}^{(l)}(\theta)$  does not have this property, then we permute the estimated source recto image with the corresponding verso in order to achieve this condition. Note that, thanks to (13), (11) and (12), we have

$$\tilde{P}_{R,\iota}^{(l)}(\theta) = (\tilde{A}_{R,\iota}^{(l)}(\theta))^{-1} C_R (\tilde{A}_{R,\iota}^{(l)}(\theta))^{-T} = (\tilde{A}_{R,\iota}^{(l)}(\theta))^{-1} x_R^T x_R (\tilde{A}_{R,\iota}^{(l)}(\theta))^{-T} = s_{R,\iota}^{(l)}(\theta)^T \tilde{s}_{R,\iota}^{(l)}(\theta).$$

So, from (20) we obtain

$$(\tilde{s}_{rR,\iota}^{(l)}(\theta))^T \cdot \tilde{s}_{vR,\iota}^{(l)}(\theta) = k_R^{(l)}.$$

However, we remark that we assumed that our estimated sources have intensity values between 0 and  $m_R$ . Thus, we do the orthogonal projection of our estimate  $s_{R,\iota}^{(l)}(\theta)$  in the space  $[0, m_R]^{n^2 \times 2}$  with respect to the Frobenius norm. Namely, we apply to the estimate of the sources the following function, which to every vector  $s \in \mathbb{R}^{n^2}$  associates the  $n^2$ -dimensional vector  $\tau(s)$ , whose elements are

$$(\tau(s))_i = \begin{cases} 0, & \text{if } s_i \leq 0, \\ s_i, & \text{if } 0 < s_i \leq m_R, \\ m_R, & \text{if } s_i > m_R, \end{cases} \quad i = 1, \dots, n^2. \tag{44}$$

Note that the function  $\tau$  defined in (44) is not of class  $C^1$ . However, in order to prove that the proposed minimization algorithm has a superlinear order of convergence, we can approximate  $\tau$  with the next function  $\bar{\tau}$ , which is of class  $LC^3$  on  $\mathbb{R}^{n^2}$ , whose elements are given by

$$(\bar{\tau}(s))_i = \begin{cases} 0, & \text{if } s_i \leq 0, \\ p_7(s_i), & \text{if } 0 < s_i \leq 1, \\ s_i, & \text{if } 1 < s_i \leq m_R - 1, \\ q_7(s_i), & \text{if } m_R - 1 < s_i \leq m_R \\ m_R, & \text{if } s_i > m_R, \end{cases} \quad i = 1, \dots, n^2, \tag{45}$$

where

$$\begin{aligned}p_7(x) &= -10x^7 + 36x^6 - 45x^5 + 20x^4, \\ q_7(x) &= m - p_7(m - x), \quad x \in \mathbb{R}.\end{aligned}\tag{46}$$

In order to obtain (46), we consider a generic polynomial  $p_7 = \sum_{i=0}^7 c_i x^i$ , posed

$$\begin{aligned} 0 &= p_7(0) = p'_7(0) = p''_7(0) = p'''_7(0) = p''_7(1) = p'''_7(1), \\ 1 &= p_7(1) = p'_7(1), \end{aligned}$$

and obtain  $c_i = 0$  for all  $i = 0, 1, 2, 3$ ,  $c_4 = 20$ ,  $c_5 = -45$ ,  $c_6 = 36$  and  $c_7 = -10$ , by solving the system

$$\begin{cases} c_4 + c_5 + c_6 + c_7 &= 1 \\ 4c_4 + 5c_5 + 6c_6 + 7c_7 &= 1 \\ 12c_4 + 20c_5 + 30c_6 + 42c_7 &= 0 \\ 24c_4 + 60c_5 + 120c_6 + 210c_7 &= 0 \end{cases}.$$

The polynomial  $q_7$  is obtained by requiring that its graph is obtained from that of the polynomial  $p_7$  by means of a rotation with respect to the point  $(m_R/2, m_R/2)$ .

By this transformation, the projections of the estimated source images  $\tau(\tilde{s}_{rR,\iota}^{(l)}(\theta))$  and  $\tau(\tilde{s}_{vR,\iota}^{(l)}(\theta))$  turn to be nonnegative (see also [11, 13, 22, 43, 45]). From now on, we refer to the above projections as the new considered source estimates. Thus, the estimated source overlapping level is a nonnegative value, and it is zero if and only if there is no overlapping text from the recto to the verso of the estimated source document. Then we choose the values of  $\theta$  and  $\iota$  which allow to estimate source images with the smallest source overlapping level. Hence, among the possible values of  $\theta$  and  $\iota$ , we choose a couple  $(\theta^{(l+1)}, \iota^{(l+1)})$  which is a minimum of the following *objective function*:

$$f^{(l)}(\theta, \iota, C_R) = (\tau(\tilde{s}_{rR,\iota}^{(l)}(\theta)))^T \cdot \tau(\tilde{s}_{vR,\iota}^{(l)}(\theta)). \quad (47)$$

Note that the index  $l$  indicates that the objective function  $f^{(l)}(\theta, \iota, C_R)$  depends on the previous estimated source overlapping level  $k_R^{(l)}$ . Thus, we can write the objective function also as

$$g(k_R^{(l)}, \theta, \iota, C_R) = f^{(l)}(\theta, \iota, C_R). \quad (48)$$

Now we pose

$$k_R^{(l+1)} = f^{(l)}(\theta^{(l+1)}, \iota^{(l+1)}, C_R)$$

and we iterate this process until a fix point is reached, that is when we find an index  $l$  with  $k_R^{(l+1)} = k_R^{(l)}$ . We see that, when we reach a fixed point  $k_R^{(l+1)} = k_R^{(l)}$ , then in all our experimental cases we get  $\tau(\tilde{s}_{rR,\iota}^{(l)}(\theta)) = \tilde{s}_{rR,\iota}^{(l)}(\theta)$  and  $\tau(\tilde{s}_{vR,\iota}^{(l)}(\theta)) = \tilde{s}_{vR,\iota}^{(l)}(\theta)$ . Thus,  $\tilde{s}_{rR,\iota}^{(l)}(\theta)$  and  $\tilde{s}_{vR,\iota}^{(l)}(\theta)$  are nonnegative matrices, and assuming that the positive pixels of the recto of the estimated document are not a subset of the positive pixels of the estimated verso, or vice versa, we have that the estimated mixing matrix  $\tilde{A}_{R,\iota}^{(l)}(\theta)$  is nonnegative. So, since  $\tilde{A}_{R,\iota}^{(l)}(\theta)$  satisfies (4), then  $\tilde{A}_{R,\iota}^{(l)}(\theta)$  is a stochastic matrix, as we required. Moreover, we have that  $\tilde{A}_{R,\iota}^{(l)}(\theta) \cdot \tilde{s}_{R,\iota}^{(l)}(\theta)^T$ , with  $\tilde{A}_{R,\iota}^{(l)}(\theta) \in \mathbb{R}_{+}^{2 \times 2}$  and  $\tilde{s}_{R,\iota}^{(l)}(\theta)^T \in \mathbb{R}_{+}^{2 \times n^2}$ , is a nonnegative factorization of the matrix  $x^T \in \mathbb{R}_{+}^{2 \times n^2}$  (see also [13, 22, 43, 45]).

The algorithm related to our method for the red component in the case  $\det C_R \neq 0$  is the following.

```

function MATODS( $x_R$ )
 $C_R = x_R^T x_R;$ 
 $k_R^{(-1)} = -2\varepsilon;$ 
 $k_R^{(0)} = 0;$ 
 $l = 0;$ 
while ( $|k_R^{(l)} - k_R^{(l-1)}| \geq \varepsilon$ ) do
     $[\theta^{(l+1)}, \iota^{(l+1)}] = \text{argmin} (\text{function } g(k_R^{(l)}, \cdot, \cdot, C_R));$ 
     $k_R^{(l+1)} = g(k_R^{(l)}, \theta^{(l+1)}, \iota^{(l+1)}, C_R);$ 
     $l = l + 1;$ 
end while
 $Z_{R,\iota^{(l)}}(\theta^{(l)}) = C_R^{1/2} Q_{\iota^{(l)}}(\theta^{(l)});$ 
compute  $\tilde{s}_{rR,\iota^{(l)}}(\theta^{(l)})$  and  $\tilde{s}_{vR,\iota^{(l)}}(\theta^{(l)})$  as in (43);
return  $\tilde{s}_{R,\iota^{(l)}}(\theta^{(l)})$ 

```

where  $\varepsilon$  is a fixed positive real number, which is a suitable tolerance threshold, while the function  $g(\cdot, \cdot, \cdot, \cdot)$  is computed as follows.

```

function  $g(k, \theta, \iota, C_R)$ 
 $Z_{R,\iota}(\theta) = C_R^{1/2} Q_{\iota}(\theta);$ 
compute  $\tilde{s}_{rR,\iota}(\theta)$  and  $\tilde{s}_{vR,\iota}(\theta)$  as in (43);
return  $(\tau(\tilde{s}_{rR,\iota}(\theta)))^T \cdot \tau(\tilde{s}_{vR,\iota}(\theta))$ 

```

In the next section we present the procedure we use in order to minimizes the objective function  $g(k_R^{(l)}, \cdot, \cdot, C_R)$ . An analogous algorithm is proposed also for restoring the green and blue components. We refer to this method as the *Minimum Amount of Text Overlapping in Document Separation* (MATODS) algorithm, which is a parameter free procedure, that makes it an unsupervised technique.

## 4 The objective function minimization algorithms

In this section we study the problem of finding the minimum of the objective function  $g(k, \cdot, \iota, C)$  (see equations (47) and (48)), for  $\iota \in \{1, -1\}$  and for a positive definite matrix  $C \in \mathbb{R}^{2 \times 2}$ . We minimize the functions  $g(k, \cdot, 1, C)$  and  $g(k, \cdot, -1, C)$ , and pose  $\iota^{(l)} = 1$  if  $\min_{\theta \in [0, 2\pi]} g(k, \cdot, 1, C) \leq \min_{\theta \in [0, 2\pi]} g(k, \cdot, -1, C)$ , and  $\iota^{(l)} = -1$  otherwise. We start by analyzing a stochastic technique that assure the convergence to the minimum in probability.

### 4.1 The simulated annealing

The simulated annealing techniques have the aim to define a sequence, which converges to the global minimum of a function, not necessarily convex (see also [21]). However, since it is dealt with an asymptotic behaviour, in general it is not possible to assure the convergence to the minimum after a finite number of steps.

To apply the annealing technique, for each temperature  $T_h$ , where  $h \in \mathbb{N}$  is fixed and

$\lim_{h \rightarrow +\infty} T_h = 0$ , we use the Metropolis Sampler, in order to update the variable  $\theta$  (see also [44, 58]). For each fixed  $h \in \mathbb{N}$ , a sequence  $\theta_j^{(h)}$ ,  $j = 0, \dots, L_h$  of estimates of  $\theta$  is constructed. Given  $\theta_j^{(h)}$ , at the step  $j+1$  the proposed  $\theta_{j+1}^{(h)}$  is given by  $\theta_j^{(h)} + \nu$ , where  $\nu$  is a random variable, having uniform distribution in the interval  $(-\delta, \delta)$ , with given  $\delta \in \mathbb{R}^+$ . Hence at the step  $j+1$ , as a new estimate of  $\theta$  we choose either  $\theta_j^{(h)}$  or  $\theta_{j+1}^{(h)}$ . Let  $\Delta g = g(k, \theta_j^{(h)}, \iota, C) - g(k, \theta_{j+1}^{(h)}, \iota, C)$ . We accept  $\theta_{j+1}^{(h)}$  when  $\Delta g > 0$  or with probability  $e^{\frac{\Delta g}{T_h}}$  when  $\Delta g \leq 0$ . By iterating, for every  $h \in \mathbb{N}$  it is possible to construct a Markov chain  $\theta_j^{(h)}$ ,  $j = 0, 1, 2, \dots$ , convergent in  $L^2$  and in probability to an equilibrium state having probability

$$\pi^{(h)}(\theta) = \frac{e^{-\frac{g(k, \theta, \iota, C)}{T_h}}}{\int_0^{2\pi} e^{-\frac{g(k, \theta, \iota, C)}{T_h}} d\theta},$$

fixed  $k$ ,  $\iota$  and  $C$ , where the involved integral is intended in the discrete sense (see also [58, Theorem 8.2.2 (a)]). As  $h$  tends to  $+\infty$ , if

$$T_h \geq \frac{\Delta}{\ln h}, \quad (49)$$

where  $\Delta$  denotes the *maximal local increase* of  $g(k, \cdot, \iota, C)$  (see also [58]), then the stationary probability distribution of the Markov chain converges in probability to the set of the global minima of  $g(k, \cdot, \iota, C)$  (see also [58, Theorem 8.2.3]).

In the practical cases, it is impossible to obtain asymptotic results, and furthermore the assumption (49) it is not advisable in terms of computational times, and thus one has to establish: an initial value of the temperature  $T_0$ ; the number of steps of the Metropolis technique, that is the length  $L_h$  of the involved Markov chain; a suitable function which expresses the decay of the temperature; a stop criterion.

The initial temperature  $T_0$  must be sufficiently high, in order to accept the variations of configurations with high probability. In correspondence with the temperature  $T_0$ , let  $\chi(T_0) = A(T_0)/P(T_0)$ , where  $A(T_0)$  and  $P(T_0)$  are the numbers of the accepted and proposed transitions, respectively, at the temperature  $T_0$ . Successively, we impose  $\chi(T_0) \simeq 1$ . Let  $n_1$  (resp.  $n_2$ ) the number of the decreasing (resp. increasing) transitions in correspondence with the temperature  $T_0$ . Observe that  $n_1 + n_2 = L_0$ , where  $L_0$  is the length of the Markov chain associated with the temperature  $T_0$ . Let us denote by  $\langle \Delta g \rangle^+$  the mean value of  $\Delta g$  associated with the transition which increases the energy. We assume the following approximation:

$$\chi(T_0) = \frac{n_1 + n_2 e^{-\frac{\langle \Delta g \rangle^+}{T_0}}}{n_1 + n_2},$$

obtaining

$$T_0 = \frac{\langle \Delta g \rangle^+}{\ln \left( \frac{n_2}{n_2 \chi(T_0) - n_1 (1 - \chi(T_0))} \right)}. \quad (50)$$

In order to estimate  $T_0$  by means of (50), we can compute experimentally  $n_1$ ,  $n_2$  and  $\langle \Delta g \rangle^+$ , where  $\chi(T_0)$  is a suitable positive constant close to 1.

As mentioned before, to obtain convergence of the global minimum of the function  $g(k, \cdot, \iota, C)$ , it is necessary to have a logarithmic decay of the temperature. Anyway, to get good results, it is possible to suppose to have a linear decay, namely  $T_{h+1} = \gamma T_h$ , where  $\gamma$  is a suitable real constant, which in general is taken between 0.95 and 0.99 (see also [1, 58]). At the last step, we establish that the stop criterion is as follows: when the values of the estimated  $\theta$  remain constant after a complete Markov chain, then we stop.

The simulated annealing algorithm can be expressed as follows:

```

function SA( $k, \iota, C$ )
 $h = 0;$ 
 $\theta_1^{(0)} = 0;$ 
 $\theta_1^{(-1)} = \theta_1^{(0)} + 2\varepsilon;$ 
while ( $|\theta_1^{(h)} - \theta_1^{(h-1)}| > \varepsilon$ ) do
    for  $j=1$  to  $L_h - 1$  do
         $\theta_{j+1}^{(h)} = \theta_j^{(h)} + random(-\delta, \delta);$ 
         $\Delta g = g(k, \theta_j^{(h)}, \iota, C) - g(k, \theta_{j+1}^{(h)}, \iota, C);$ 
        if (( $\Delta g \leq 0$ ) and ( $random(0, 1) > e^{\frac{\Delta g}{T_k}}$ )) then
             $\theta_{j+1}^{(h)} = \theta_j^{(h)};$ 
        end if
    end for
     $\theta_1^{(h+1)} = \theta_{L_h}^{(h)};$ 
     $T_{h+1} = \gamma T_h;$ 
     $h = h + 1;$ 
end while
return  $\theta_1^{(h)}$ 

```

where  $\varepsilon$  is a suitable tolerance threshold. We refer to this algorithm as *Simulated Annealing* (SA).

## 4.2 Local quasi-convexity of the objective function

Here we analyze experimentally the trend of the objective function  $g(k, \cdot, \iota, C)$  (see equations (47) and (48)) to be minimized, for fixed  $k \geq 0$ ,  $\iota \in \{1, -1\}$  and  $C \in \mathbb{R}^{2 \times 2}$  definite positive matrix. First, we observe that  $g(k, \cdot, \iota, C)$  is a periodic function with period  $\pi$ . Indeed, from (18) we have  $Q_\iota(\theta + \pi) = -Q_\iota(\theta)$ ,  $\iota \in \{1, -1\}$ . Then, from (19) we get  $Z_{R,\iota}(\theta + \pi) = -Z_{R,\iota}(\theta)$ ,  $\iota \in \{1, -1\}$ . Finally, from (43), we obtain that the equation related to the estimated sources  $\tilde{s}_{R,\iota}^{(l)}(\theta + \pi) = \tilde{s}_{R,\iota}^{(l)}(\theta)$  holds for  $\iota \in \{1, -1\}$  and for every positive definite matrix  $C_R \in \mathbb{R}^{2 \times 2}$ . In Figures 4–9 we present some examples of graphs of the function  $g(k, \cdot, \iota, C)$ . In order to obtain such graphs, we take the following mixing matrices

$$A_R = \begin{pmatrix} 0.6 & 0.4 \\ 0.4 & 0.6 \end{pmatrix}, A_G = \begin{pmatrix} 0.6 & 0.4 \\ 0.4 & 0.6 \end{pmatrix}, A_B = \begin{pmatrix} 0.6 & 0.4 \\ 0.4 & 0.6 \end{pmatrix},$$

and consider as original sources the images in Figures 12–15. Then, by (3) we construct the observed data and the related overlapping matrix  $C_R$ ,  $C_G$ , and  $C_B$ . Recalling that

the value of  $k$  is estimated independently on each of the three channels, we saw experimentally that, during the execution of the MATODS algorithm, the value of  $k$  is always increasing, as it is shown in Figure 3.

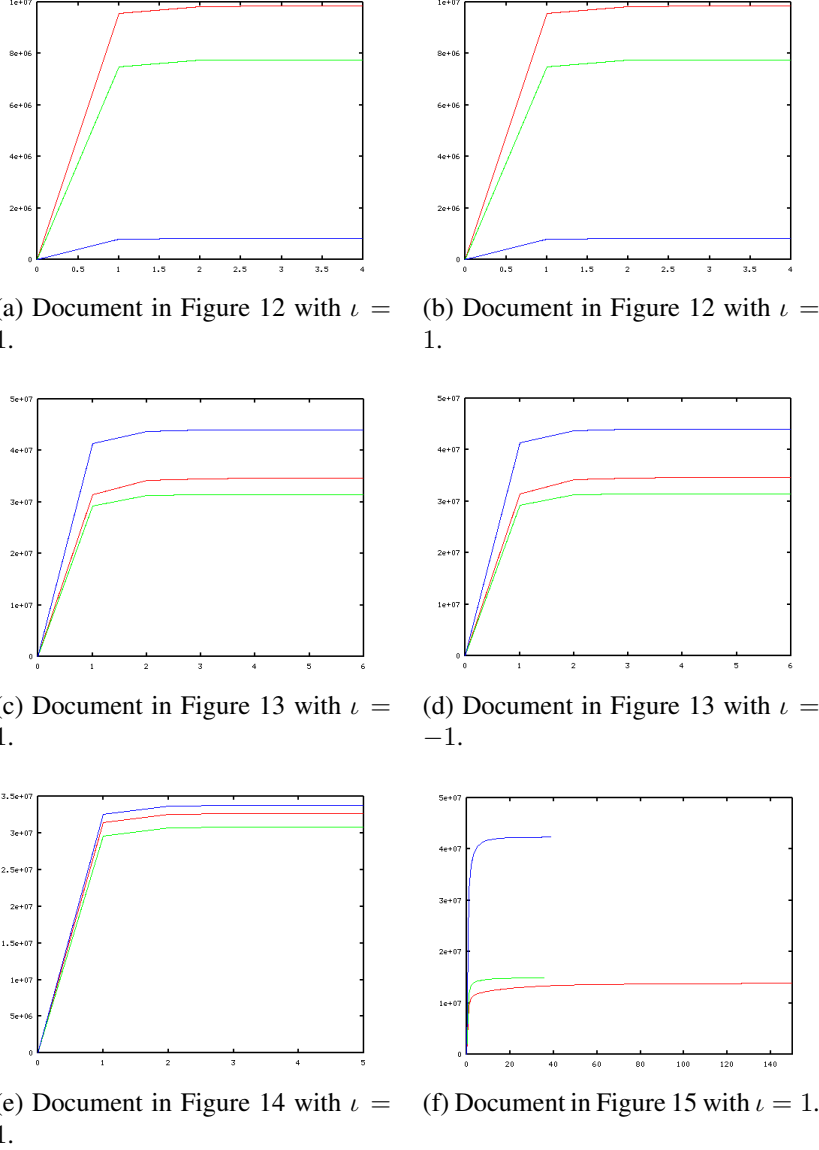


Figure 3: Trend of  $k_R^{(l)}$ ,  $k_G^{(l)}$  and  $k_B^{(l)}$  during the execution of MATODS

In Figure 4, we deal with the document in Figure 12 where  $\iota = 1$  is fixed. We recall that, in order to assume that the system (26) is well-defined, we have to impose that (see (38))

$$k \geq \frac{\det(C_R)}{(\bar{c}_{11}^R - \bar{c}_{21}^R)^2 + (\bar{c}_{12}^R - \bar{c}_{22}^R)^2} = k_{sup}^R,$$

$$k \geq \frac{\det(C_G)}{(\bar{c}_{11}^G - \bar{c}_{21}^G)^2 + (\bar{c}_{12}^G - \bar{c}_{22}^G)^2} = k_{sup}^G,$$

$$k \geq \frac{\det(C_B)}{(\bar{c}_{11}^B - \bar{c}_{21}^B)^2 + (\bar{c}_{12}^B - \bar{c}_{22}^B)^2} = k_{sup}^B.$$

In Figure 3 (a) we see that  $k$ , in the three RGB channels, converges monotonically to the source overlapping levels  $k_R$ ,  $k_G$  and  $k_B$ , respectively. In this case, we have  $k_R = 9855291 < k_{sup}^R = 132751132.62$ ,  $k_G = 7753236 < k_{sup}^G = 105650226.17$ ,  $k_B = 834224 < k_{sup}^B = 11122735.89$ . Indeed, the values source overlapping level upper bounds  $k_{sup}^R$ ,  $k_{sup}^G$  and  $k_{sup}^B$  are much closer to data overlapping levels  $d_R = 139503525.96$ ,  $d_G = 108090739.20$ ,  $d_B = 11444930.24$ . Since the source overlapping levels are in general much smaller than the respective data overlapping levels, we can assume that, during the execution of the MATODS algorithm in the three channels, the value of  $k$  is always smaller than  $k_{sup}^R$ ,  $k_{sup}^G$  or  $k_{sup}^B$ , respectively.

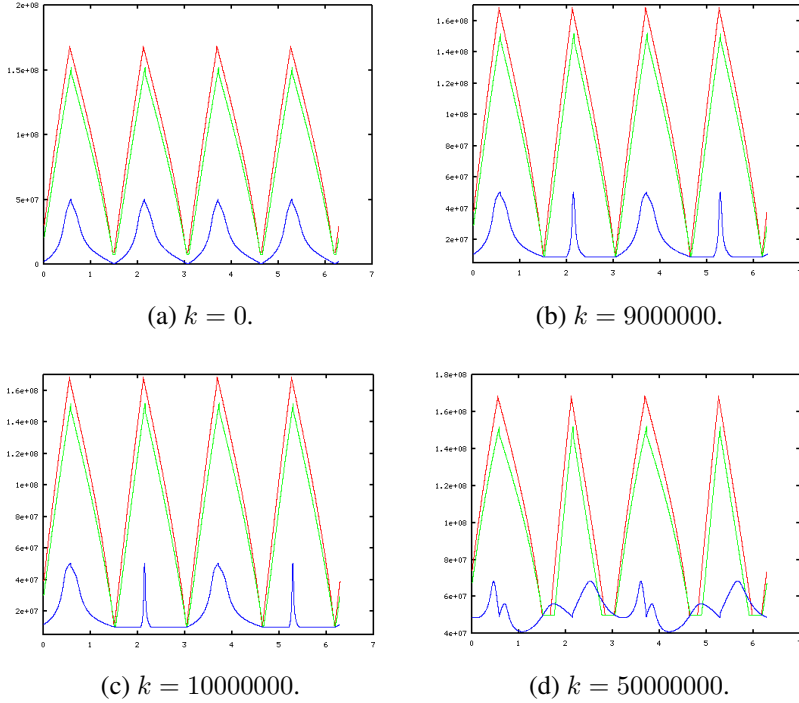


Figure 4: Graphs of the objective functions  $g(k, \cdot, 1, C_R)$ ,  $g(k, \cdot, 1, C_G)$  and  $g(k, \cdot, 1, C_B)$  in correspondence with the document in Figure 12.

In Figure 4 the values of  $k$  are the following:  $k = 0$ , that is the MATODS source overlapping level initial value for all three channels;  $k = 9000000$ , which is near to the red ideal source overlapping level  $k_R$ ;  $k = 10000000$ , which is close but smaller than the green source overlapping level upper bound  $k_{sup}^G$ ;  $k = 50000000$ , which is greater than all source overlapping level upper bounds.

We observe that, in this case, the points of discontinuity of the objective functions  $g(k, \cdot, 1, C_R)$ ,  $g(k, \cdot, 1, C_G)$  and  $g(k, \cdot, 1, C_B)$ , for all  $k$  smaller than their source overlapping level upper bounds, are  $\varphi_R^{(1)} = 0.53873315$ ,  $\varphi_R^{(2)} = 3.68032580$ ,  $\varphi_R^{(5)} = 5.25112213$  and  $\varphi_R^{(6)} = 2.10952948$ , for the red channel,  $\varphi_G^{(1)} = 0.57955014$ ,  $\varphi_G^{(2)} = 3.72114279$ ,  $\varphi_G^{(5)} = 5.29193912$  and  $\varphi_G^{(6)} = 2.15034646$ , for the green channel,  $\varphi_B^{(1)} = 0.57021981$ ,  $\varphi_B^{(2)} = 3.71181247$ ,  $\varphi_B^{(5)} = 5.28260880$  and  $\varphi_B^{(6)} = 2.14101614$ , for the blue channel

(see also equations (39) and (41)). In Figures 4 we note that, when  $k$  is smaller than the source overlapping level upper bounds then for all three channels the objective functions  $g(k, \cdot, 1, C_R)$ ,  $g(k, \cdot, 1, C_G)$  and  $g(k, \cdot, 1, C_B)$  turn to be quasi-convex in the intervals included between any two successive points of discontinuity. We recall that a function  $f : [a, b] \rightarrow \mathbb{R}$  is *quasi-convex* iff

$$f((1 - \alpha)\theta_1 + \alpha\theta_2) \leq \max\{f(\theta_1), f(\theta_2)\},$$

for each  $\alpha \in [0, 1]$  and  $\theta_1, \theta_2 \in [a, b]$  with  $\theta_1 \neq \theta_2$ . A function  $f : [a, b] \subset \mathbb{R} \rightarrow \mathbb{R}$  is said to be *weakly unimodal* iff there exists a value  $\widehat{\theta}$ , for which it is weakly monotonically increasing for  $\theta \in [a, \widehat{\theta}]$  and weakly monotonically decreasing for  $\theta \in [\widehat{\theta}, b]$ . A function  $f : [a, b] \subset \mathbb{R} \rightarrow \mathbb{R}$  is *quasi-convex* in the convex and compact set  $[a, b] \subset S$  iff it is weakly unimodal. When  $f : S \subset \mathbb{R}^n \rightarrow \mathbb{R}$ , similar definitions can be done. In this case quasi-convex functions are weakly unimodal functions, but not all the weakly unimodal functions are quasi-convex (see also [4, 35]).

Concerning Figure 5, we consider again the document in Figure 12, choose  $\iota = -1$  and take the same values of  $k$ . In this case, the values of the points of discontinuity of the objective functions  $g(k, \cdot, -1, C_R)$ ,  $g(k, \cdot, -1, C_G)$  and  $g(k, \cdot, -1, C_B)$  are given by  $\varphi_R^{(3)} = 1.03206318$ ,  $\varphi_R^{(4)} = 4.17365583$ ,  $\varphi_R^{(7)} = 5.74445216$  and  $\varphi_R^{(8)} = 2.60285950$  for the red channel,  $\varphi_G^{(3)} = 0.99124619$ ,  $\varphi_G^{(4)} = 4.13283884$ ,  $\varphi_G^{(7)} = 5.70363517$  and  $\varphi_G^{(8)} = 2.56204252$  for the green channel,  $\varphi_B^{(3)} = 1.00057651$ ,  $\varphi_B^{(4)} = 4.14216917$ ,  $\varphi_B^{(7)} = 5.71296549$  and  $\varphi_B^{(8)} = 2.57137284$  for the blue channel (see also equations (40) and (42)). Such values are the unique ones which differ from those of the previous case. In Figure 5 we note that, when  $k$  is smaller than the upper bounds, the objective functions  $g(k, \cdot, -1, C_R)$ ,  $g(k, \cdot, -1, C_G)$  and  $g(k, \cdot, -1, C_B)$  are quasi-convex on each interval which lies between any two successive points of discontinuity.

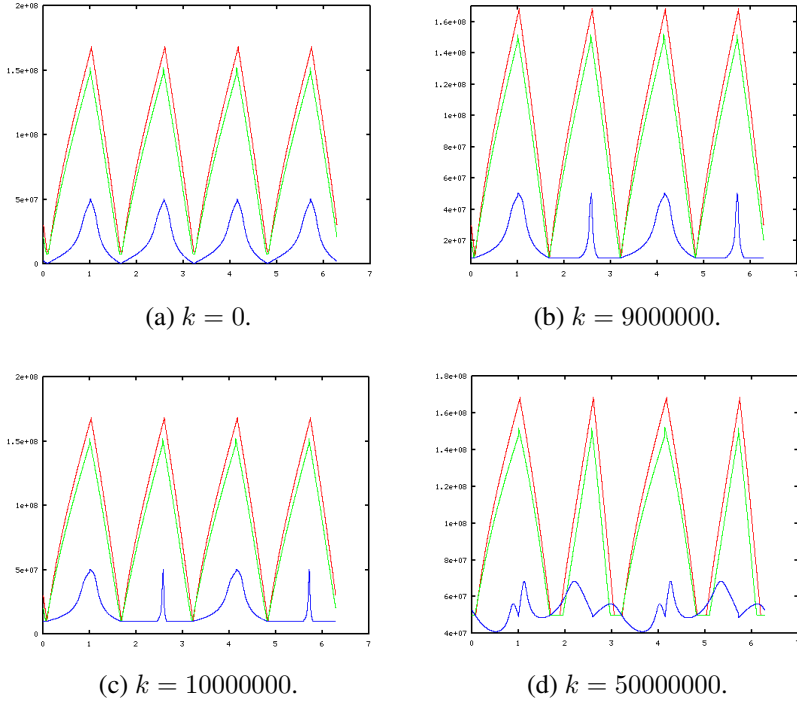


Figure 5: Graphs of the objective functions  $g(k, \cdot, -1, C_R)$ ,  $g(k, \cdot, -1, C_G)$  and  $g(k, \cdot, -1, C_B)$  in correspondence with the document in Figure 12.

In Figure 6, we take the document in Figure 13 and choose  $\iota = 1$ . Also in this case, it is  $k_R = 34612679 < k_{sup}^R = 131593024.23 < d_R = 136166103.08$ ,  $k_G = 31495751 < k_{sup}^G = 130553408.73 < d_G = 141445576.28$ ,  $k_B = 44013514 < k_{sup}^B = 157271106.68 < d_B = 172518952.96$ . The discontinuity of the objective functions  $g(k, \cdot, 1, C_R)$ ,  $g(k, \cdot, 1, C_G)$  and  $g(k, \cdot, 1, C_B)$  are given by  $\varphi_R^{(1)} = 0.56948411$ ,  $\varphi_R^{(2)} = 3.71107676$ ,  $\varphi_R^{(5)} = 5.28187309$  and  $\varphi_R^{(6)} = 2.14028043$  for the red channel,  $\varphi_G^{(1)} = 0.50318323$ ,  $\varphi_G^{(2)} = 3.64477588$ ,  $\varphi_G^{(5)} = 5.215572207$  and  $\varphi_G^{(6)} = 2.07397955$ , for the green channel, and  $\varphi_B^{(1)} = 0.48885097$ ,  $\varphi_B^{(2)} = 3.63044362$ ,  $\varphi_B^{(5)} = 5.20123995$  and  $\varphi_B^{(6)} = 2.05964730$  for the blue channel. We choose  $k = 0$ , because it is the MATODS initial estimate,  $k = 40000000$ , since it is near to all ideal source overlapping levels,  $k = 100000000$ , as it is close, but inferior, to all source overlapping level upper bounds, and  $k = 200000000$ , because it is beyond these upper bounds. In Figure 6 we note that, when  $k$  is smaller than its source overlapping level upper bound, the objective functions  $g(k, \cdot, 1, C_R)$ ,  $g(k, \cdot, 1, C_G)$  and  $g(k, \cdot, 1, C_B)$  are quasi-convex on each interval which lies between any two successive points of discontinuity.

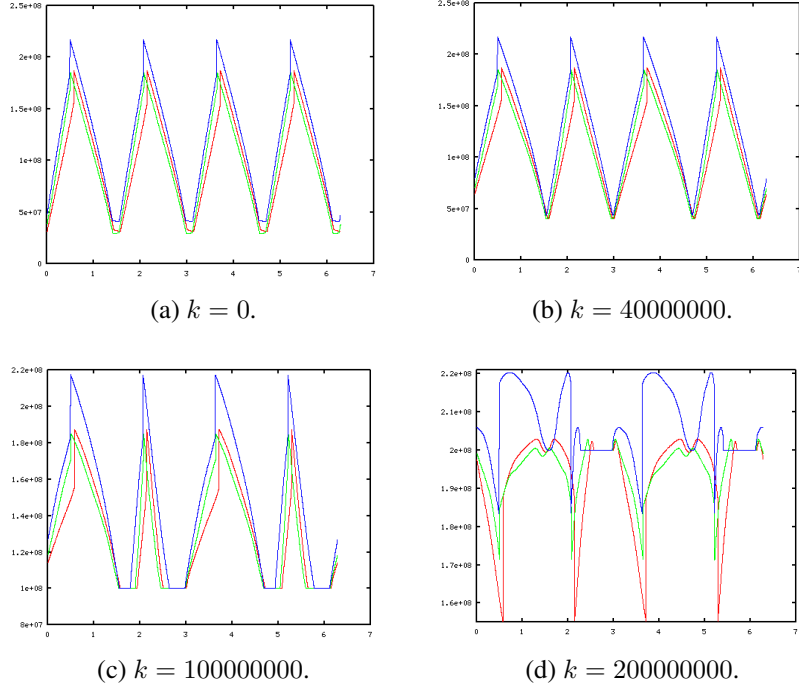


Figure 6: Graphs of the objective functions  $g(k, \cdot, 1, C_R)$ ,  $g(k, \cdot, 1, C_G)$  and  $g(k, \cdot, 1, C_B)$  in correspondence with the document in Figure 13.

In Figure 7, we consider the document in Figure 13 again, but we take  $\iota = -1$  and use the same values of  $k$ . In this case, the values of the points of discontinuity of the objective functions  $g(k, \cdot, -1, C_R)$ ,  $g(k, \cdot, -1, C_G)$  and  $g(k, \cdot, -1, C_B)$  are given by  $\varphi_R^{(3)} = 1.00131222$ ,  $\varphi_R^{(4)} = 4.14290487$ ,  $\varphi_R^{(7)} = 5.71370120$  and  $\varphi_R^{(8)} = 2.57210855$ , for the red channel,  $\varphi_G^{(3)} = 1.06761310$ ,  $\varphi_G^{(4)} = 4.20920575$ ,  $\varphi_G^{(7)} = 5.78000208$  and  $\varphi_G^{(8)} = 2.63840943$  for the green channel,  $\varphi_B^{(3)} = 1.08194536$ ,  $\varphi_B^{(4)} = 4.22353801$ ,  $\varphi_B^{(7)} = 5.79433434$  and  $\varphi_B^{(8)} = 2.65274169$ , for the blue channel. Note that, in Figure 7, when  $k$  is smaller than its upper bound, for all three channels the objective functions  $g(k, \cdot, -1, C_R)$ ,  $g(k, \cdot, -1, C_G)$  and  $g(k, \cdot, -1, C_B)$  are quasi-convex on each interval which lies between any two successive points of discontinuity.

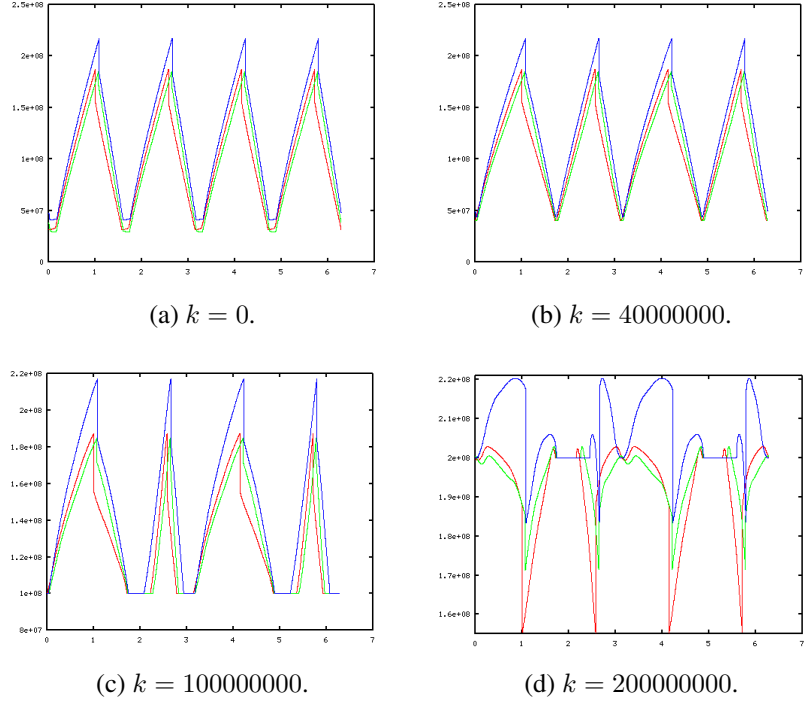


Figure 7: Graphs of the objective functions  $g(k, \cdot, -1, C_R)$ ,  $g(k, \cdot, -1, C_G)$  and  $g(k, \cdot, -1, C_B)$  in correspondence with the document in Figure 13.

From now on, since the graphs obtained with  $\iota = 1$  and  $\iota = -1$  are very similar, we consider only the case  $\iota = 1$ . Concerning the graphs in Figure 8, we take the document in Figure 14. In this case we have the inequalities  $k_R = 32685410 < d_R = 72365832.56 < k_{sup}^R = 73936335.04$ ,  $k_G = 30815153 < d_G = 68222469.08 < k_{sup}^G = 69702847.74$ ,  $k_B = 33805612 < d_B = 74981471.44 < k_{sup}^B = 76611523.60$ . The discontinuity of the objective functions  $g(k, \cdot, 1, C_R)$ ,  $g(k, \cdot, 1, C_G)$  and  $g(k, \cdot, 1, C_B)$  are  $\varphi_R^{(1)} = 0.81450982$ ,  $\varphi_R^{(2)} = 3.95610247$ ,  $\varphi_R^{(5)} = 5.52689880$  and  $\varphi_R^{(6)} = 2.38530615$ , for the red channel,  $\varphi_G^{(1)} = 0.81453870$ ,  $\varphi_G^{(2)} = 3.95613135$ ,  $\varphi_G^{(5)} = 5.52692768$  and  $\varphi_G^{(6)} = 2.38533503$ , for the green channel,  $\varphi_B^{(1)} = 0.81446681$ ,  $\varphi_B^{(2)} = 3.95605946$ ,  $\varphi_B^{(5)} = 5.52685579$  and  $\varphi_B^{(6)} = 2.38526314$ , for the blue channel. Here, we choose  $k = 0$ , that is the initial value,  $k = 30000000$  which is close to all ideal solutions,  $k = 65000000$  which is inferior but near to all upper bounds and  $k = 90000000$  which is higher than all upper bounds. Finally in Figure 8, when  $k$  is smaller than its upper bound, the objective functions  $g(k, \cdot, 1, C_R)$ ,  $g(k, \cdot, 1, C_G)$  and  $g(k, \cdot, 1, C_B)$  are quasi-convex on each interval which lies between any two successive points of discontinuity.

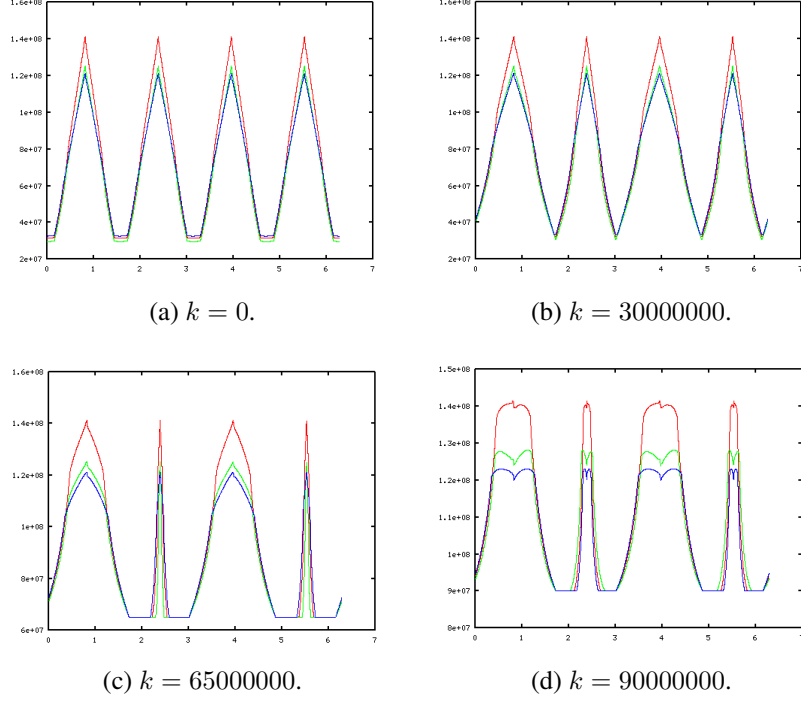


Figure 8: Graphs of the objective functions  $g(k, \cdot, 1, C_R)$ ,  $g(k, \cdot, 1, C_G)$  and  $g(k, \cdot, 1, C_B)$  in correspondence with the document in Figure 14.

The Figure 9 is obtained by considering the document in Figure 15. Here we get  $k_R = 15812614 < k_{sup}^R = 44683913.34 < d_R = 79303165.36$ ,  $k_G = 14928144 < k_{sup}^G = 64082928.34 < d_G = 65712248.40$ ,  $k_B = 78431743 < d_B = 144848191.56 < k_{sup}^B = 147729606.55$ . Thus, we choose to show the graphs for  $k = 0$ ,  $k = 15000000$ ,  $k = 40000000$  and  $k = 70000000$ . The points of discontinuity of the objective functions  $g(k, \cdot, 1, C_R)$ ,  $g(k, \cdot, 1, C_G)$  and  $g(k, \cdot, 1, C_B)$  are  $\varphi_R^{(1)} = 1.41814710$ ,  $\varphi_R^{(2)} = 4.55973976$ ,  $\varphi_R^{(5)} = 6.13053609$  and  $\varphi_R^{(6)} = 2.98894343$  for the red channel,  $\varphi_G^{(1)} = 0.98719285$ ,  $\varphi_G^{(2)} = 4.12878550$ ,  $\varphi_G^{(5)} = 5.69958183$  and  $\varphi_G^{(6)} = 2.55798917$  for the green channel,  $\varphi_B^{(1)} = 0.85077026$ ,  $\varphi_B^{(2)} = 3.99236291$ ,  $\varphi_B^{(5)} = 5.56315924$  and  $\varphi_B^{(6)} = 2.42156658$  for the blue channel. In Figure 9 we note again that, when  $k$  is smaller than its upper bound, for all three channels the objective functions are quasi-convex on every interval which lies between any two successive points of discontinuity.

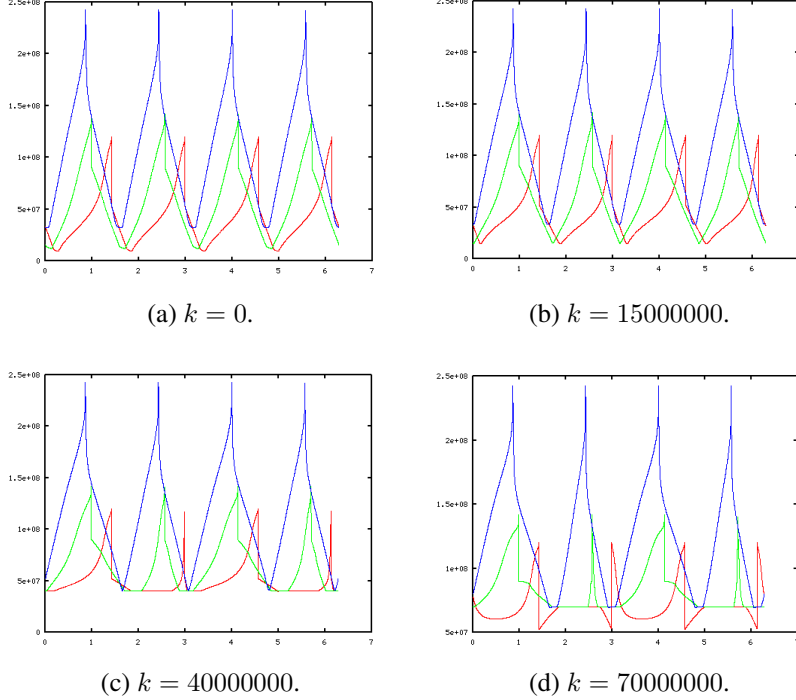


Figure 9: Graphs of the objective functions  $g(k, \cdot, 1, C_R)$ ,  $g(k, \cdot, 1, C_G)$  and  $g(k, \cdot, 1, C_B)$  in correspondence with the document in Figure 15.

Thus, for all graphs in Figures 4–9, when  $k$  is smaller than its upper bound (which is always true during the execution of the MATODS algorithm) the objective functions  $g(k, \cdot, \iota, C_R)$ ,  $g(k, \cdot, \iota, C_G)$  and  $g(k, \cdot, \iota, C_B)$  are quasi-convex on each interval which lies between any two successive points of discontinuity. Moreover the values of the local minima, on each interval where an objective function is quasi-convex, are almost identical. Thus, to find the minimum of an objective function, it is sufficient to minimize it in an interval which lies between any two successive points of discontinuity, where the involved function is quasi-convex. In our experiments similar results were obtained also by choosing any mixing matrix different from those chosen in (67).

In the sequel we give some different algorithms, which can be used to find the minimum in an interval in which the involved function is quasi-convex. Successively, we compare the obtained results, to establish the algorithm to use. In order to compare the convergence speed of such algorithms, we recall that the sequence  $\{\theta^{(h)}\}_h$  converges to  $\hat{\theta}$  with *strong order*  $p$  and *asymptotic costant*  $\gamma > 0$  if and only if

$$\lim_{h \rightarrow +\infty} \frac{|\theta^{(h+1)} - \hat{\theta}|}{|\theta^{(h)} - \hat{\theta}|^p} = \gamma.$$

When  $p = 1$ , the asymptotic costant  $\gamma$  is also called *convergence factor*. We say that the sequence  $\{\theta^{(h)}\}_h$  converges to  $\hat{\theta}$  with *weak order*  $p$  if and only if

$$\liminf_{h \rightarrow +\infty} (-\ln |\theta^{(h)} - \hat{\theta}|^p)^{1/h} = p.$$

Note that strong convergence implies weak convergence, but in general the converse does not hold.

### 4.3 The three point search

In this section we describe an algorithm to minimize the objective function  $g(k, \cdot, \iota, C)$  in one of the intervals in which it is supposed to be quasi-convex. Given a generic step of length  $p_h$ , we consider the vector

$$\psi^{(h)} = [\theta^{(h)} - p_h \quad \theta^{(h)} \quad \theta^{(h)} + p_h].$$

We now denote the corresponding values of the objective function by

$$\xi^{(h)} = [g(k, \psi_1^{(h)}, \iota, C) \quad g(k, \psi_2^{(h)}, \iota, C) \quad g(k, \psi_3^{(h)}, \iota, C)].$$

Supposed that in the interval  $[a, b]$  the function  $g(k, \cdot, \iota, C)$  is quasi-convex, we apply the following algorithm.

```

function TPS( $k, C_R, a, b$ )
 $h = 0;$ 
 $\psi^{(0)} = [a \quad (a + b)/2 \quad b];$ 
 $\xi^{(0)} = [g(k, \psi_1^{(0)}, \iota, C) \quad g(k, \psi_2^{(0)}, \iota, C) \quad g(k, \psi_3^{(0)}, \iota, C)];$ 
 $p_0 = (b - a)/2;$ 
if ( $\xi_1^{(0)} < \xi_2^{(0)}$ ) then
    while (( $\xi_1^{(0)} < \xi_2^{(0)}$ ) and ( $p_h > \varepsilon$ )) do
         $\psi_3^{(0)} = \psi_2^{(0)};$ 
         $\xi_3^{(0)} = \xi_2^{(0)};$ 
         $\psi_2^{(0)} = (\psi_1^{(0)} + \psi_3^{(0)})/2;$ 
         $\xi_2^{(0)} = g(k, \psi_2^{(0)}, \iota, C);$ 
         $p_0 = p_0/2;$ 
    end while
else
    while (( $\xi_3^{(0)} < \xi_2^{(0)}$ ) and ( $p_h > \varepsilon$ )) do
         $\psi_1^{(0)} = \psi_2^{(0)};$ 
         $\xi_1^{(0)} = \xi_2^{(0)};$ 
         $\psi_2^{(0)} = (\psi_1^{(0)} + \psi_3^{(0)})/2;$ 
         $\xi_2^{(0)} = g(k, \psi_2^{(0)}, \iota, C);$ 
         $p_0 = p_0/2;$ 
    end while
end if
while ( $p_h > \varepsilon$ ) do
    if (( $\xi_2^{(h)} < \xi_1^{(h)}$ ) and ( $\xi_2^{(h)} < \xi_3^{(h)}$ )) then
        if ( $\xi_1^{(h)} < \xi_3^{(h)}$ ) then
             $\psi_3^{(h+1)} = \psi_2^{(h)};$ 
             $\xi_3^{(h+1)} = \xi_2^{(h)};$ 
        else
             $\psi_1^{(h+1)} = \psi_2^{(h)};$ 
             $\xi_1^{(h+1)} = \xi_2^{(h)};$ 
        end if
    end if

```

```

 $\psi_2^{(h+1)} = (\psi_1^{(h+1)} + \psi_3^{(h+1)})/2;$ 
 $\xi_2^{(h+1)} = g(k, \psi_2^{(h+1)}, \iota, C);$ 
 $p_{h+1} = p_h/2;$ 
else
  if ( $\xi_1^{(h)} < \xi_3^{(h)}$ ) then
     $\psi^{(h+1)} = [\psi_1^{(h)} - p_h \quad \psi_1^{(h)} \quad \psi_2^{(h)}];$ 
     $\xi^{(h+1)} = [g(k, \psi_1^{(h+1)}, \iota, C) \quad \xi_1^{(h)} \quad \xi_2^{(h)}];$ 
  else
     $\psi^{(h+1)} = [\psi_2^{(h)} \quad \psi_3^{(h)} \quad \psi_3^{(h)} + p_h];$ 
     $\xi^{(h+1)} = [\xi_2^{(h)} \quad \xi_3^{(h)} \quad g(k, \psi_3^{(h+1)}, \iota, C)];$ 
  end if
   $p_{h+1} = p_h;$ 
end if
 $h = h + 1;$ 
end while
return  $\psi_2^{(h)}$ 

```

where  $\varepsilon$  is a positive real number which indicates a suitable tolerance. Such algorithm is formed by an if block and a while block. The if block is necessary to ensure that the conditions

$$\psi_1^{(0)}, \psi_2^{(0)}, \psi_3^{(0)} \in [a, b], \quad \xi_2^{(0)} \leq \xi_1^{(0)}, \quad \xi_2^{(0)} \leq \xi_3^{(0)} \quad (51)$$

hold. The main while body has three cases. In the first one, the value of the function at the point  $\psi_2^{(h)}$  is less than those evaluated at the other two nodes (see Figure 10 (a)). In this case, the node which assumes the greater value is removed and the intermediate point between the other two nodes is added, halving the size step  $p^{(h)}$  (see Figure 10 (b)). In the second case, the value of the function at the node  $\psi_1^{(h)}$  is greater than or equal to the one at the node  $\psi_2^{(h)}$ , which is greater than or equal to the one at the node  $\psi_3^{(h)}$  (see Figure 10 (c)). In this case we eliminate the node  $\psi_1^{(h)}$  and add a node to the right of  $\psi_3^{(h)}$  with distance  $p^{(h)}$  (see Figure 10 (d)). Analogously, in the third case, the value of the function at the node  $\psi_3^{(h)}$  is greater than or equal to the one at the node  $\psi_2^{(h)}$ , which is greater than or equal to the one at the node  $\psi_1^{(h)}$ . So we delete the node  $\psi_3^{(h)}$  and add a node to the left of  $\psi_1^{(h)}$  with distance  $p^{(h)}$ . Since the function  $g(k; \cdot, \iota, C)$  is quasi-convex, there are no other possible cases.

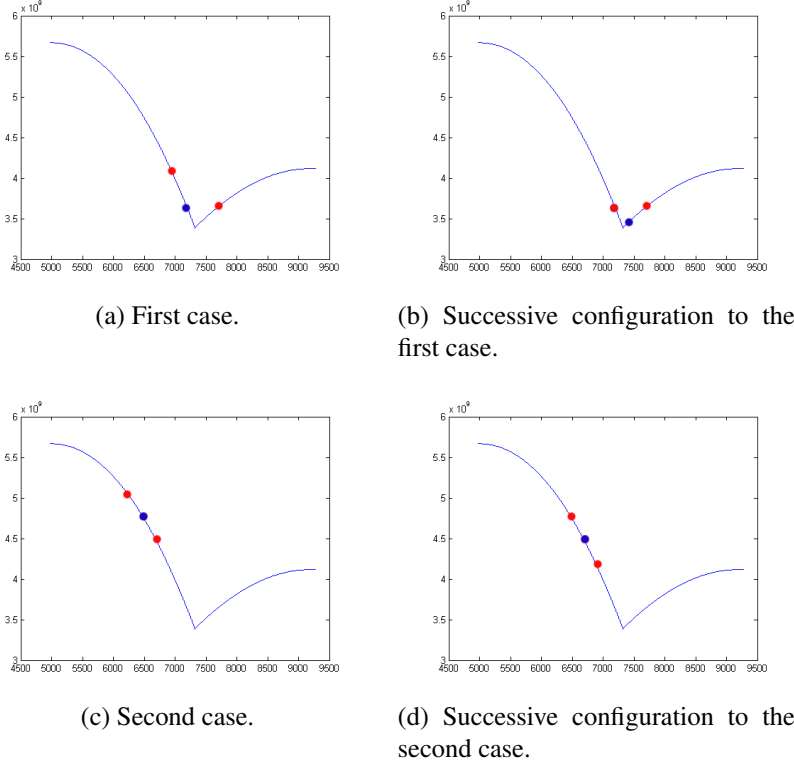


Figure 10: Cases in the body of the while in the TPS algorithm.

Note that at each iteration it is necessary only one evaluation of the function  $g(k, \cdot, \iota, C)$ . Furthermore, observe that in the body of the while, at every step  $h$  at which the algorithm halves the length  $p_h$ , it is

$$\xi_2^{(h)} \leq \xi_1^{(h)}, \quad \xi_2^{(h)} \leq \xi_3^{(h)}. \quad (52)$$

Let  $\hat{\theta}$  be a minimizer of the function  $g(k, \cdot, \iota, C)$ . From (52), since  $g(k, \cdot, \iota, C)$  is quasi-convex, we have

$$\hat{\theta} \in [\xi_1^{(h)}, \xi_2^{(h)}], \quad (53)$$

at every step  $h$  at which the algorithm halves the length of the step. Note that from (51) we deduce that the property (53) holds also for  $h = 0$ . Furthermore, observe that by the conditions (51), the algorithm halves the length of the step when  $h = 0$ .

**Theorem 4.1.** *Suppose that at the step  $h - 1$  the algorithm halves the length of the step  $p_{h-1}$ , then the TPS algorithm halves again the length of the step not later than the step  $h + 2$ . That is*

$$p_{h+3} \leq \frac{1}{2} p_h \quad (54)$$

holds.

*Proof.* We suppose that at the step  $h - 1$  we halve the length of the step so that  $p^{(h)} = p^{(h-1)}/2$ , and we delete, let us say, the node  $\psi_1^{(h-1)}$ . Let  $\hat{\theta}$  be a minimizer of the functions  $g(k, \cdot, \iota, C)$ . Suppose first that  $\psi_2^{(h-1)} = \psi_1^{(h)} \leq \hat{\theta}$ , then we have two cases. The first is when  $\xi_2^{(h)} < \xi_1^{(h)}$ . In this case,  $\xi_2^{(h)}$  is the smallest value of the vector  $\xi^{(h)}$ , and hence the size of the step is halved at the step  $h$ . The second case is when  $\xi_2^{(h)} \geq \xi_1^{(h)}$ . In this case

$\psi_1^{(h-1)} < \psi_1^{(h+1)} < \psi_2^{(h+1)}$ ,  $\xi_1^{(h+1)} < \xi_2^{(h+1)}$  and  $\xi_2^{(h+1)} = \xi_1^{(h)} < \xi_3^{(h+1)} = \xi_2^{(h)}$ , hence the length step is halved at the step  $h + 1$ . Now we assume that  $\psi_2^{(h-1)} = \psi_1^{(h)} > \hat{\theta}$ . Then,  $\xi_1^{(h)} < \xi_2^{(h)} < \xi_3^{(h)}$ . So,  $\psi_1^{(h+1)} = \psi_1^{(h)} - p^{(h)} = \psi_1^{(h-1)} + p^{(h)}$ . If the length step is not halved at the step  $h + 1$ , then  $\xi_1^{(h+2)} = \xi_1^{(h-1)} > \xi_3^{(h+2)} = \xi_2^{(h-1)}$  and  $\xi_2^{(h+2)} = \xi_1^{(h+1)} < \xi_1^{(h+2)} = \xi_2^{(h+1)}$ . So, at the step  $h + 3$  the length step is halved. When we eliminate the node  $\psi_2^{(h-1)}$  at the step  $h - 1$ , we proceed similarly.  $\square$

The relation (54) can be also obtained by imposing the condition

$$\frac{p_{h+1}}{p_h} \leq \left(\frac{1}{2}\right)^{\frac{1}{3}} \simeq 0.7937,$$

so we obtain that the algorithm has a linear convergence with a factor of convergence of at least 0.7937. Note that, in the best cases, the length of the step can be halved at each step, and so a convergence factor of 0.5 is obtained. Note that, if at the step  $h - 1$  the algorithm halves the length of the step and if at the step  $h + 1$  the length of the step is not yet halved, it has to be halved at the next step. Moreover, at the  $h + 2$ -th step, the value of the function  $g(k, \cdot, \iota, C)$  to be evaluated is assumed exactly at the node deleted at the step  $h - 1$ . Thus, the steps  $h + 1$  and  $h + 2$  can be unified using only one evaluation of the function  $g(k, \cdot, \iota, C)$ , by means of the following algorithm.

```

function TPS( $k, C_R, a, b$ )
   $h = 0;$ 
   $\psi^{(0)} = [a \quad (a + b)/2 \quad b];$ 
   $\xi^{(0)} = [g(k, \psi_1^{(0)}, \iota, C) \quad g(k, \psi_2^{(0)}, \iota, C) \quad g(k, \psi_3^{(0)}, \iota, C)];$ 
   $p_0 = (b - a)/2;$ 
  if ( $\xi_1^{(0)} < \xi_2^{(0)}$ ) then
    while (( $\xi_1^{(0)} < \xi_2^{(0)}$ ) and ( $p_h > \varepsilon$ )) do
       $\psi_3^{(0)} = \psi_2^{(0)};$ 
       $\xi_3^{(0)} = \xi_2^{(0)};$ 
       $\psi_2^{(0)} = (\psi_1^{(0)} + \psi_3^{(0)})/2;$ 
       $\xi_2^{(0)} = g(k, \psi_2^{(0)}, \iota, C);$ 
       $p_0 = p_0/2;$ 
    end while
  else
    while (( $\xi_3^{(0)} < \xi_2^{(0)}$ ) and ( $p_h > \varepsilon$ )) do
       $\psi_1^{(0)} = \psi_2^{(0)};$ 
       $\xi_1^{(0)} = \xi_2^{(0)};$ 
       $\psi_2^{(0)} = (\psi_1^{(0)} + \psi_3^{(0)})/2;$ 
       $\xi_2^{(0)} = g(k, \psi_2^{(0)}, \iota, C);$ 
       $p_0 = p_0/2;$ 
    end while
  end if
  while ( $p_h > \varepsilon$ ) do
    if (( $\xi_2^{(h)} < \xi_1^{(h)}$ ) and ( $\xi_2^{(h)} < \xi_3^{(h)}$ )) then
      if ( $\xi_1^{(h)} < \xi_3^{(h)}$ ) then

```

```

aux =  $\xi_3^{(h)}$ ;
 $\psi_3^{(h+1)} = \psi_2^{(h)}$ ;
 $\xi_3^{(h+1)} = \xi_2^{(h)}$ ;
v = 0;

else
    aux =  $\xi_1^{(h)}$ ;
     $\psi_1^{(h+1)} = \psi_2^{(h)}$ ;
     $\xi_1^{(h+1)} = \xi_2^{(h)}$ ;
    v = 0;
end if
 $\psi_2^{(h+1)} = (\psi_1^{(h+1)} + \psi_3^{(h+1)})/2$ ;
 $\xi_2^{(h+1)} = g(k, \psi_2^{(h+1)}, \iota, C)$ ;
 $p_{h+1} = p_h/2$ ;

else
    if ( $\xi_1^{(h)} < \xi_3^{(h)}$ ) then
        if (v ≠ 1) then
             $\psi^{(h+1)} = [\psi_1^{(h)} - p_h \quad \psi_1^{(h)} \quad \psi_2^{(h)}]$ ;
             $\xi^{(h+1)} = [g(k, \psi_1^{(h+1)}, \iota, C) \quad \xi_1^{(h)} \quad \xi_2^{(h)}]$ ;
             $p_{h+1} = p_h$ ;
            v = 1;
        else
             $p_{h+1} = p_h/2$ ;
            v = 0;
        if (aux <  $\xi_2^{(h)}$ ) then
             $\psi^{(h+1)} = [\psi_1^{(h)} - 2p_h \quad \psi_1^{(h)} - p_h \quad \psi_1^{(h)}]$ ;
             $\xi^{(h+1)} = [aux \quad g(k, \psi_2^{(h+1)}, \iota, C) \quad \xi_1^{(h)}]$ ;
            aux =  $\xi_2^{(h)}$ ;
        else
             $\psi^{(h+1)} = [\psi_1^{(h)} \quad \psi_2^{(h)} - p_h \quad \psi_2^{(h)}]$ ;
             $\xi^{(h+1)} = [\xi_1^{(h)} \quad g(k, \psi_2^{(h+1)}, \iota, C) \quad \xi_2^{(h)}]$ ;
        end if
    end if
else
    if (v ≠ 1) then
         $\psi^{(h+1)} = [\psi_2^{(h)} \quad \psi_3^{(h)} \quad \psi_3^{(h)} + p_h]$ ;
         $\xi^{(h+1)} = [\xi_2^{(h)} \quad \xi_3^{(h)} \quad g(k, \psi_3^{(h+1)}, \iota, C)]$ ;
         $p_{h+1} = p_h$ ;
        v = 1;
    else
         $p_{h+1} = p_h/2$ ;
        v = 0;
    if (aux <  $\xi_2^{(h)}$ ) then
         $\psi^{(h+1)} = [\psi_3^{(h)} \quad \psi_3^{(h)} + p_h \quad \psi_3^{(h)} + 2p_h]$ ;
         $\xi^{(h+1)} = [\xi_3^{(h)} \quad g(k, \psi_2^{(h+1)}, \iota, C) \quad aux]$ ;
        aux =  $\xi_2^{(h)}$ ;
    end if
end if

```

```

else
     $\psi^{(h+1)} = [\psi_2^{(h)} \quad \psi_2^{(h)} + p_h \quad \psi_3^{(h)}];$ 
     $\xi^{(h+1)} = [\xi_2^{(h)} \quad g(k, \psi_2^{(h+1)}, \iota, C) \quad \xi_3^{(h)}];$ 
end if
end if
end if
end if
end while
return  $\psi_2^{(h)}$ .

```

Thus, asymptotically we have the relation

$$p_{h+2} \leq \frac{1}{2}p_h.$$

This relation can be also obtained by imposing the condition

$$\frac{p_{h+1}}{p_h} \leq \left(\frac{1}{2}\right)^{\frac{1}{2}} \simeq 0.70711,$$

so the algorithm has a linear convergence with a factor of convergence smaller than or equal to 0.70711. We refer to this algorithm as *Three Point Search* (TPS).

#### 4.4 The golden section search

In this section we present an algorithm in which the uncertainty interval is reduced by a constant factor by means of one valuation of the function  $g(k, \cdot, \iota, C)$  (see also [38]). Here we consider the vector

$$\psi^{(h)} = [\psi_1^{(h)} \quad \psi_2^{(h)} \quad \psi_3^{(h)} \quad \psi_4^{(h)}]. \quad (55)$$

Let  $(a, b)$  be the initial uncertainty interval, containing the minimum of the function  $g(k, \cdot, \iota, C)$ , and let  $\phi = (\sqrt{5} + 1)/2$  be the *golden ratio* or *golden section*, then we apply the following algorithm:

```

function GSS( $k, C_R, a, b$ )
     $h = 0;$ 
     $\psi_1^{(0)} = a;$ 
     $\psi_4^{(0)} = b;$ 
     $\psi_2^{(0)} = \psi_4^{(0)} - (\psi_4^{(0)} - \psi_1^{(0)})/\phi;$ 
     $\psi_3^{(0)} = \psi_1^{(0)} + (\psi_4^{(0)} - \psi_1^{(0)})/\phi;$ 
    while ( $|\psi_4^{(h)} - \psi_1^{(h)}| > \varepsilon$ ) do
        if ( $g(k, \psi_2^{(h)}, \iota, C) < g(k, \psi_3^{(h)}, \iota, C)$ ) then
             $\psi^{(h+1)} = [\psi_1^{(h)} \quad \psi_4^{(h+1)} - (\psi_4^{(h+1)} - \psi_1^{(h+1)})/\phi \quad \psi_1^{(h+1)} + (\psi_4^{(h+1)} - \psi_1^{(h+1)})/\phi \quad \psi_3^{(h)}];$ 
        else
             $\psi^{(h+1)} = [\psi_2^{(h)} \quad \psi_4^{(h+1)} - (\psi_4^{(h+1)} - \psi_1^{(h+1)})/\phi \quad \psi_1^{(h+1)} + (\psi_4^{(h+1)} - \psi_1^{(h+1)})/\phi \quad \psi_4^{(h)}];$ 
        end if
    
```

```

 $h = h + 1;$ 
end while
return  $\psi_2^{(h)}$ 

```

where  $\varepsilon$  is a suitable tolerance threshold. In the body of the while we have two cases. In the first one,  $g(k, \psi_2^{(h)}, \iota, C) < g(k, \psi_3^{(h)}, \iota, C)$  (see Figure 11 (a) and (b)). So the minimizer  $\hat{\theta}$  of the functions  $g(k, \cdot, \iota, C)$  lies between  $\psi_1^{(h)}$  and  $\psi_3^{(h)}$ , thus the new uncertainty interval is  $[\psi_1^{(h)}, \psi_3^{(h)}]$ . In the second one,  $g(k, \psi_2^{(h)}, \iota, C) \geq g(k, \psi_3^{(h)}, \iota, C)$  (see Figure 11 (c) and (d)). Thus  $\hat{\theta}$  lies between  $\psi_2^{(h)}$  and  $\psi_4^{(h)}$ , so the new uncertainty interval is  $[\psi_2^{(h)}, \psi_4^{(h)}]$ .

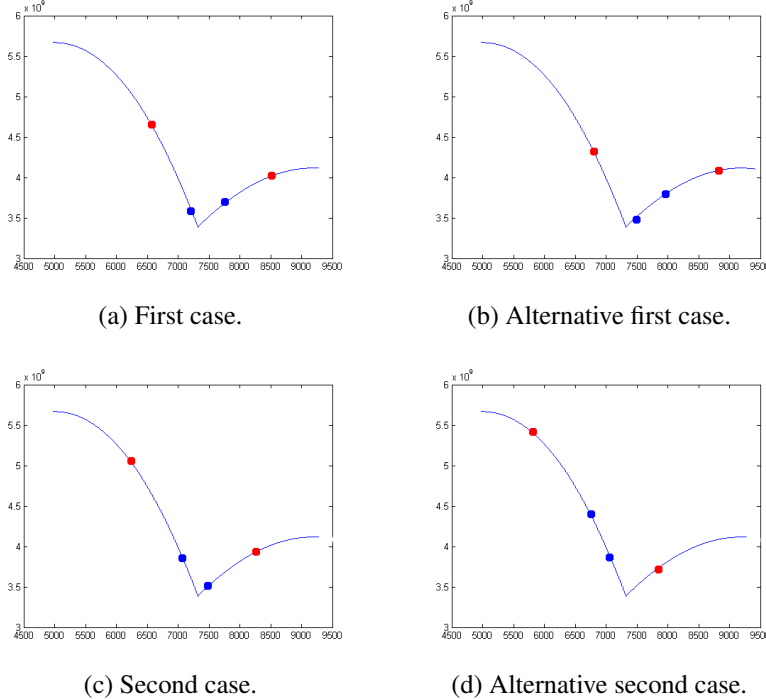


Figure 11: Cases in the body of the while of the GSS algorithm.

In both cases it is

$$\psi_2^{(h)} = \psi_4^{(h)} - \frac{\psi_4^{(h)} - \psi_1^{(h)}}{\phi} \quad (56)$$

and

$$\psi_3^{(h)} = \psi_1^{(h)} + \frac{\psi_4^{(h)} - \psi_1^{(h)}}{\phi}. \quad (57)$$

Let  $\ell^{(h+1)} = \psi_4^{(h+1)} - \psi_1^{(h+1)}$  be the length of the uncertainty interval at the step  $h + 1$ . If  $g(k, \psi_2^{(h)}, \iota, C) < g(k, \psi_3^{(h)}, \iota, C)$ , then from the equation (57) we have

$$\ell^{(h+1)} = \psi_3^{(h)} - \psi_1^{(h)} = \psi_1^{(h)} + \frac{\psi_4^{(h)} - \psi_1^{(h)}}{\phi} - \psi_1^{(h)} = \frac{\psi_4^{(h)} - \psi_1^{(h)}}{\phi}, \quad (58)$$

while, if  $g(k, \psi_2^{(h)}, \iota, C) \geq g(k, \psi_3^{(h)}, \iota, C)$ , then from the equation (56) we get

$$\ell^{(h+1)} = \psi_4^{(h)} - \psi_2^{(h)} = \psi_4^{(h)} - \psi_4^{(h)} + \frac{\psi_4^{(h)} - \psi_1^{(h)}}{\phi} = \frac{\psi_4^{(h)} - \psi_1^{(h)}}{\phi}. \quad (59)$$

Thus, we obtain

$$\ell^{(h+1)} = \psi_4^{(h+1)} - \psi_1^{(h+1)} = \frac{\psi_4^{(h)} - \psi_1^{(h)}}{\phi} = \frac{\ell^{(h)}}{\phi}. \quad (60)$$

So, in any case, the uncertainty interval is reduced at each step by a constant factor. Now, in order to compute the factor of convergence of the method, first we have to show that at each step just one valuation of the function  $g(k, \cdot, \iota, C)$  is necessary.

To prove this, we observe that the golden section has the following property:

$$\frac{1}{\phi^2} = \left( \frac{\sqrt{5}-1}{2} \right)^2 = \frac{3-\sqrt{5}}{2} = 1 - \frac{\sqrt{5}-1}{2} = 1 - \frac{1}{\phi}.$$

From this, if  $g(k, \psi_2^{(h)}, \iota, C) < g(k, \psi_3^{(h)}, \iota, C)$  then from the equations (56), (57) and (58) we get

$$\begin{aligned} \psi_3^{(h+1)} &= \psi_1^{(h+1)} + \frac{\psi_4^{(h+1)} - \psi_1^{(h+1)}}{\phi} = \psi_1^{(h)} + \frac{\psi_3^{(h)} - \psi_1^{(h)}}{\phi} \\ &= \psi_1^{(h)} + \frac{\frac{\psi_4^{(h)} - \psi_1^{(h)}}{\phi}}{\phi} = \left( 1 - \frac{1}{\phi^2} \right) \psi_1^{(h)} + \frac{1}{\phi^2} \psi_4^{(h)} \\ &= \frac{1}{\phi} \psi_1^{(h)} + \left( 1 - \frac{1}{\phi} \right) \psi_4^{(h)} = \psi_4^{(h)} - \frac{\psi_4^{(h)} - \psi_1^{(h)}}{\phi} \\ &= \psi_2^{(h)}, \end{aligned}$$

while, if  $g(k, \psi_2^{(h)}, \iota, C) \geq g(k, \psi_3^{(h)}, \iota, C)$ , from the equations (56), (57) and (59) we have

$$\begin{aligned} \psi_2^{(h+1)} &= \psi_4^{(h+1)} - \frac{\psi_4^{(h+1)} - \psi_1^{(h+1)}}{\phi} = \psi_4^{(h)} - \frac{\psi_4^{(h)} - \psi_2^{(h)}}{\phi} \\ &= \psi_4^{(h)} - \frac{\frac{\psi_4^{(h)} - \psi_1^{(h)}}{\phi}}{\phi} = \left( 1 - \frac{1}{\phi^2} \right) \psi_4^{(h)} + \frac{1}{\phi^2} \psi_1^{(h)} \\ &= \frac{1}{\phi} \psi_4^{(h)} + \left( 1 - \frac{1}{\phi} \right) \psi_1^{(h)} = \psi_1^{(h)} + \frac{\psi_4^{(h)} - \psi_1^{(h)}}{\phi} \\ &= \psi_3^{(h)}. \end{aligned}$$

Thus, if we define

$$\xi^{(h)} = [g(k, \psi_1^{(h)}, \iota, C) \quad g(k, \psi_2^{(h)}, \iota, C) \quad g(k, \psi_3^{(h)}, \iota, C) \quad g(k, \psi_4^{(h)}, \iota, C)],$$

the algorithm can be written as follows:

```

function GSS( $k, C_R, a, b$ )
 $h = 0;$ 
 $\psi_1^{(0)} = a;$ 
 $\psi_4^{(0)} = b;$ 
 $\psi_2^{(0)} = \psi_4^{(0)} - (\psi_4^{(0)} - \psi_1^{(0)})/\phi;$ 
 $\psi_3^{(0)} = \psi_1^{(0)} + (\psi_4^{(0)} - \psi_1^{(0)})/\phi;$ 
 $\xi^{(0)} = [g(k, \psi_1^{(0)}, \iota, C) \quad g(k, \psi_2^{(0)}, \iota, C) \quad g(k, \psi_3^{(0)}, \iota, C) \quad g(k, \psi_4^{(0)}, \iota, C)];$ 
while ( $|\psi_4^{(h)} - \psi_1^{(h)}| > \varepsilon$ ) do
    if ( $\xi_2^{(h)} < \xi_3^{(h)}$ ) then
         $\psi^{(h+1)} = [\psi_1^{(h)} \quad \psi_4^{(h+1)} - (\psi_4^{(h+1)} - \psi_1^{(h+1)})/\phi \quad \psi_2^{(h)} \quad \psi_3^{(h)}];$ 
         $\xi^{(h+1)} = [\xi_1^{(h)} \quad g(k, \psi_2^{(h+1)}, \iota, C) \quad \xi_2^{(h)} \quad \xi_3^{(h)}];$ 
    else
         $\psi^{(h+1)} = [\psi_2^{(h)} \quad \psi_3^{(h)} \quad \psi_1^{(h+1)} + (\psi_4^{(h+1)} - \psi_1^{(h+1)})/\phi \quad \psi_4^{(h)}];$ 
         $\xi^{(h+1)} = [\xi_2^{(h)} \quad \xi_3^{(h)} \quad g(k, \psi_3^{(h+1)}, \iota, C) \quad \xi_4^{(h)}];$ 
    end if
     $h = h + 1;$ 
end while
return  $\psi_2^{(h)}$ .

```

During each iterate, in every case, the function  $g(k, \cdot, \iota, C)$  is evaluated only one time, so, from the equation (60), the algorithm has a linear convergence with factor of convergence given by

$$\frac{l^{(h+1)}}{l^{(h)}} = \frac{\psi_4^{(h+1)} - \psi_1^{(h+1)}}{\psi_4^{(h)} - \psi_1^{(h)}} = \frac{\frac{\psi_4^{(h)} - \psi_1^{(h)}}{\phi}}{\psi_4^{(h)} - \psi_1^{(h)}} = \frac{1}{\phi} = \frac{\sqrt{5} - 1}{2} \simeq 0.61803.$$

We refer to this algorithm as *Golden Section Search* (GSS).

## 4.5 Successive parabolic interpolation

Given a finite sequence of approximations of the required minimum, the method introduced in this section constructs a parabola which interpolates the objective function  $g(k, \cdot, \iota, C)$  in the last three terms of the considered sequence and add a new term to the sequence, corresponding to the argument of the minimum of the obtained parabola (see also [9, 34]). That is, given the sequence  $\theta^{(0)}, \dots, \theta^{(h+2)}$ , we call  $p_2(\theta)$  the interpolation polynomial of the function  $g(k, \cdot, \iota, C)$  at the point  $\theta^{(h)}, \theta^{(h+1)}, \theta^{(h+2)}$ , and choose  $\theta^{(h+3)}$  by posing

$$p'_2(\theta^{(h+3)}) = 0. \tag{61}$$

We recall that the divided differences of the function  $g(k, \cdot, \iota, C)$  are

$$g[\theta^{(h)}] = g(k, \theta^{(h)}, \iota, C), \quad h = 0, 1, \dots,$$

and

$$g[\theta^{(h)}, \theta^{(h+1)}, \dots, \theta^{(h+k-1)}, \theta^{(h+k)}] = \frac{g[\theta^{(h+1)}, \theta^{(h+2)}, \dots, \theta^{(h+k)}] - g[\theta^{(h)}, \theta^{(h+1)}, \dots, \theta^{(h+k-1)}]}{\theta^{(h+k)} - \theta^{(h)}} \\ h = 0, 1, \dots, k = 1, 2, \dots .$$

It is possible to prove that, if  $g(k, \cdot, \iota, C) \in C^2([a, b])$ , where  $[a, b]$  contains the argument of the minimum of  $g(k, \cdot, \iota, C)$ , then the sequence  $\{\theta^{(h)}\}_{h \in \mathbb{N}}$  is well-defined (see also [9]). If

$$g[\theta^{(h)}, \theta^{(h+1)}, \theta^{(h+2)}] \neq 0,$$

then the unique solution of (61) is

$$\theta^{(h+3)} = \frac{1}{2} \left( \theta^{(h+1)} + \theta^{(h+2)} - \frac{g[\theta^{(h+1)}, \theta^{(h+2)}]}{g[\theta^{(h)}, \theta^{(h+1)}, \theta^{(h+2)}]} \right). \quad (62)$$

Fix  $n \in \mathbb{N}$ , a function  $f : [a, b] \rightarrow \mathbb{R}$  is said to be of class  $LC^n([a, b])$  iff its  $n$ -th derivative exists and is Lipschitz, namely iff there exists a positive real number  $M_0$  with

$$\sup_{x, y \in [a, b], |x-y| \leq \delta} |f(x) - f(y)| \leq M_0 \delta$$

for each  $\delta > 0$ . The following result holds.

**Theorem 4.2.** (see also [9, Theorem 3.7.1]) *Let  $g(k, \cdot, \iota, C) : [a, b] \rightarrow \mathbb{R}$  be of class  $LC^3([a, b])$ , and  $\hat{\theta} \in ]a, b[$  be such that  $g'(k, \hat{\theta}, \iota, C) = 0$  and  $g''(k, \hat{\theta}, \iota, C) \neq 0$ . If  $\theta^{(0)}$ ,  $\theta^{(1)}$ ,  $\theta^{(2)}$  are distinct and sufficiently close to  $\hat{\theta}$ , then a sequence  $\{\theta^{(h)}\}_{h \in \mathbb{N}}$  is univoquely defined by (62), and  $\{\theta^{(h)}\}_{h \in \mathbb{N}}$  either converges with strong order  $p \simeq 1.325$ , or converges with weak order  $p = ((3 + \sqrt{5})/2)^{1/3} \simeq 1.378$ .*

Note that, if in the expression of  $g(k, \cdot, 1, C_R)$  we use the function  $\bar{\tau}$  in (45) instead of  $\tau$  in (44), then, using classical results of Analysis, it is not difficult to check that  $g(k, \cdot, 1, C_R)$  is of class  $LC^3((\varphi_R^{(1)} + \eta, \varphi_R^{(6)} - \eta))$ . So, Theorem 4.2 can be applied.

The relative algorithm is the following

```

function SPI( $k, C_R$ )
   $h = 0;$ 
   $\theta^{(0)} = \varphi_R^{(1)} + \eta;$ 
   $\theta^{(1)} = \varphi_R^{(6)} - \eta;$ 
   $\theta^{(2)} = (\theta^{(0)} + \theta^{(1)})/2;$ 
   $\xi^{(h)} = g(k, \theta^{(h)}, \iota, C);$ 
   $\xi^{(h+1)} = g(k, \theta^{(h+1)}, \iota, C);$ 
   $\xi^{(h+2)} = g(k, \theta^{(h+2)}, \iota, C);$ 
   $g[\theta^{(h)}, \theta^{(h+1)}] = \frac{\xi^{(h+1)} - \xi^{(h)}}{\theta^{(h+1)} - \theta^{(h)}};$ 
  while ( $|\theta^{(h+2)} - \theta^{(h+1)}| > \varepsilon$ ) do
     $g[\theta^{(h+1)}, \theta^{(h+2)}] = \frac{\xi^{(h+2)} - \xi^{(h+1)}}{\theta^{(h+2)} - \theta^{(h+1)}};$ 
     $g[\theta^{(h)}, \theta^{(h+1)}, \theta^{(h+2)}] = \frac{g[\theta^{(h+1)}, \theta^{(h+2)}] - g[\theta^{(h)}, \theta^{(h+1)}]}{\theta^{(h+2)} - \theta^{(h)}};$ 
     $\theta^{(h+3)} = \frac{1}{2} \left( \theta^{(h+1)} + \theta^{(h+2)} - \frac{g[\theta^{(h+1)}, \theta^{(h+2)}]}{g[\theta^{(h)}, \theta^{(h+1)}, \theta^{(h+2)}]} \right);$ 
     $\xi^{(h+3)} = g(k, \theta^{(h+3)}, \iota, C);$ 
     $h = h + 1;$ 
  end while
return  $\theta^{(h+2)}$ 

```

where  $\varepsilon$  is the tolerance threshold. To accelerate the order of convergence of the sequence  $(\theta^{(h)})$ , we can pose

$$\theta^{(h+3)} = \Xi^{(h)} - \left( \frac{g[\theta^{(h-1)}, \theta^{(h)}, \theta^{(h+1)}, \theta^{(h+2)}]}{2g[\theta^{(h)}, \theta^{(h+1)}, \theta^{(h+2)}]} \right) \Upsilon^{(h)}, \quad (63)$$

where

$$\Xi^{(h)} = \frac{1}{2} \left( \theta^{(h+1)} + \theta^{(h+2)} - \frac{g[\theta^{(h+1)}, \theta^{(h+2)}]}{g[\theta^{(h)}, \theta^{(h+1)}, \theta^{(h+2)}]} \right)$$

and

$$\begin{aligned} \Upsilon^{(h)} &= (\theta^{(h)} - \Xi^{(h)})(\theta^{(h+1)} - \Xi^{(h)}) + (\theta^{(h)} - \Xi^{(h)})(\theta^{(h+2)} - \Xi^{(h)}) \\ &+ (\theta^{(h+1)} - \Xi^{(h)})(\theta^{(h+2)} - \Xi^{(h)}). \end{aligned}$$

Indeed, we have the following

**Theorem 4.3.** (see also [9, Theorem 3.8.1]) *Let  $g(k, \cdot, \iota, C) : [a, b] \rightarrow \mathbb{R}$  be of class  $LC^3([a, b])$ ,  $\hat{\theta} \in ]a, b[$  be such that  $g'(k, \hat{\theta}, \iota, C) = 0$  and  $g''(k, \hat{\theta}, \iota, C) \neq 0$ . If  $\theta^{(0)}, \theta^{(1)}, \theta^{(2)}$  are distinct and sufficiently close to  $\hat{\theta}$ , then the sequence  $\{\theta^{(h)}\}_{h \in \mathbb{N}}$  is univoquely defined by (63), and  $\{\theta^{(h)}\}_{h \in \mathbb{N}}$  converges with weak order  $p \simeq 1.465$ .*

The relative algorithm is the following

```

function SPI( $k, C_R$ )
   $h = 0;$ 
   $\theta^{(0)} = \varphi_R^{(1)} + \eta;$ 
   $\theta^{(1)} = \varphi_R^{(6)} - \eta;$ 
   $\theta^{(2)} = (\theta^{(0)} + \theta^{(1)})/2;$ 
   $\xi^{(h)} = g(k, \theta^{(h)}, \iota, C);$ 
   $\xi^{(h+1)} = g(k, \theta^{(h+1)}, \iota, C);$ 
   $\xi^{(h+2)} = g(k, \theta^{(h+2)}, \iota, C);$ 
   $g[\theta^{(h)}, \theta^{(h+1)}] = \frac{\xi^{(h+1)} - \xi^{(h)}}{\theta^{(h+1)} - \theta^{(h)}};$ 
   $g[\theta^{(h+1)}, \theta^{(h+2)}] = \frac{\xi^{(h+2)} - \xi^{(h+1)}}{\theta^{(h+2)} - \theta^{(h+1)}};$ 
   $g[\theta^{(h)}, \theta^{(h+1)}, \theta^{(h+2)}] = \frac{g[\theta^{(h+1)}, \theta^{(h+2)}] - g[\theta^{(h)}, \theta^{(h+1)}]}{\theta^{(h+2)} - \theta^{(h)}};$ 
   $\theta^{(h+3)} = \frac{1}{2} \left( \theta^{(h+1)} + \theta^{(h+2)} - \frac{g[\theta^{(h+1)}, \theta^{(h+2)}]}{g[\theta^{(h)}, \theta^{(h+1)}, \theta^{(h+2)}]} \right);$ 
   $\xi^{(h+3)} = g(k, \theta^{(h+3)}, \iota, C);$ 
   $h = h + 1;$ 
  while  $(|\theta^{(h+2)} - \theta^{(h+1)}| > \varepsilon)$  do
     $g[\theta^{(h+1)}, \theta^{(h+2)}] = \frac{\xi^{(h+2)} - \xi^{(h+1)}}{\theta^{(h+2)} - \theta^{(h+1)}};$ 
     $g[\theta^{(h)}, \theta^{(h+1)}, \theta^{(h+2)}] = \frac{g[\theta^{(h+1)}, \theta^{(h+2)}] - g[\theta^{(h)}, \theta^{(h+1)}]}{\theta^{(h+2)} - \theta^{(h)}};$ 
     $\Xi^{(h)} = \frac{1}{2} \left( \theta^{(h+1)} + \theta^{(h+2)} - \frac{g[\theta^{(h+1)}, \theta^{(h+2)}]}{g[\theta^{(h)}, \theta^{(h+1)}, \theta^{(h+2)}]} \right);$ 
     $\Upsilon^{(h)} = (\theta^{(h)} - \Xi^{(h)})(\theta^{(h+1)} - \Xi^{(h)}) + (\theta^{(h)} - \Xi^{(h)})(\theta^{(h+2)} - \Xi^{(h)}) + (\theta^{(h+1)} - \Xi^{(h)})(\theta^{(h+2)} - \Xi^{(h)});$ 
     $g[\theta^{(h-1)}, \theta^{(h)}, \theta^{(h+1)}, \theta^{(h+2)}] = \frac{g[\theta^{(h)}, \theta^{(h+1)}, \theta^{(h+2)}] - g[\theta^{(h-1)}, \theta^{(h)}, \theta^{(h+1)}]}{\theta^{(h+2)} - \theta^{(h-1)}};$ 
     $\theta^{(h+3)} = \Xi^{(h)} - \left( \frac{g[\theta^{(h-1)}, \theta^{(h)}, \theta^{(h+1)}, \theta^{(h+2)}]}{2g[\theta^{(h)}, \theta^{(h+1)}, \theta^{(h+2)}]} \right) \Upsilon^{(h)};$ 

```

```

 $\xi^{(h+3)} = g(k, \theta^{(h+3)}, \iota, C);$ 
 $h = h + 1;$ 
end while
return  $\theta^{(h+2)}$ .

```

where  $\varepsilon$  is the tolerance threshold.

We refer to this algorithm as *Successive Parabolic Interpolation* (SPI).

## 4.6 Hybrid SPI and GSS

In our case the SPI algorithm could not converge to the desired solutions, since the derivative of the function  $g(k, \cdot, \iota, C)$ , on each interval lying between any two successive points of discontinuity, can vanish also in correspondence of the points which are not minimizers. Moreover, it is possible that the updates of the solution do not belong to the initial uncertainty interval, that is the interval in which the objective function is quasi-convex. We saw experimentally that, in general, the SPI algorithm does not converge to the minimum of the function  $g(k, \cdot, \iota, C)$ . To guarantee the convergence to that minimum a hybrid *Successive Parabolic Interpolation* and *Golden Section Search* technique is necessary (see also [9]).

By means of this algorithm, a sequence  $\{\theta^{(h)}\}_{h \in \mathbb{N}}$  such that

$$g(k, \theta^{(h)}, 1, C_R) \geq g(k, \theta^{(h+1)}, 1, C_R) \quad h = 0, 1, \dots, \quad (64)$$

is constructed, while at the  $h$ -th step we have an uncertainty interval, say  $[a^{(h)}, b^{(h)}]$ .

Given  $\varphi_R^{(1)}$  and  $\varphi_R^{(6)}$  as in the equations (39) and (41) and  $\eta \in \mathbb{R}^+$  small enough, we take the initial uncertainty interval as  $[a^{(0)} = \varphi_R^{(1)} + \eta, b^{(0)} = \varphi_R^{(6)} - \eta]$ . Let  $\phi = (\sqrt{5} + 1)/2$  be the *golden ratio* or *golden section*. The sequence is initialized as

$$\theta^{(0)} = \theta^{(1)} = \theta^{(2)} = a^{(2)} + \frac{b^{(2)} - a^{(2)}}{\phi},$$

which is equivalent to a golden section search step.

The main step of the successive parabolic interpolation algorithm can be written as

$$\theta^{(h+3)} = \theta^{(h+2)} + \frac{p}{q},$$

where

$$p = (\theta^{(h+2)} - \theta^{(h)})^2(g(k, \theta^{(h+2)}, 1, C_R) - g(k, \theta^{(h+1)}, 1, C_R)) \\ - (\theta^{(h+2)} - \theta^{(h+1)})^2(g(k, \theta^{(h+2)}, 1, C_R) - g(k, \theta^{(h)}, 1, C_R))$$

and

$$q = 2(\theta^{(h+2)} - \theta^{(h)})(g(k, \theta^{(h+2)}, 1, C_R) - g(k, \theta^{(h+1)}, 1, C_R)) \\ - 2(\theta^{(h+2)} - \theta^{(h+1)})(g(k, \theta^{(h+2)}, 1, C_R) - g(k, \theta^{(h)}, 1, C_R)).$$

If some of the points  $\theta^{(h)}$ ,  $\theta^{(h+1)}$  and  $\theta^{(h+2)}$  coincide or the parabola degenerates in a line (in this case,  $q = 0$ ), or if the successive parabolic interpolation updating is outside of

the current uncertainty interval  $[a^{(h)}, b^{(h)}]$ , then an updating is done by the golden section search algorithm.

This algorithm can be described as follows:

```

function SPI-GSS( $k, C_R$ )
 $h = 0;$ 
 $[a^{(0)}, b^{(0)}] = [\varphi_R^{(1)} + \eta, \varphi_R^{(6)} - \eta];$ 
 $\theta^{(0)} = \theta^{(1)} = \theta^{(2)} = a^{(2)} + (b^{(2)} - a^{(2)})/\phi;$ 
while ( $|\theta^{(h+2)} - \theta^{(h+1)}| > \varepsilon$ ) do
     $p = (\theta^{(h+2)} - \theta^{(h)})^2(g(k, \theta^{(h+2)}, \iota, C_R) - g(k, \theta^{(h+1)}, \iota, C_R));$ 
     $p = p - (\theta^{(h+2)} - \theta^{(h+1)})^2(g(k, \theta^{(h+2)}, \iota, C_R) - g(k, \theta^{(h)}, \iota, C_R));$ 
     $q = 2(\theta^{(h+2)} - \theta^{(h)})(g(k, \theta^{(h+2)}, \iota, C_R) - g(k, \theta^{(h+1)}, \iota, C_R));$ 
     $q = q - 2(\theta^{(h+2)} - \theta^{(h+1)})(g(k, \theta^{(h+2)}, \iota, C_R) - g(k, \theta^{(h)}, \iota, C_R));$ 
    if (( $q \neq 0$ ) and ( $\theta^{(h+2)} + p/q \in [a^{(h)}, b^{(h)}]$ )) then
         $\theta^{(h+3)} = \theta^{(h+2)} + p/q;$ 
    else
        if ( $\theta^{(h+2)} < (a^{(h+2)} + b^{(h+2)})/2$ ) then
             $\theta^{(h+3)} = \theta^{(h+2)} + (b^{(h+2)} - \theta^{(h+2)})/r;$ 
        else
             $\theta^{(h+3)} = \theta^{(h+2)} + (a^{(h+2)} - \theta^{(h+2)})/r;$ 
        end if
    end if
    Compute the new uncertainty interval  $[a^{(h+1)}, b^{(h+1)}];$ 
    Order  $\{\theta^{(i)}\}_{i=h, \dots, h+3}$  in such a way that (64) holds;
     $h = h + 1;$ 
end while
return  $\theta^{(h+2)}$ 

```

where  $\varepsilon$  is a suitable tolerance threshold.

During the last steps, usually the algorithm stops choosing golden section search steps and computes only parabolic interpolation steps. Thus, the asymptotic convergence depends only on the SPI algorithm. We refer to this algorithm as *Successive Parabolic Interpolation–Golden Section Search* (SPI-GSS).

## 4.7 The Newton method

To find the minimum of the function  $g(k, \cdot, \iota, C)$ , it is possible to apply the classical Newton method to its derivative, that is the following algorithm is performed:

```

function Newton( $k, C_R$ )
 $h = 0;$ 
 $\theta^{(1)} = (\varphi_R^{(1)} + \varphi_R^{(6)})/2;$ 
 $\theta^{(0)} = \theta^{(1)} + 2\varepsilon;$ 
while ( $|\theta^{(h+1)} - \theta^{(h)}| > \varepsilon$ ) do
     $h = h + 1;$ 
     $\theta^{(h+1)} = \theta^{(h)} - \frac{g'(k, \theta^{(h)}, \iota, C_R)}{g''(k, \theta^{(h)}, \iota, C_R)};$ 
end while

```

**return**  $\theta^{(h+1)}$

where  $\varepsilon$  is the tolerance threshold, and

$$\begin{aligned} g(k_R^{(l)}, \theta, \iota, C_R) &= f^{(l)}(\theta, \iota, C_R) = (\tau(\tilde{s}_{rR,\iota}^{(l)}(\theta)))^T \cdot \tau(\tilde{s}_{vR,\iota}^{(l)}(\theta)) \\ &= \sum_{i=1}^{n^2} (\tau(\tilde{s}_{rR,\iota}^{(l)}(\theta)))_i (\tau(\tilde{s}_{vR,\iota}^{(l)}(\theta)))_i, \end{aligned}$$

and  $\tau$  is as in (44). Note that

$$\frac{\partial(\tau(\cdot)_i)}{\partial s_j} = \begin{cases} 0, & \text{if } s_j > 0, \\ \delta_{i,j}, & \text{if } 0 < s_j < m_R, \\ 0, & \text{if } s_j > m_R, \end{cases} \quad i, j = 1, \dots, n^2, \quad (65)$$

where  $\delta_{i,j}$  denotes the *Kronecker delta*. When the following quantities make sense, we get

$$\frac{d}{d\theta} f^{(l)}(\theta, \iota, C_R) = \sum_{i=1}^{n^2} \left( \tau(\tilde{s}_{vR,\iota}^{(l)}(\theta))_i \left( \frac{d}{d\theta} (\tau(\tilde{s}_{rR,\iota}^{(l)}(\theta))_i) + (\tau(\tilde{s}_{rR,\iota}^{(l)}(\theta)))_i \left( \frac{d}{d\theta} (\tau(\tilde{s}_{vR,\iota}^{(l)}(\theta)))_i \right) \right) \right)$$

where for each  $i = 1, 2, \dots, n^2$  it is

$$\begin{aligned} \frac{d}{d\theta} (\tau(\tilde{s}_{rR,\iota}^{(l)}(\theta))_i) &= \sum_{j=1}^{n^2} \frac{\partial(\tau(\cdot)_i)}{\partial s_j} ((\tilde{s}_{rR,\iota}^{(l)}(\theta))_j) \cdot ((\tilde{s}_{rR,\iota}^{(l)}(\theta))_j)' = \\ &= \frac{\partial(\tau(\cdot)_i)}{\partial s_i} ((\tilde{s}_{rR,\iota}^{(l)}(\theta))_i) \cdot ((\tilde{s}_{rR,\iota}^{(l)}(\theta))_i)' = \\ &= \begin{cases} ((\tilde{s}_{rR,\iota}^{(l)}(\theta))_i)', & \text{if } 0 < (\tilde{s}_{rR,\iota}^{(l)}(\theta))_i < m_R, \\ 0, & \text{otherwise} \end{cases}; \end{aligned}$$

$$\begin{aligned} \frac{d}{d\theta} (\tau(\tilde{s}_{vR,\iota}^{(l)}(\theta))_i) &= \sum_{j=1}^{n^2} \frac{\partial(\tau(\cdot)_i)}{\partial s_j} ((\tilde{s}_{vR,\iota}^{(l)}(\theta))_j) \cdot ((\tilde{s}_{vR,\iota}^{(l)}(\theta))_j)' = \\ &= \frac{\partial(\tau(\cdot)_i)}{\partial s_i} ((\tilde{s}_{vR,\iota}^{(l)}(\theta))_i) \cdot ((\tilde{s}_{vR,\iota}^{(l)}(\theta))_i)' = \\ &= \begin{cases} ((\tilde{s}_{vR,\iota}^{(l)}(\theta))_i)', & \text{if } 0 < (\tilde{s}_{vR,\iota}^{(l)}(\theta))_i < m_R, \\ 0, & \text{otherwise} \end{cases}. \end{aligned}$$

Moreover, we have:

$$\begin{aligned} \frac{d^2}{d\theta^2} f^{(l)}(\theta, \iota, C_R) &= \sum_{i=1}^{n^2} \left( \tau(\tilde{s}_{vR,\iota}^{(l)}(\theta))_i \left( \frac{d^2}{d\theta^2} (\tau(\tilde{s}_{rR,\iota}^{(l)}(\theta))_i) + (\tau(\tilde{s}_{rR,\iota}^{(l)}(\theta)))_i \left( \frac{d^2}{d\theta^2} (\tau(\tilde{s}_{vR,\iota}^{(l)}(\theta)))_i \right) \right) \right) + \\ &+ 2 \left( \frac{d}{d\theta} (\tau(\tilde{s}_{rR,\iota}^{(l)}(\theta))_i) \right) \left( \frac{d}{d\theta} (\tau(\tilde{s}_{vR,\iota}^{(l)}(\theta)))_i \right), \end{aligned}$$

where

$$\frac{d^2}{d\theta^2} (\tau(\tilde{s}_{rR,\iota}^{(l)}(\theta))_i) = \begin{cases} ((\tilde{s}_{rR,\iota}^{(l)}(\theta))_i)'', & \text{if } 0 < (\tilde{s}_{rR,\iota}^{(l)}(\theta))_i < m_R, \\ 0, & \text{otherwise} \end{cases};$$

$$\frac{d^2}{d\theta^2}(\tau(\tilde{s}_{vR,\iota}^{(l)}(\theta))_i) = \begin{cases} ((\tilde{s}_{vR,\iota}^{(l)}(\theta))_i)'' & \text{if } 0 < (\tilde{s}_{vR,\iota}^{(l)}(\theta))_i < m_R, \\ 0 & \text{otherwise} \end{cases}.$$

For every  $i = 1, 2, \dots, n^2$ , we get:

$$(\tilde{s}_{rR,\iota}^{(l)}(\theta))_i = y_{11}^{R,\iota,(l)}(\theta)(x_{rR})_i + y_{12}^{R,\iota,(l)}(\theta)(x_{vR})_i,$$

$$(\tilde{s}_{vR,\iota}^{(l)}(\theta))_i = y_{21}^{R,\iota,(l)}(\theta)(x_{rR})_i + y_{22}^{R,\iota,(l)}(\theta)(x_{vR})_i,$$

$$((\tilde{s}_{rR,\iota}^{(l)}(\theta))_i)' = (y_{11}^{R,\iota,(l)})'(\theta)(x_{rR})_i + (y_{12}^{R,\iota,(l)})'(\theta)(x_{vR})_i,$$

$$((\tilde{s}_{vR,\iota}^{(l)}(\theta))_i)'' = (y_{21}^{R,\iota,(l)})''(\theta)(x_{rR})_i + (y_{22}^{R,\iota,(l)})''(\theta)(x_{vR})_i,$$

$$((\tilde{s}_{rR,\iota}^{(l)}(\theta))_i)'' = (y_{11}^{R,\iota,(l)})''(\theta)(x_{rR})_i + (y_{12}^{R,\iota,(l)})''(\theta)(x_{vR})_i,$$

$$((\tilde{s}_{vR,\iota}^{(l)}(\theta))_i)'' = (y_{21}^{R,\iota,(l)})''(\theta)(x_{rR})_i + (y_{22}^{R,\iota,(l)})''(\theta)(x_{vR})_i,$$

where

$$\begin{aligned} y_{11}^{R,\iota,(l)}(\theta) &= \frac{z_{22}^{R,\iota}(\theta)(\det(C_R) - k_R^{(l)}(z_{11}^{R,\iota}(\theta) - z_{21}^{R,\iota}(\theta))^2)}{(z_{22}^{R,\iota}(\theta) - z_{12}^{R,\iota}(\theta))\det(C_R)} - z_{21}^{R,\iota}(\theta) \frac{k_R^{(l)}(z_{11}^{R,\iota}(\theta) - z_{21}^{R,\iota}(\theta))}{\det(C_R)}, \\ y_{12}^{R,\iota,(l)}(\theta) &= -\frac{z_{12}^{R,\iota}(\theta)(\det(C_R) - k_R^{(l)}(z_{11}^{R,\iota}(\theta) - z_{21}^{R,\iota}(\theta))^2)}{(z_{22}^{R,\iota}(\theta) - z_{12}^{R,\iota}(\theta))\det(C_R)} + z_{11}^{R,\iota}(\theta) \frac{k_R^{(l)}(z_{11}^{R,\iota}(\theta) - z_{21}^{R,\iota}(\theta))}{\det(C_R)}, \\ y_{21}^{R,\iota,(l)}(\theta) &= -\frac{z_{21}^{R,\iota}(\theta)}{z_{11}^{R,\iota}(\theta) - z_{21}^{R,\iota}(\theta)}, \\ y_{22}^{R,\iota,(l)}(\theta) &= \frac{z_{11}^{R,\iota}(\theta)}{z_{11}^{R,\iota}(\theta) - z_{21}^{R,\iota}(\theta)}. \end{aligned}$$

We have

$$\begin{aligned} (y_{11}^{R,\iota,(l)})'(\theta) &= -\frac{z_{22}^{R,\iota}(\theta)((z_{22}^{R,\iota})'(\theta) - (z_{12}^{R,\iota})'(\theta))(\det(C_R) - k_R^{(l)}(z_{11}^{R,\iota}(\theta) - z_{21}^{R,\iota}(\theta))^2)}{(z_{22}^{R,\iota}(\theta) - z_{12}^{R,\iota}(\theta))^2\det(C_R)} + \\ &\quad + \frac{(z_{22}^{R,\iota})'(\theta)(\det(C_R) - k_R^{(l)}(z_{11}^{R,\iota}(\theta) - z_{21}^{R,\iota}(\theta))^2)}{(z_{22}^{R,\iota}(\theta) - z_{12}^{R,\iota}(\theta))\det(C_R)} - \\ &\quad - \frac{k_R^{(l)}(z_{21}^{R,\iota})'(\theta)(z_{11}^{R,\iota}(\theta) - z_{21}^{R,\iota}(\theta))}{\det(C_R)} - \\ &\quad - 2\frac{k_R^{(l)}z_{22}^{R,\iota}(\theta)(z_{11}^{R,\iota}(\theta) - z_{21}^{R,\iota}(\theta))((z_{11}^{R,\iota})'(\theta) - (z_{21}^{R,\iota})'(\theta))}{(z_{22}^{R,\iota}(\theta) - z_{12}^{R,\iota}(\theta))\det(C_R)} - \\ &\quad - \frac{k_R^{(l)}z_{21}^{R,\iota}(\theta)((z_{11}^{R,\iota})'(\theta) - (z_{21}^{R,\iota})'(\theta))}{\det(C_R)} \end{aligned}$$

Therefore,

$$\begin{aligned}
(y_{11}^{R,\iota,(l)})''(\theta) &= -\frac{z_{22}^{R,\iota}(\theta)((z_{22}^{R,\iota})''(\theta) - (z_{12}^{R,\iota})''(\theta))(\det(C_R) - k_R^{(l)}(z_{11}^{R,\iota}(\theta) - z_{21}^{R,\iota}(\theta))^2)}{(z_{22}^{R,\iota}(\theta) - z_{12}^{R,\iota}(\theta))^2 \det(C_R)} + \\
&+ \frac{(z_{22}^{R,\iota})''(\theta)(\det(C_R) - k_R^{(l)}(z_{11}^{R,\iota}(\theta) - z_{21}^{R,\iota}(\theta))^2)}{(z_{22}^{R,\iota}(\theta) - z_{12}^{R,\iota}(\theta)) \det(C_R)} + \\
&+ 2 \frac{z_{22}^{R,\iota}(\theta)((z_{22}^{R,\iota})'(\theta) - (z_{12}^{R,\iota})'(\theta))^2 (\det(C_R) - k_R^{(l)}(z_{11}^{R,\iota}(\theta) - z_{21}^{R,\iota}(\theta))^2)}{(z_{22}^{R,\iota}(\theta) - z_{12}^{R,\iota}(\theta))^3 \det(C_R)} - \\
&- 2 \frac{(z_{22}^{R,\iota})'(\theta)((z_{22}^{R,\iota})'(\theta) - (z_{12}^{R,\iota})'(\theta))(\det(C_R) - k_R^{(l)}(z_{11}^{R,\iota}(\theta) - z_{21}^{R,\iota}(\theta))^2)}{(z_{22}^{R,\iota}(\theta) - z_{12}^{R,\iota}(\theta))^2 \det(C_R)} + \\
&+ 4 \frac{k_R^{(l)} z_{22}^{R,\iota}(\theta)(z_{11}^{R,\iota}(\theta) - z_{21}^{R,\iota}(\theta))((z_{11}^{R,\iota})'(\theta) - (z_{21}^{R,\iota})'(\theta))((z_{22}^{R,\iota})'(\theta) - (z_{12}^{R,\iota})'(\theta))}{(z_{22}^{R,\iota}(\theta) - z_{12}^{R,\iota}(\theta))^2 \det(C_R)} - \\
&- 4 \frac{k_R^{(l)} z_{22}'(\theta)((z_{11}^{R,\iota})'(\theta) - (z_{21}^{R,\iota})'(\theta))(z_{11}^{R,\iota}(\theta) - z_{21}^{R,\iota}(\theta))}{(z_{22}^{R,\iota}(\theta) - z_{12}^{R,\iota}(\theta)) \det(C_R)} - \\
&- \frac{k_R^{(l)}(z_{11}^{R,\iota}(\theta) - z_{21}^{R,\iota}(\theta))(z_{21}^{R,\iota})''(\theta)}{\det(C_R)} - \\
&- 2 \frac{k_R^{(l)} z_{22}^{R,\iota}(\theta)(z_{11}^{R,\iota}(\theta) - z_{21}^{R,\iota}(\theta))((z_{11}^{R,\iota})''(\theta) - (z_{21}^{R,\iota})''(\theta))}{(z_{22}^{R,\iota}(\theta) - z_{12}^{R,\iota}(\theta)) \det(C_R)} - \\
&- \frac{k_R^{(l)}(z_{11}''(\theta) - z_{21}''(\theta))z_{21}^{R,\iota}(\theta)}{\det(C_R)} - \\
&- 2 \frac{k_R^{(l)} z_{21}'(\theta)(z_{11}'(\theta) - z_{21}'(\theta))}{(\det(C_R))} - \\
&- 2 \frac{k_R^{(l)} z_{22}^{R,\iota}(\theta)(z_{11}'(\theta) - z_{21}'(\theta))}{(z_{22}^{R,\iota}(\theta) - z_{12}^{R,\iota}(\theta)) \det(C_R)},
\end{aligned}$$

and hence

$$\begin{aligned}
(y_{12}^{R,\iota,(l)})''(\theta) &= \frac{z_{12}^{R,\iota}(\theta)((z_{22}^{R,\iota})''(\theta) - (z_{12}^{R,\iota})''(\theta))(\det(C_R) - k_R^{(l)}(z_{11}^{R,\iota}(\theta) - z_{21}^{R,\iota}(\theta))^2)}{(z_{22}^{R,\iota}(\theta) - ((z_{12}^{R,\iota}(\theta)))^2 \det(C_R))} - \\
&\quad - \frac{(z_{12}^{R,\iota})''(\theta)(\det(C_R) - k_R^{(l)}(z_{11}^{R,\iota}(\theta) - (z_{21}^{R,\iota}(\theta)))^2)}{(z_{22}^{R,\iota}(\theta) - z_{12}^{R,\iota}(\theta)) \det(C_R)} - \\
&\quad - 2 \frac{z_{12}^{R,\iota}(\theta)((z_{22}^{R,\iota})'(\theta) - ((z_{12}^{R,\iota})'(\theta)))^2 (\det(C_R) - k_R^{(l)}(z_{11}^{R,\iota}(\theta) - z_{21}^{R,\iota}(\theta))^2)}{(z_{22}^{R,\iota}(\theta) - z_{12}^{R,\iota}(\theta))^3 \det(C_R)} + \\
&\quad + 2 \frac{(z_{12}^{R,\iota})'(\theta)((z_{22}^{R,\iota})'(\theta) - (z_{12}^{R,\iota})'(\theta))(\det(C_R) - k_R^{(l)}(z_{11}^{R,\iota}(\theta) - z_{21}^{R,\iota}(\theta))^2)}{(z_{22}^{R,\iota}(\theta) - z_{12}^{R,\iota}(\theta))^2 \det(C_R)} - \\
&\quad - 4 \frac{k_R^{(l)} z_{12}^{R,\iota}(\theta)(z_{11}^{R,\iota}(\theta) - z_{21}^{R,\iota}(\theta))((z_{11}^{R,\iota})'(\theta) - (z_{21}^{R,\iota})'(\theta))((z_{22}^{R,\iota})'(\theta) - (z_{12}^{R,\iota})'(\theta))}{(z_{22}^{R,\iota}(\theta) - z_{12}^{R,\iota}(\theta))^2 \det(C_R)} + \\
&\quad + 4 \frac{k_R^{(l)}(z_{12}^{R,\iota})'(\theta)((z_{11}^{R,\iota})'(\theta) - (z_{21}^{R,\iota})'(\theta))(z_{11}^{R,\iota}(\theta) - z_{21}^{R,\iota}(\theta))}{(z_{22}^{R,\iota}(\theta) - z_{12}^{R,\iota}(\theta)) \det(C_R)} + \\
&\quad + \frac{k_R^{(l)}(z_{11}^{R,\iota}(\theta) - z_{21}^{R,\iota}(\theta))(z_{11}^{R,\iota})''(\theta)}{\det(C_R)} + \\
&\quad + 2 \frac{k_R^{(l)} z_{12}^{R,\iota}(\theta)(z_{11}^{R,\iota}(\theta) - z_{21}^{R,\iota}(\theta))((z_{11}^{R,\iota})''(\theta) - (z_{21}^{R,\iota})''(\theta))}{(z_{22}^{R,\iota}(\theta) - z_{12}^{R,\iota}(\theta)) \det(C_R)} + \\
&\quad + \frac{k_R^{(l)}((z_{11}^{R,\iota})''(\theta) - (z_{21}^{R,\iota})''(\theta)) z_{11}^{R,\iota}(\theta)}{\det(C_R)} + \\
&\quad + 2 \frac{k_R^{(l)}(z_{11}^{R,\iota})'(\theta)((z_{11}^{R,\iota})'(\theta) - (z_{21}^{R,\iota})'(\theta))}{(\det(C_R))} + \\
&\quad + 2 \frac{k_R^{(l)} z_{12}^{R,\iota}(\theta)((z_{11}^{R,\iota})'(\theta) - (z_{21}^{R,\iota})'(\theta))}{(z_{22}^{R,\iota}(\theta) - z_{12}^{R,\iota}(\theta)) \det(C_R)}.
\end{aligned}$$

Moreover, we get

$$\begin{aligned}
(y_{21}^{R,\iota,(l)})'(\theta) &= \frac{z_{21}^{R,\iota}(\theta)((z_{11}^{R,\iota})'(\theta) - (z_{21}^{R,\iota})'(\theta))}{(z_{11}^{R,\iota}(\theta) - z_{21}^{R,\iota}(\theta))^2} - \frac{(z_{21}^{R,\iota})'(\theta)}{z_{11}^{R,\iota}(\theta) - z_{21}^{R,\iota}(\theta)}, \\
(y_{21}^{R,\iota,(l)})''(\theta) &= \frac{z_{21}^{R,\iota}(\theta)((z_{11}^{R,\iota})''(\theta) - (z_{21}^{R,\iota})''(\theta))}{(z_{11}^{R,\iota}(\theta) - z_{21}^{R,\iota}(\theta))^2} - \frac{(z_{21}^{R,\iota})''(\theta)}{z_{11}^{R,\iota}(\theta) - z_{21}^{R,\iota}(\theta)} + \\
&\quad + \frac{2(z_{21}^{R,\iota})'(\theta)((z_{11}^{R,\iota})'(\theta) - (z_{21}^{R,\iota})'(\theta))}{(z_{11}^{R,\iota}(\theta) - z_{21}^{R,\iota}(\theta))^2} - \frac{2z_{21}^{R,\iota}(\theta)((z_{11}^{R,\iota})'(\theta) - (z_{21}^{R,\iota})'(\theta))^2}{(z_{11}^{R,\iota}(\theta) - z_{21}^{R,\iota}(\theta))^3}, \\
(y_{22}^{R,\iota,(l)})'(\theta) &= \frac{z_{11}^{R,\iota}(\theta)((z_{11}^{R,\iota})'(\theta) - (z_{21}^{R,\iota})'(\theta))}{(z_{11}^{R,\iota}(\theta) - z_{21}^{R,\iota}(\theta))^2} + \frac{(z_{11}^{R,\iota})'(\theta)}{z_{11}^{R,\iota}(\theta) - z_{21}^{R,\iota}(\theta)}, \\
(y_{22}^{R,\iota,(l)})''(\theta) &= - \frac{z_{11}^{R,\iota}(\theta)((z_{11}^{R,\iota})''(\theta) - (z_{21}^{R,\iota})''(\theta))}{(z_{11}^{R,\iota}(\theta) - z_{21}^{R,\iota}(\theta))^2} + \frac{(z_{11}^{R,\iota})''(\theta)}{z_{11}^{R,\iota}(\theta) - z_{21}^{R,\iota}(\theta)} - \\
&\quad - \frac{2(z_{11}^{R,\iota})'(\theta)((z_{11}^{R,\iota})'(\theta) - (z_{21}^{R,\iota})'(\theta))}{(z_{11}^{R,\iota}(\theta) - z_{21}^{R,\iota}(\theta))^2} + \frac{2z_{11}^{R,\iota}(\theta)((z_{11}^{R,\iota})'(\theta) - (z_{21}^{R,\iota})'(\theta))^2}{(z_{11}^{R,\iota}(\theta) - z_{21}^{R,\iota}(\theta))^3}.
\end{aligned}$$

Let  $\widehat{\theta}$  be a minimizer of the function  $g(k, \cdot, \iota, C)$ . If  $g''(k, \widehat{\theta}, \iota, C) \neq 0$ , then the Newton method is locally convergent with order 2. Anyway, we experimentally check that in our case the Newton method does not converge to a minimizer of the function  $g(k, \cdot, \iota, C)$ .

## 4.8 The Armijo Line Search

Another method based on the derivative of the function  $g(k, \cdot, \iota, C)$  is the *Armijo Line Search* (ALS). The relative algorithm is the following

```

function ALS( $k, C_R$ )
 $h = 0;$ 
 $\theta^{(1)} = (\varphi_R^{(1)} + \varphi_R^{(6)})/2;$ 
 $\theta^{(0)} = \theta^{(1)} + 2\varepsilon;$ 
while ( $|\theta^{(h+1)} - \theta^{(h)}| > \varepsilon$ ) do
     $h = h + 1;$ 
     $\theta^{(h+1)} = \theta^{(h)};$ 
     $\xi^{(h+1)} = g(k, \theta^{(h)}, \iota, C_R);$ 
     $der = g'(k, \theta^{(h)}, \iota, C_R);$ 
     $i = 0;$ 
     $\bar{\theta}^{(i)} = \theta^{(h)} - der;$ 
    while ( $\bar{\theta}^{(i)} \notin [\varphi_R^{(1)} + \eta, \varphi_R^{(6)} - \eta]$ ) do
         $i = i + 1;$ 
         $\bar{\theta}^{(i)} = \theta^{(h)} - der/2^i;$ 
    end while
     $\bar{\xi}^{(i)} = g(k, \bar{\theta}^{(i)}, \iota, C_R);$ 
    while ( $\bar{\xi}^{(i)} > \xi^{(h+1)} - |der|/2^{i+1}$ ) do
        if ( $\bar{\xi}^{(i)} < \xi^{(h+1)}$ ) then
             $\theta^{(h+1)} = \bar{\theta}^{(i)};$ 
             $\xi^{(h+1)} = \bar{\xi}^{(i)};$ 
        end if
         $i = i + 1;$ 
         $\bar{\theta}^{(i)} = \theta^{(h)} - der/2^i;$ 
         $\bar{\xi}^{(i)} = g(k, \bar{\theta}^{(i)}, \iota, C_R);$ 
    end while
    if ( $\bar{\xi}^{(i)} < \xi^{(h+1)}$ ) then
         $\theta^{(h+1)} = \bar{\theta}^{(i)};$ 
         $\xi^{(h+1)} = \bar{\xi}^{(i)};$ 
    end if
end while
return  $\theta^{(h+1)}$ 

```

where  $\varepsilon$  is a suitable threshold tolerance. The following result holds.

**Theorem 4.4.** (see also [8, Theorem 11], [48, Theorem 5.4.1.8]) *Let  $g(k, \cdot, \iota, C) : [a, b] \rightarrow \mathbb{R}_0^+$  and  $\theta^{(0)} \in [a, b]$  be such that the set  $K = \{\theta \in [a, b] : g(k, \theta, \iota, C_R) \leq g(k, \theta^{(0)}, \iota, C_R)\}$  is compact and  $g(k, \cdot, \iota, C_R) \in C^1(A)$ , where  $K \subset A$  and  $A \subset [a, b]$  is open. Then every*

sequence  $\{\theta^{(h)}\}_{h \in \mathbb{N}}$  defined by the ALS method has at least a limit point  $\theta \in K$ , and every limit point is a stationary point for  $h$ .

## 4.9 Comparison of the results

We initially compared the results of methods which do not use derivatives, like the SA, TPS, GSS, SPI-GSS algorithms. We tested them in restoring the documents of the Figures (12)-(15), which were mixed with the mixture matrix (67). In Tables 1 and 2 there are the calculation times and the mean square errors, indicated with MSE, with respect to the ideal documents of the four previously presented algorithms. From these tables we deduce that the algorithm SPI-GSS is the most efficient in terms of computational costs, among the considered ones. Moreover, we tested the SPI-GSS algorithm with  $\iota = 1$  fixed. The related results are presented in Table 3. We observe that the errors in terms of MSE are similar to those found in Table 2 where  $\iota$  was not fixed, while the computational costs are substantially halved. From now on, we do not minimize with respect to  $\iota$ , but we fix  $\iota = 1$ . Successively we compare the SPI-GSS technique with the Armijo algorithm. The results are shown in Table 3, in which we deduce that the SPI-GSS algorithm is more efficient, and thus we choose it for minimizing functions with MATODS techniques.

Ideal Document	SA			TPS		
	Time	MSE recto	MSE verso	Time	MSE recto	MSE verso
Figure 12	32.78 s	$1.15 \cdot 10^{-6}$	$2.24 \cdot 10^{-8}$	0.50 s	$1.09 \cdot 10^{-10}$	$2.94 \cdot 10^{-11}$
Figure 13	47.08 s	$3.01 \cdot 10^{-7}$	$8.36 \cdot 10^{-8}$	0.67 s	$4.16 \cdot 10^{-9}$	$6.54 \cdot 10^{-10}$
Figure 14	41.55 s	$7.40 \cdot 10^{-8}$	$1.02 \cdot 10^{-7}$	0.71 s	$6.74 \cdot 10^{-8}$	$9.44 \cdot 10^{-8}$
Figure 15	515.80 s	0.63	5.35	7.24 s	0.63	5.35

Table 1: Results obtained by algorithms SA and TPS.

Ideal Document	GSS			SPI-GSS		
	Time	MSE recto	MSE verso	Time	MSE recto	MSE verso
Figure 12	0.42 s	$2.75 \cdot 10^{-10}$	$3.00 \cdot 10^{-12}$	0.40 s	$1.47 \cdot 10^{-10}$	$1.71 \cdot 10^{-11}$
Figure 13	0.64 s	$5.30 \cdot 10^{-9}$	$7.51 \cdot 10^{-10}$	0.61 s	$5.62 \cdot 10^{-9}$	$9.02 \cdot 10^{-10}$
Figure 14	0.59 s	$6.96 \cdot 10^{-8}$	$9.74 \cdot 10^{-8}$	0.56 s	$6.92 \cdot 10^{-8}$	$9.68 \cdot 10^{-8}$
Figure 15	7.64 s	0.63	5.35	5.37 s	0.63	5.35

Table 2: Results obtained by algorithms GSS and SPI-GSS.

## 5 A not translation invariant model

Actually the linear model is not always realistic, because in many ancient documents the infiltration of the ink is not spatially uniform. Thus, in order to obtain a not translation invariant model for our problem, we proceed as follows. For the red component we consider

Ideal Document	SPI-GSS			ALS		
	Time	MSE recto	MSE verso	Time	MSE recto	MSE verso
Figure 12	0.20 s	$1.34 \cdot 10^{-10}$	$4.26 \cdot 10^{-11}$	0.47 s	$3.78 \cdot 10^{-10}$	$1.28 \cdot 10^{-15}$
Figure 13	0.30 s	$3.69 \cdot 10^{-9}$	$6.27 \cdot 10^{-10}$	0.95 s	$6.05 \cdot 10^{-9}$	$9.12 \cdot 10^{-10}$
Figure 14	0.27 s	$6.88 \cdot 10^{-8}$	$9.63 \cdot 10^{-8}$	1.27 s	$7.02 \cdot 10^{-8}$	$9.81 \cdot 10^{-8}$
Figure 15	3.28 s	0.63	5.35	6.71 s	0.63	5.35

Table 3: Results obtained by algorithms SPI-GSS, NL-SOR and ALS by fixing  $\iota = 1$ .

different subimages  $\bar{x}_R^{(p,q)}$ ,  $p, q = 1, \dots, \lceil \frac{n-\bar{n}}{\nu} \rceil$ , of a fixed size  $\bar{n} \times \bar{n}$  and solve the linear problem in each subimage. These subimages are chosen in such a way that the range of each of them is obtained from the previous range, by shifting  $\nu$  pixels in the horizontal or vertical way. Finally, we pose the light intensity value of every pixel of the estimated source  $\tilde{s}_R$  as the arithmetic mean of the light intensity of estimated subsources value in which such a pixel belongs. If we assume that  $n$  and  $\bar{n}$  are multiples of  $\nu$ , then the main procedure for the red component is the following.

```

function NIT-MATODS( $x_R$ )
  Initialize  $\tilde{s}_R$  as a null matrix;
  for  $p = 1$  to  $n - \bar{n}$  with step  $\nu$  do
    for  $q = 1$  to  $n - \bar{n}$  with step  $\nu$  do
      for  $i = 1$  to  $\bar{n}$  do
        for  $j = 1$  to  $\bar{n}$  do
           $\bar{x}_{rR i,j}^{(p,q)} = x_{rR i+p,j+q};$ 
           $\bar{x}_{vR i,j}^{(p,q)} = x_{vR i+p,j+q};$ 
        end for
      end for
       $\bar{s}_R^{(p,q)} = \text{MATODS}(\bar{x}_R^{(p,q)})$ 
       $dim_y = \min\{\bar{n}/\nu, \lceil (i+p)/\nu \rceil, \lceil (n+1-i-p)/\nu \rceil\};$ 
       $dim_x = \min\{\bar{n}/\nu, \lceil (j+q)/\nu \rceil, \lceil (n+1-j-q)/\nu \rceil\};$ 
      for  $i = 1$  to  $\bar{n}$  do
        for  $j = 1$  to  $\bar{n}$  do
           $\tilde{s}_{rR i+p,j+q} = \tilde{s}_{rR i+p,j+q} + \bar{s}_{rR i,j}^{(p,q)} / (dim_x \cdot dim_y);$ 
           $\tilde{s}_{vR i+p,j+q} = \tilde{s}_{vR i+p,j+q} + \bar{s}_{vR i,j}^{(p,q)} / (dim_x \cdot dim_y);$ 
        end for
      end for
    end for
  end for
return  $\tilde{s}_R$ 

```

We refer to this method as *Not Invariant for Translation MATODS* (NIT-MATODS) algorithm.

## 6 Experimental results

We have implemented both MATODS and NIT-MATODS algorithms in C language in an Ubuntu operating system on a computer with a  $2.80GHz$  processor. In this section we illustrate our experimental results. In particular we first compare the MATODS algorithm with other methods existing in literature and then we see how the NIT-MATODS algorithm works in restoring real ancient documents.

For restoring color image documents of dimension  $256 \times 256$  in most cases MATODS has a computation time less than one second, as we saw in the previous section, so we compare it with other fast and unsupervised methods as FastICA, SW, W and PCA algorithms. We proceed as follows. First, we generate a synthetic data document from a given mixing matrix and a fixed source document using the linear model in equation (3). Then we compare the estimated sources with the given source document by means of the *Mean Squared Error* (MSE) and the *Peak Signal-to-Noise Ratio* (PSNR). Since we deal with data overlapping matrices, in order to better compare the W, SW and PCA techniques with our algorithm, we apply the pre-processing phase as in equation (5) also to such algorithms. At the end of execution of FastICA, SW, W and PCA algorithms, we normalize the estimated mixture matrices in order to make them stochastic. Moreover, for these algorithms, as we assumed that the mixing matrix  $A_R$  is a diagonally predominant matrix, if the estimated matrix does not have this property, then we permute the estimated source recto image with the corresponding verso, in order to achieve this condition, and then we apply an orthogonal projection operator in order to have estimated results in the space  $[0, 255]^{n^2 \times 6}$ . As source documents we consider the  $256 \times 256$  documents in Figures 12-18.

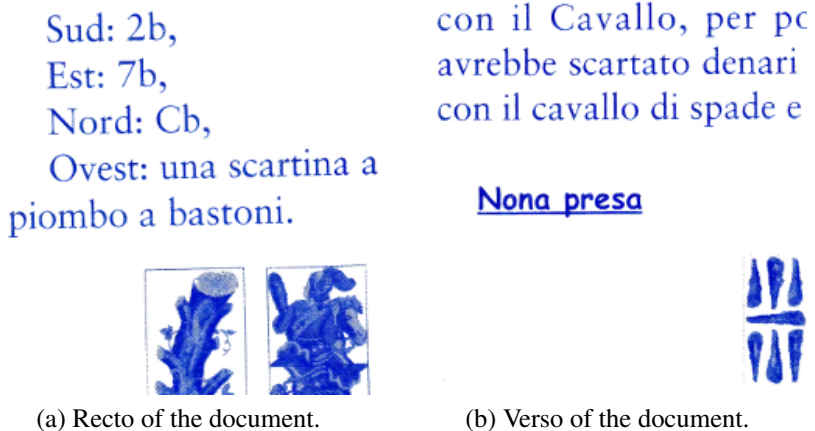
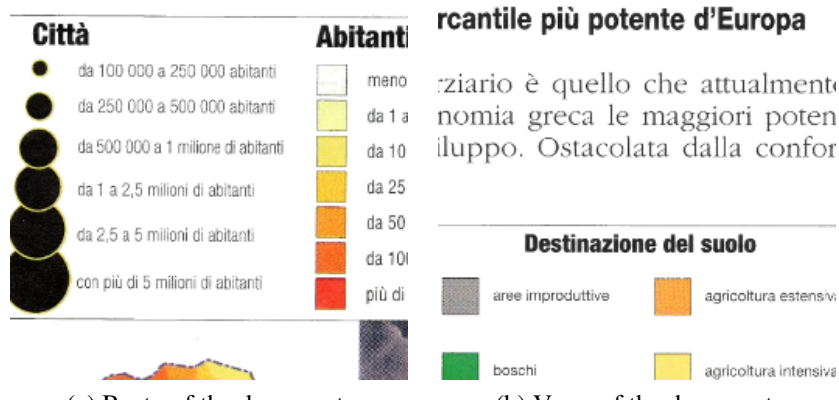


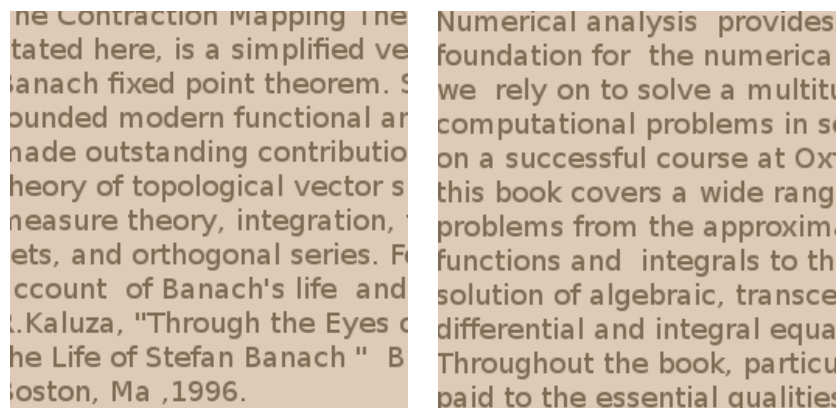
Figure 12: Ideal sources.



(a) Recto of the document.

(b) Verso of the document.

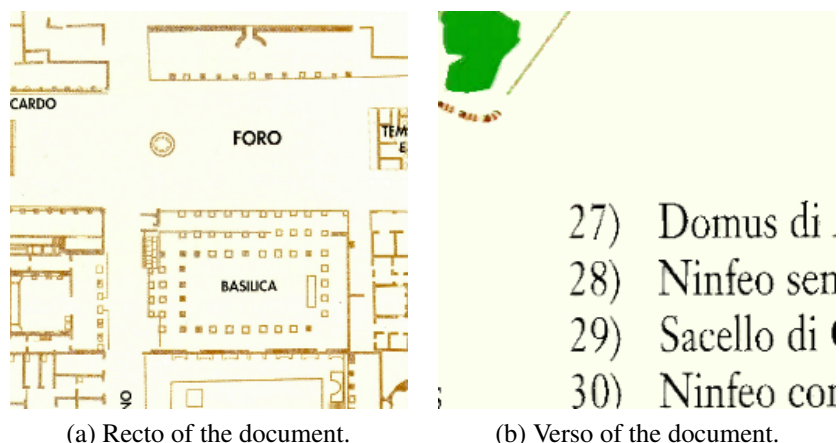
Figure 13: Ideal sources.



(a) Recto of the document.

(b) Verso of the document.

Figure 14: Ideal sources



(a) Recto of the document.

(b) Verso of the document.

Figure 15: Ideal sources.

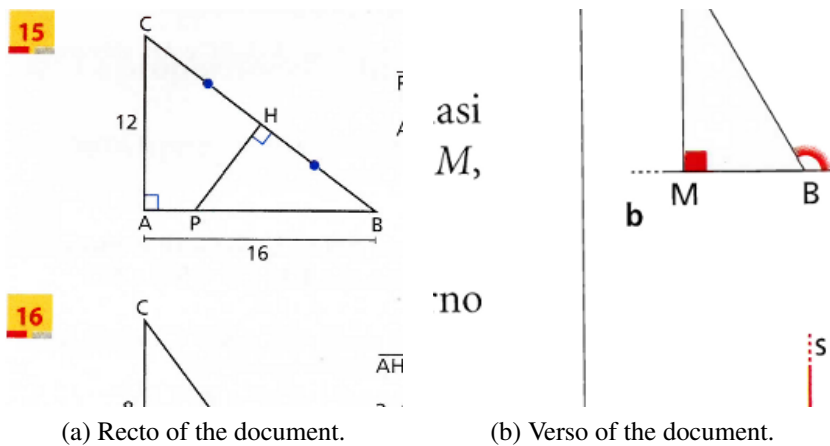


Figure 16: Ideal sources.

tagliare an-  
ne ed incol-  
nzionato in  
st'ultima doma-  
me il tema della  
non sia solame-

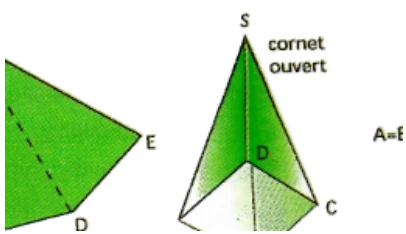


Figure 17: Ideal sources.

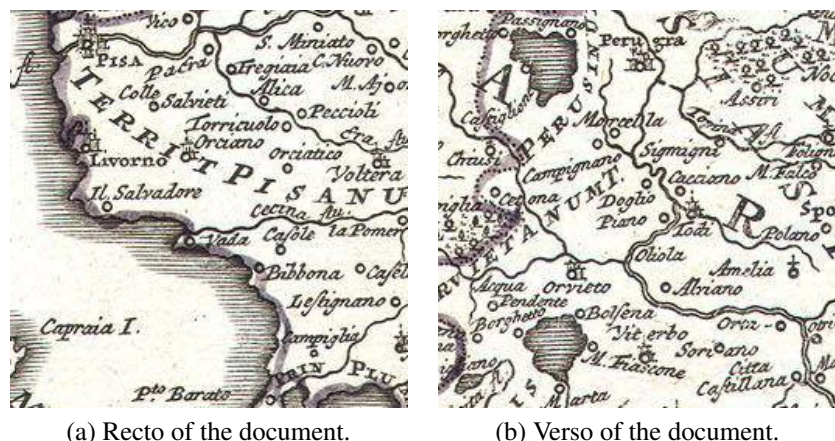


Figure 18: Ideal sources.

First, we have mixed our documents with the mixture matrices

$$A_R = \begin{pmatrix} 0.7 & 0.3 \\ 0.3 & 0.7 \end{pmatrix}, A_G = \begin{pmatrix} 0.7 & 0.3 \\ 0.3 & 0.7 \end{pmatrix}, A_B = \begin{pmatrix} 0.7 & 0.3 \\ 0.3 & 0.7 \end{pmatrix}. \quad (66)$$

In Tables 4 and 5 there are the MSE with respect to the original documents obtained by means of the algorithms MATODS, FastICA, SW, W and PCA. Note that, in general, the errors obtained by means of the W and PCA algorithms are larger than the corresponding ones obtained by MATODS, FastICA and SW. This confirms the observations made in [53]. Thus, being the level of mixing degradation in the subsequent experimental tests greater than the one here presented, from now on we give the results related only to MATODS, FastICA and SW algorithms. Note that, in such tables, the MATODS algorithm obtains always a MSE smaller than the other ones.

Ideal Document	MATODS		FastICA		SW	
	MSE recto	MSE verso	MSE recto	MSE verso	MSE recto	MSE verso
Figure 12	$1.54 \cdot 10^{-10}$	$4.15 \cdot 10^{-11}$	53.27	1.45	0.15	4.87
Figure 13	$3.56 \cdot 10^{-9}$	$6.21 \cdot 10^{-10}$	17.71	12.14	15.84	40.66
Figure 14	$6.93 \cdot 10^{-8}$	$9.69 \cdot 10^{-8}$	171.23	30.92	74.87	68.74
Figure 15	1.09	6.99	20.62	25.67	45.40	20.41
Figure 16	$1.25 \cdot 10^{-5}$	$5.04 \cdot 10^{-12}$	4.46	1.78	0.22	1.86
Figure 17	$1.13 \cdot 10^{-9}$	$4.54 \cdot 10^{-11}$	130.81	24.84	21.77	34.97
Figure 18	0.15	0.19	42.77	70.79	341.69	342.18

Table 4: Errors of algorithms MATODS, FastICA and SW with the mixture matrix as in (66) in terms of MSE.

Ideal Document	W		PCA	
	MSE recto	MSE verso	MSE recto	MSE verso
Figure 12	55.56	2.38	890.46	473.76
Figure 13	134.82	30.12	1035.10	853.17
Figure 14	40.20	43.94	3610.01	3794.41
Figure 15	39.07	106.85	1636.92	899.77
Figure 16	22.57	2.16	478.03	382.44
Figure 17	296.42	36.80	525.31	112.09
Figure 18	245.89	262.93	9249.91	10330.02

Table 5: Errors of the algorithms W and PCA with the mixture matrix as in (66) in terms of MSE.

In Tables 6 and 7 there are the PSNR with respect to the same algorithms. The PSNR is used to evaluate the quality of an image compressed in connection with the original one. This index of quality of images is defined as the ratio between the greatest power of a signal and the noise power, which can invalidate the faithfulness of its compressed representation.

Since several signals have a very large dynamic wideness, the PSNR is in general expressed in terms of logarithmic scale of decibels. In particular, it is

$$PSNR = 20 \log_{10} \left( \frac{255}{\sqrt{MSE}} \right).$$

As this function is decreasing, to evaluate the goodness of the results in terms of PSNR one has to consider the highest values which correspond to the lowest ones in terms of MSE.

Ideal document	MATODS		FastICA		SW	
	PSNR recto	PSNR verso	PSNR recto	PSNR verso	PSNR recto	PSNR verso
Figure 12	146.27	151.95	30.87	46.53	56.48	41.26
Figure 13	132.62	140.20	35.65	37.29	36.13	32.04
Figure 14	119.73	118.27	25.80	33.23	29.39	29.76
Figure 15	47.75	39.69	34.99	34.04	31.56	35.03
Figure 16	97.18	161.11	41.64	45.62	54.63	45.43
Figure 17	137.59	151.56	26.96	34.18	34.75	32.69
Figure 18	56.23	55.26	31.82	29.63	22.79	22.79

Table 6: Errors of the algorithms MATODS, FastICA and SW with the mixture matrix as in (66) in terms of PSNR.

Ideal document	W		PCA	
	PSNR recto	PSNR verso	PSNR recto	PSNR verso
Figure 12	30.68	44.36	18.64	21.38
Figure 13	26.83	33.34	17.98	18.82
Figure 14	32.09	31.70	12.56	12.34
Figure 15	32.21	27.84	15.99	18.59
Figure 16	34.60	44.78	21.34	22.31
Figure 17	23.41	32.47	20.93	27.64
Figure 18	24.22	23.93	8.47	7.99

Table 7: Errors of the algorithms W and PCA with the mixture matrix as in (66) in terms of PSNR.

In Table 8 there are the errors in terms of MSE related to the mixture matrices obtained by all considered algorithms. Note that the difference between the ideal mixing matrices in (66) and the MATODS estimated mixing matrices is substantially zero.

Document	MATODS	FastICA	SW	W	PCA
Figure 12	$9.95 \cdot 10^{-15}$	0.0052	$6.71 \cdot 10^{-4}$	0.0030	0.020
Figure 13	$2.29 \cdot 10^{-13}$	0.0031	0.0017	0.0046	0.020
Figure 14	$3.32 \cdot 10^{-11}$	0.049	0.0026	0.0049	0.038
Figure 15	$1.80 \cdot 10^{-4}$	0.012	0.0037	0.0073	0.021
Figure 16	$1.61 \cdot 10^{-9}$	0.0020	$5.30 \cdot 10^{-4}$	0.0023	0.025
Figure 17	$3.97 \cdot 10^{-14}$	0.019	0.0053	0.011	0.0083
Figure 18	$1.71 \cdot 10^{-5}$	0.0066	0.0048	0.0086	0.038

Table 8: Errors of the mixing matrices estimated by the algorithms MATODS, FastICA and SW with respect to the mixture matrix as in (66) in terms of MSE.

In Figures 19 (a) and (b) there are the mixtures of the document obtained with the mask (66), while in Figures 19 (c) and (d) the results of the MATODS are presented. Figures 20 (a) and (b) contain the results obtained by means of the FastICA, while in Figures 20 (c) and (d) the results obtained by the SW algorithm are presented. In Figures 21 (a) and (b) there are the results obtained with the W technique, while Figures 21 (c) and (d) contain the results of the PCA algorithm.

The image shows a rectangular document page with a mix of two different texts. One text is in a dark gray font and the other in a lighter gray font. The dark text discusses the Banach fixed point theorem and its applications in functional analysis. The light text is a numerical analysis textbook summary.

(a) Recto of the mixture.

The image shows a rectangular document page with a mix of two different texts. One text is in a dark gray font and the other in a lighter gray font. The dark text discusses the Banach fixed point theorem and its applications in functional analysis. The light text is a numerical analysis textbook summary.

(b) Verso of the mixture.

The image shows a rectangular document page with a mix of two different texts. One text is in a dark gray font and the other in a lighter gray font. The dark text discusses the Banach fixed point theorem and its applications in functional analysis. The light text is a numerical analysis textbook summary.

(c) Recto estimated by MATODS.

The image shows a rectangular document page with a mix of two different texts. One text is in a dark gray font and the other in a lighter gray font. The dark text discusses the Banach fixed point theorem and its applications in functional analysis. The light text is a numerical analysis textbook summary.

(d) Verso estimated by MATODS.

Figure 19: Document in Figure 14 mixed with a mixture matrix as in (66).

The Contraction Mapping Theorem stated here, is a simplified version of the Banach fixed point theorem. S. Banach made outstanding contributions to the theory of topological vector spaces, measure theory, integration, sets, and orthogonal series. For an account of Banach's life and work see Kaluza, "Through the Eyes of a Mathematician: A Short Account of the Life of Stefan Banach." Boston, Ma., 1996.

(a) Recto estimated by FastICA.

The Contraction Mapping Theorem stated here, is a simplified version of the Banach fixed point theorem. S. Banach made outstanding contributions to the theory of topological vector spaces, measure theory, integration, sets, and orthogonal series. For an account of Banach's life and work see Kaluza, "Through the Eyes of a Mathematician: A Short Account of the Life of Stefan Banach." Boston, Ma., 1996.

(c) Recto estimated by SW.

Numerical analysis provides the foundation for the numerical methods we rely on to solve a multitude of computational problems in science and engineering. This book is based on a successful course at Oxford University and covers a wide range of problems from the approximation of functions and integrals to the solution of algebraic, transcendental and differential equations. Throughout the book, particular attention is paid to the essential qualities

(b) Verso estimated by FastICA.

Numerical analysis provides the foundation for the numerical methods we rely on to solve a multitude of computational problems in science and engineering. This book is based on a successful course at Oxford University and covers a wide range of problems from the approximation of functions and integrals to the solution of algebraic, transcendental and differential equations. Throughout the book, particular attention is paid to the essential qualities

(d) Verso estimated by SW.

Figure 20: Document in Figure 14 mixed by a mixture matrix as in (66).

The Contraction Mapping Theorem stated here, is a simplified version of the Banach fixed point theorem. It founded modern functional analysis and made outstanding contributions to the theory of topological vector spaces, measure theory, integration, Banach algebras, and orthogonal series. For an account of Banach's life and work see Kaluza, "Through the Eyes of a Mathematician: A Short Account of the Life of Stefan Banach." Boston, MA, 1996.

(a) Recto estimated by W.

The Contraction Mapping Theorem stated here, is a simplified version of the Banach fixed point theorem. It founded modern functional analysis and made outstanding contributions to the theory of topological vector spaces, measure theory, integration, Banach algebras, and orthogonal series. For an account of Banach's life and work see Kaluza, "Through the Eyes of a Mathematician: A Short Account of the Life of Stefan Banach." Boston, MA, 1996.

(c) Recto estimated by PCA.

Numerical analysis provides the foundation for the numerical methods we rely on to solve a multitude of computational problems in science and engineering. Based on a successful course at Oxford University, this book covers a wide range of problems from the approximation of functions and integrals to the solution of algebraic, transcendental, differential and integral equations. Throughout the book, particular attention is paid to the essential qualities

(b) Verso estimated by W.

Numerical analysis provides the foundation for the numerical methods we rely on to solve a multitude of computational problems in science and engineering. Based on a successful course at Oxford University, this book covers a wide range of problems from the approximation of functions and integrals to the solution of algebraic, transcendental, differential and integral equations. Throughout the book, particular attention is paid to the essential qualities

(d) Verso estimated by PCA.

Figure 21: Document in Figure 14 mixed by a mixture matrix as in (66).

Now we consider the same documents mixed by the following mixture matrices

$$A_R = \begin{pmatrix} 0.6 & 0.4 \\ 0.4 & 0.6 \end{pmatrix}, A_G = \begin{pmatrix} 0.6 & 0.4 \\ 0.4 & 0.6 \end{pmatrix}, A_B = \begin{pmatrix} 0.6 & 0.4 \\ 0.4 & 0.6 \end{pmatrix}. \quad (67)$$

In Table 9 the errors in terms of MSE are illustrated. In Table 10 the PSNR with respect to the original source documents of the estimated ones by the considered algorithms are presented. Table 11 contains the errors in terms of the MSE related to the obtained mixing matrices. We observe that MATODS allows to obtain better results than the other algorithms, as it is readily seen.

Ideal Document	MATODS		FastICA		SW	
	MSE recto	MSE verso	MSE recto	MSE verso	MSE recto	MSE verso
Figure 12	$1.34 \cdot 10^{-10}$	$4.26 \cdot 10^{-11}$	58.60	2.03	0.89	4.56
Figure 13	$3.69 \cdot 10^{-9}$	$6.27 \cdot 10^{-10}$	21.89	14.76	21.92	38.51
Figure 14	$6.88 \cdot 10^{-8}$	$9.63 \cdot 10^{-8}$	245.40	111.11	73.94	69.74
Figure 15	0.63	5.35	61.37	118.79	42.99	24.11
Figure 16	$1.24 \cdot 10^{-5}$	$5.42 \cdot 10^{-12}$	5.82	2.30	0.56	1.76
Figure 17	$9.07 \cdot 10^{-10}$	$3.67 \cdot 10^{-11}$	491.63	198.74	63.14	37.30
Figure 18	0.12	3.46	37.17	58.61	337.60	344.68

Table 9: Errors of the algorithms MATODS, FastICA and SW with the mixture matrix as in (67) in terms of MSE.

Ideal document	MATODS		FastICA		SW	
	PSNR recto	PSNR verso	PSNR recto	PSNR verso	PSNR recto	PSNR verso
Figure 12	146.87	151.84	30.45	45.07	48.64	41.54
Figure 13	132.46	140.16	34.73	36.44	34.72	32.28
Figure 14	119.76	118.30	24.23	27.67	29.44	29.70
Figure 15	50.16	40.85	30.25	27.38	31.80	34.31
Figure 16	97.18	160.79	40.48	44.52	50.62	45.67
Figure 17	138.55	152.49	21.21	25.15	30.13	32.41
Figure 18	57.36	42.74	32.43	30.45	22.85	22.76

Table 10: Errors of the algorithms MATODS, FastICA and SW with the mixture matrix as in (67) in terms of PSNR.

In Figures 22 (a) and (b) there are the mixtures of the document obtained with the mask (67), while in Figures 22 (c) and (d) the results of the MATODS are presented. Figures 23 (a) and (b) contain the results obtained with the FastICA. In Figures 23 (c) and (d) the results obtained by means of the SW technique are presented. Note that in the SW results the colors are not quite correct. Figures 24 (a) and (b) contain the images related to the document in Figure 17 mixed by the mixture matrix (67). In Figures 24 (c) and (d) it is possible to observe the results obtained by the MATODS, while in Figures 24 (e) and (f) there are the results got by means of the FastICA. Observe that, in the results obtained with the FastICA, there are still some ink infiltrations, while by means of the MATODS we obtain substantially perfectly clean images.

Document	MATODS	FastICA	SW
Figure 12	$6.73 \cdot 10^{-15}$	0.0058	$3.46 \cdot 10^{-4}$
Figure 13	$2.25 \cdot 10^{-13}$	0.0057	$6.45 \cdot 10^{-4}$
Figure 14	$3.29 \cdot 10^{-11}$	0.024	$6.43 \cdot 10^{-4}$
Figure 15	$1.07 \cdot 10^{-4}$	0.0074	0.0013
Figure 16	$1.44 \cdot 10^{-9}$	0.0027	$2.61 \cdot 10^{-4}$
Figure 17	$3.02 \cdot 10^{-14}$	0.012	0.0023
Figure 18	$1.29 \cdot 10^{-4}$	0.0055	0.0012

Table 11: Errors of the estimated mixing matrices by the algorithms MATODS, FastICA and SW with the mixture matrix as in (67) in terms of MSE.

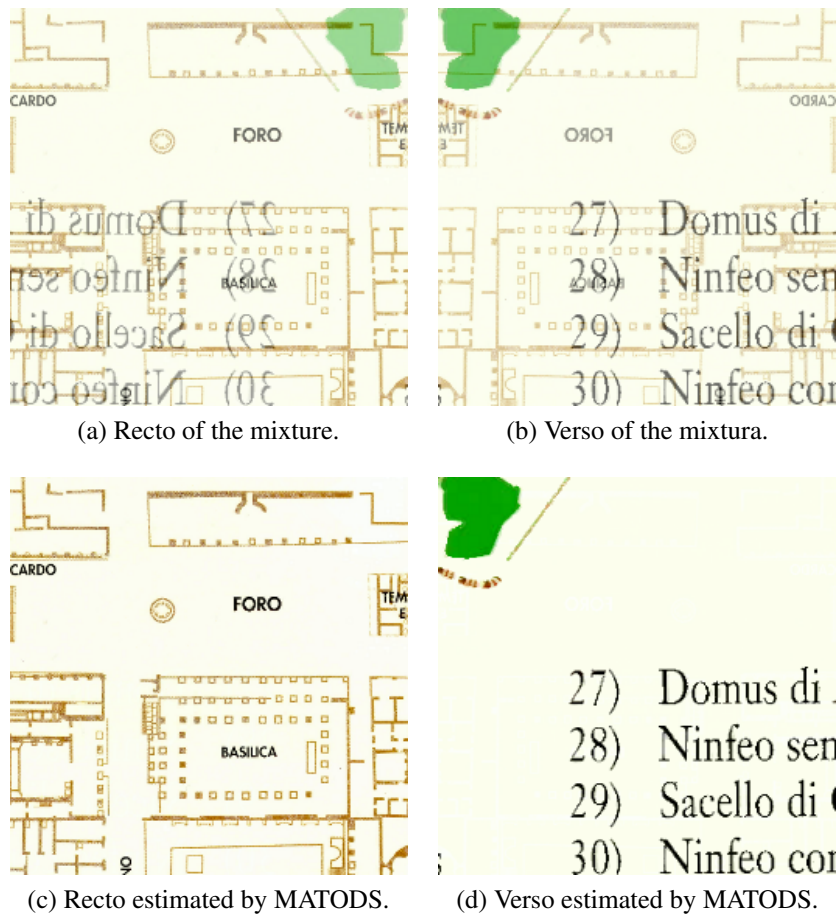
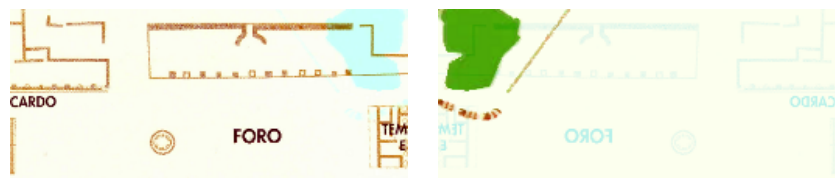


Figure 22: Document in Figure 15 mixed with a mixture matrix as in (67).



(a) Recto estimated by FastICA.



- 27) Domus di  
28) Ninfeo sen  
29) Sacello di  
30) Ninfeo cor

(b) Verso estimated by FastICA.



(c) Recto estimated by SW.



- 27) Domus di  
28) Ninfeo sen  
29) Sacello di  
30) Ninfeo cor

(d) Verso estimated by SW.

Figure 23: Document in Figure 15 mixed with a mixture matrix as in (67).

tagliare anche ed incol-

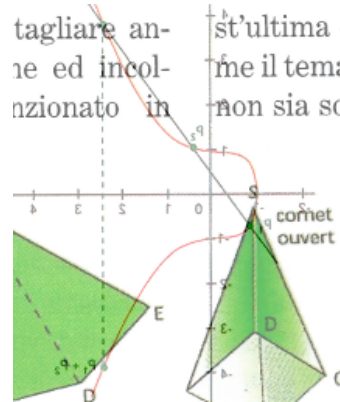
st'ultima doma  
me il tema della  
non sia solame

SA, nu-  
: le imi-  
nte, rdi,  
o in bro  
nde rdy  
sta, fet-  
ver

nzionato in

b E S T 0

$s^2$



(a) Recto of the mixture.

tagliare anche ed incol-

st'ultima doma  
me il tema della  
non sia solame

SA, nu-  
: le imi-  
nte, rdi,  
o in bro  
nde rdy  
sta, fet-  
ver

nzionato in

b E S T 0

$s^2$



(c) Recto estimated by MATODS.

tagliare anche ed incol-

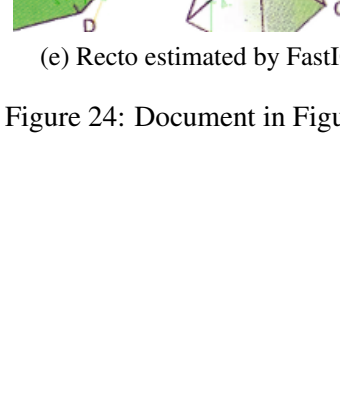
st'ultima doma  
me il tema della  
non sia solame

SA, nu-  
: le imi-  
nte, rdi,  
o in bro  
nde rdy  
sta, fet-  
ver

nzionato in

b E S T 0

$s^2$



(e) Recto estimated by FastICA.

tagliare anche ed incol-

st'ultima doma  
me il tema della  
non sia solame

SA, nu-  
: le imi-  
nte, rdi,  
o in bro  
nde rdy  
sta, fet-  
ver

nzionato in

b E S T 0

$s^2$

Now we consider the following mixture matrices:

$$A_R = \begin{pmatrix} 0.55 & 0.45 \\ 0.45 & 0.55 \end{pmatrix}, A_G = \begin{pmatrix} 0.55 & 0.45 \\ 0.45 & 0.55 \end{pmatrix}, A_B = \begin{pmatrix} 0.55 & 0.45 \\ 0.45 & 0.55 \end{pmatrix}. \quad (68)$$

Note that the mixtures obtained with such matrices have the recto very similar to the verso, and the problem turns out to be difficult to solve, since such matrices are more ill-conditioned than the previous ones. In Table 12 there are the errors in terms of MSE given by the examined algorithms. The PSNR of the involved algorithms are presented in Table 13. In Table 14 there are the errors in terms of MSE of the estimated mixture matrices.

Ideal Document	MATODS		FastICA		SW	
	MSE recto	MSE verso	MSE recto	MSE verso	MSE recto	MSE verso
Figure 12	$5.76 \cdot 10^{-11}$	$5.88 \cdot 10^{-11}$	97.82	27.61	2.04	3.66
Figure 13	$4.49 \cdot 10^{-9}$	$8.52 \cdot 10^{-10}$	192.34	105.86	27.03	34.02
Figure 14	$6.95 \cdot 10^{-8}$	$9.71 \cdot 10^{-8}$	381.62	331.93	73.07	70.62
Figure 15	0.44	4.61	198.80	243.44	39.20	27.40
Figure 16	$1.24 \cdot 10^{-5}$	$3.67 \cdot 10^{-12}$	49.58	26.03	1.04	1.46
Figure 17	$4.44 \cdot 10^{-10}$	$2.50 \cdot 10^{-11}$	951.51	807.94	93.28	34.08
Figure 18	0.11	8.06	118.10	193.36	334.49	347.00

Table 12: Errors of the algorithms MATODS, FastICA and SW with the mixture matrix as in (68) in terms of MSE.

Ideal document	MATODS		FastICA		SW	
	PSNR recto	PSNR verso	PSNR recto	PSNR verso	PSNR recto	PSNR verso
Figure 12	150.53	150.43	28.23	33.72	45.03	42.49
Figure 13	131.61	138.83	25.29	27.88	33.81	32.81
Figure 14	119.71	118.26	22.32	22.92	29.49	29.64
Figure 15	51.69	41.49	25.15	24.27	32.20	33.75
Figure 16	97.18	162.48	31.18	33.98	47.98	46.49
Figure 17	141.65	154.16	18.35	19.06	28.43	32.81
Figure 18	57.54	39.07	27.41	25.27	22.89	22.73

Table 13: Errors of the algorithms MATODS, FastICA and SW with the mixture matrix as in (68) in terms of PSNR.

In Figures 25 (a) and (b) there are the mixtures of the document in Figure 12 obtained by means of the mixture matrices (68). In Figures 12 (c) and (d) there are the results obtained with the MATODS and in Figures 12 (e) and (f) there are those got by means of the FastICA. Figures 26 (a) and (b) show the mixtures of the document in Figure 13 obtained by means of the mixture matrices (68). In Figures 13 (c) and (d) we have the results obtained with the MATODS and in Figures 13 (e) and (f) there are those obtained by means of the FastICA. In Figures 27 (a) and (b) there are the mixtures of the document in Figure 16 obtained by means of the mixture matrices (68). In Figures 27 (c) and (d) we

Document	MATODS	FastICA	SW
Figure 12	$4.28 \cdot 10^{-15}$	0.0032	$1.22 \cdot 10^{-4}$
Figure 13	$2.89 \cdot 10^{-13}$	0.0028	$2.01 \cdot 10^{-4}$
Figure 14	$3.32 \cdot 10^{-11}$	0.026	$1.61 \cdot 10^{-4}$
Figure 15	$9.27 \cdot 10^{-5}$	0.0084	$4.06 \cdot 10^{-4}$
Figure 16	$1.40 \cdot 10^{-9}$	0.0017	$9.08 \cdot 10^{-5}$
Figure 17	$1.47 \cdot 10^{-14}$	0.015	$7.38 \cdot 10^{-4}$
Figure 18	$2.73 \cdot 10^{-4}$	0.0027	$3.01 \cdot 10^{-4}$

Table 14: Errors of the estimated mixing matrices by the algorithms MATODS, FastICA and SW with the mixture matrix as in (68) in terms of MSE.

have the results obtained with the MATODS and in Figures 27 (e) and (f) there are those got by means of the FastICA. Figures 18 (a) and (b) contain the mixtures of the document in Figure 18 obtained by means of the mixture matrices (68). In Figures 18 (c) and (d) we show the results obtained with the MATODS, and in Figures 18 (e) and (f) there are those got in connection with the FastICA. Even in this context the MATODS technique obtains the best results.

Sud: 2b,  
Est: 7b,  
Nord: Cb,  
Ovest: una scartina a piombo a bastoni.



(a) Recto of the mixture.

Sud: 2b,  
Est: 7b,  
Nord: Cb,  
Ovest: una scartina a piombo a bastoni.



(c) Recto estimated by MATODS.

Sud: 2b,  
Est: 7b,  
Nord: Cb,  
Ovest: una scartina a piombo a bastoni.



(e) Recto estimated by FastICA.

con il Cavallo, per pc  
avrebbe scartato denari  
con il cavallo di spade e

Ovest: una scartina a  
Nona presa



(b) Verso of the mixture.

con il Cavallo, per pc  
avrebbe scartato denari  
con il cavallo di spade e

Nona presa



(d) Verso estimated by MATODS.

con il Cavallo, per pc  
avrebbe scartato denari  
con il cavallo di spade e

Ovest: una scartina a  
Nona presa



(f) Verso estimated by FastICA.

Figure 25: Document in Figure 12 mixed by a mixture matrix as in (68).

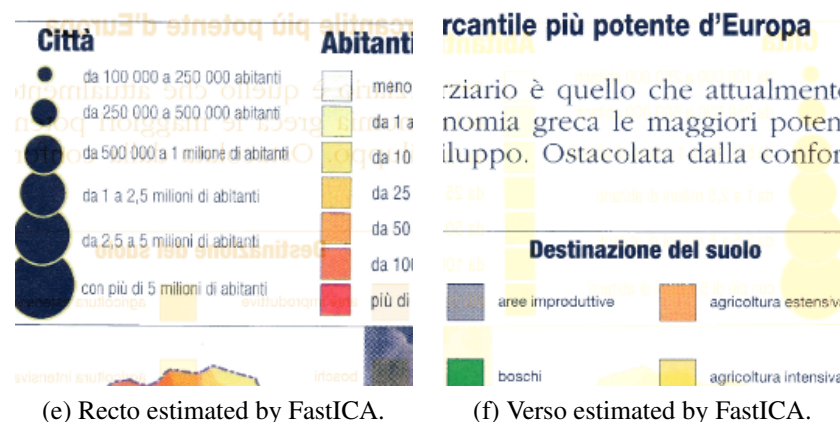
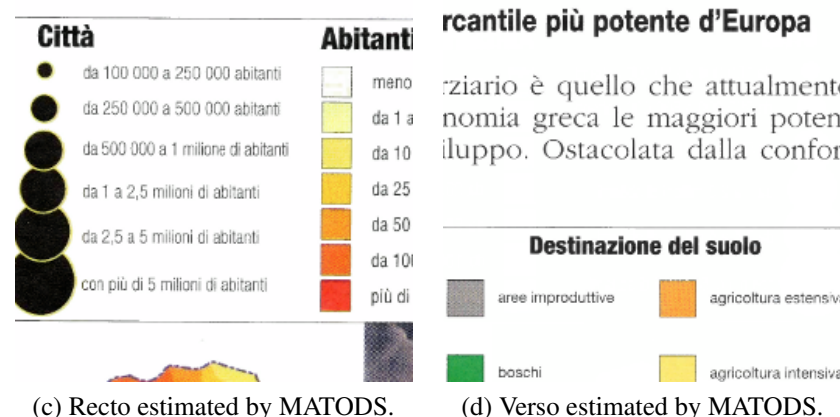
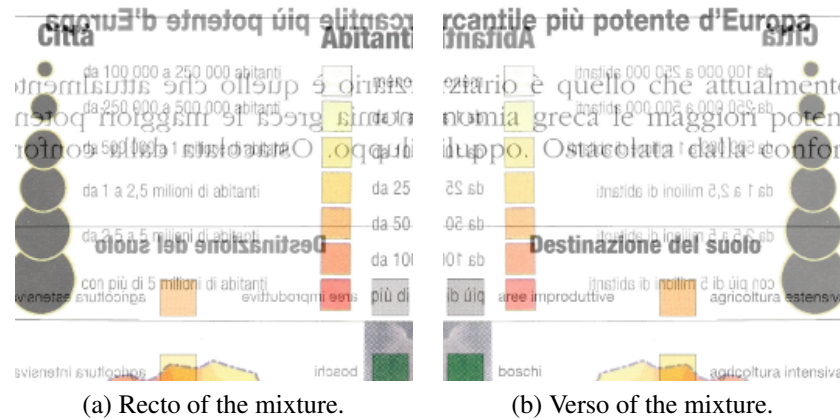


Figure 26: Document in Figure 13 mixed by a mixture matrix as in (68).

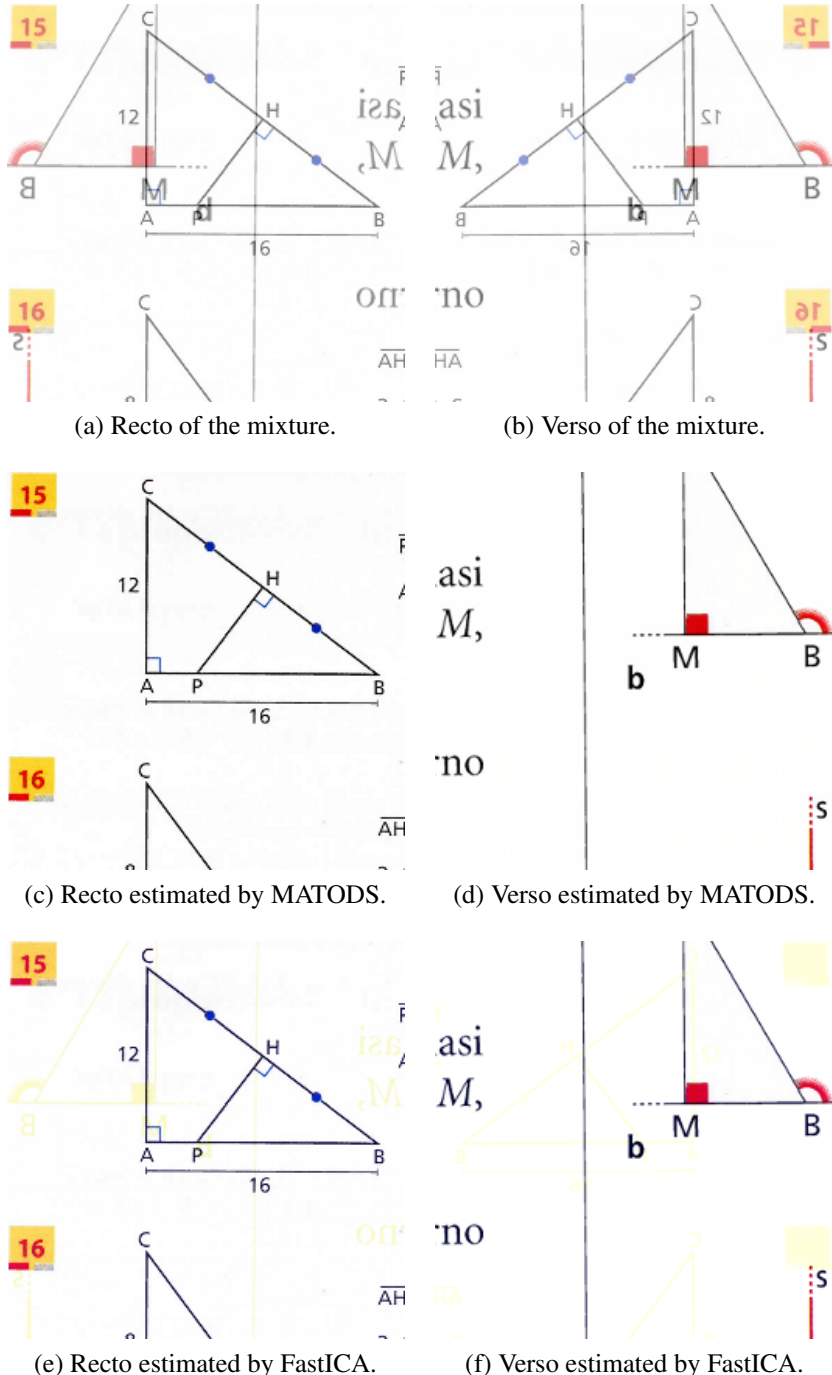


Figure 27: Document in Figure 16 mixed by a mixture matrix as in (68).



(a) Recto of the mixture.



(b) Verso of the mixture.



(c) Recto estimated by MATODS.



(d) Verso estimated by MATODS.



(e) Recto estimated by FastICA.



(f) Verso estimated by FastICA.

Figure 28: Document in Figure 18 mixed by a mixture matrix as in (68).

Now we deal with not symmetric mixture matrices. For example, let us take

$$A_R = \begin{pmatrix} 0.7 & 0.3 \\ 0.4 & 0.6 \end{pmatrix}, A_G = \begin{pmatrix} 0.6 & 0.4 \\ 0.3 & 0.7 \end{pmatrix}, A_B = \begin{pmatrix} 0.7 & 0.3 \\ 0.4 & 0.6 \end{pmatrix}. \quad (69)$$

In Table 15 there are the errors in terms of MSE. The PSNR of the considered algorithms is presented in Table 16. Table 17 contains the errors in terms of MSE related to the estimated mixing matrices.

Ideal Document	MATODS		FastICA		SW	
	MSE recto	MSE verso	MSE recto	MSE verso	MSE recto	MSE verso
Figure 12	$1.28 \cdot 10^{-10}$	$4.56 \cdot 10^{-11}$	43.71	2.27	15.27	6.28
Figure 13	$3.51 \cdot 10^{-9}$	$6.07 \cdot 10^{-10}$	19.90	17.64	39.06	40.51
Figure 14	$6.95 \cdot 10^{-8}$	$9.71 \cdot 10^{-8}$	175.96	68.05	94.41	63.01
Figure 15	0.78	5.93	18.94	33.65	48.50	13.97
Figure 16	$1.24 \cdot 10^{-5}$	$3.90 \cdot 10^{-12}$	3.33	2.91	6.18	2.35
Figure 17	$1.43 \cdot 10^{-10}$	$1.76 \cdot 10^{-11}$	258.04	96.14	132.46	49.94
Figure 18	0.12	3.46	45.77	55.89	373.00	320.18

Table 15: Errors of the algorithms MATODS, FastICA and SW with the mixture matrix as in (69) in terms of MSE.

Ideal document	MATODS		FastICA		SW	
	PSNR recto	PSNR verso	PSNR recto	PSNR verso	PSNR recto	PSNR verso
Figure 12	147.07	151.54	31.73	44.58	36.29	40.15
Figure 13	132.68	140.30	35.14	35.67	32.21	32.06
Figure 14	119.71	118.26	25.68	29.80	28.38	30.14
Figure 15	49.21	40.40	35.36	32.86	31.27	36.68
Figure 16	97.18	162.22	42.91	43.49	40.22	44.43
Figure 17	146.58	155.68	24.01	28.30	26.91	31.15
Figure 18	57.36	42.74	31.53	30.66	22.41	23.08

Table 16: Errors of the algorithms MATODS, FastICA and SW with the mixture matrix as in (69) in terms of PSNR.

Document	MATODS	FastICA	SW
Figure 12	$8.95 \cdot 10^{-15}$	0.0047	0.0018
Figure 13	$2.20 \cdot 10^{-13}$	0.0036	0.0027
Figure 14	$3.31 \cdot 10^{-11}$	0.035	0.0035
Figure 15	$9.64 \cdot 10^{-5}$	0.013	0.0057
Figure 16	$1.62 \cdot 10^{-9}$	0.0023	0.0015
Figure 17	$5.50 \cdot 10^{-15}$	0.0089	0.0037
Figure 18	$1.15 \cdot 10^{-4}$	0.0060	0.0049

Table 17: Errors of the estimated mixing matrices by the algorithms MATODS, FastICA and SW with the mixture matrix as in (69) in terms of MSE.

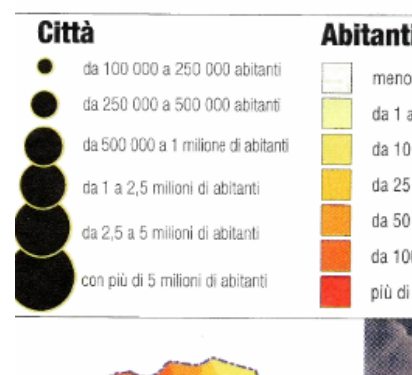
In Figures 29 (a) and (b) there are the mixtures of the document in Figure 13, obtained by means of the mixture matrices (69). In Figures 29 (c) and (d) we present the results obtained with the MATODS, while in Figures 29 (e) and (f) there are those got by means of the SW algorithm. Note that, in the results obtained by the SW method, the colors are not identical to those of the original document in Figure 13, especially if we see the picture in the bottom-right corner of the estimated recto.



(a) Recto of the mixture.



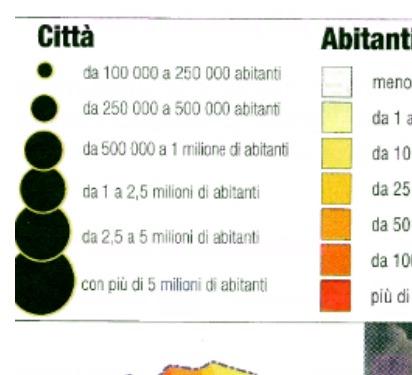
(b) Verso of the mixture.



(c) Recto estimated by MATODS.



(d) Verso estimated by MATODS.



(e) Recto estimated by SW.



(f) Verso estimated by SW.

Figure 29: Document in Figure 13 mixed with a mixture matrix as in (69).

Now we deal with a non-symmetric and not-homogeneous case. We take

$$A_R = \begin{pmatrix} 0.6 & 0.4 \\ 0.3 & 0.7 \end{pmatrix}, A_G = \begin{pmatrix} 0.7 & 0.3 \\ 0.4 & 0.6 \end{pmatrix}, A_B = \begin{pmatrix} 0.55 & 0.45 \\ 0.4 & 0.6 \end{pmatrix}. \quad (70)$$

In Table 18 there are the errors in terms of MSE. The PSNR of the considered algorithms is presented in Table 19. Table 20 contains the errors in terms of MSE related to the estimated mixing matrices.

Ideal Document	MATODS		FastICA		SW	
	MSE recto	MSE verso	MSE recto	MSE verso	MSE recto	MSE verso
Figure 12	$1.22 \cdot 10^{-10}$	$4.27 \cdot 10^{-11}$	28.98	0.29	15.87	5.68
Figure 13	$3.54 \cdot 10^{-9}$	$6.16 \cdot 10^{-10}$	38.76	18.77	20.64	43.76
Figure 14	$6.94 \cdot 10^{-8}$	$9.71 \cdot 10^{-8}$	212.02	89.25	72.42	83.52
Figure 15	0.63	5.35	33.75	60.95	47.96	33.40
Figure 16	$1.24 \cdot 10^{-5}$	$5.10 \cdot 10^{-12}$	7.05	1.88	2.54	2.26
Figure 17	$6.76 \cdot 10^{-10}$	$4.87 \cdot 10^{-11}$	470.29	181.33	30.74	30.43
Figure 18	0.12	3.46	43.04	98.59	331.54	367.22

Table 18: Errors of the algorithms MATODS, FastICA and SW with the mixture matrix as in (70) in terms of MSE.

Ideal document	MATODS		FastICA		SW	
	PSNR recto	PSNR verso	PSNR recto	PSNR verso	PSNR recto	PSNR verso
Figure 12	147.26	151.83	33.51	53.58	36.12	40.59
Figure 13	132.64	140.24	32.25	35.40	34.98	31.72
Figure 14	119.71	118.26	24.87	28.63	29.53	28.91
Figure 15	50.16	40.85	32.85	30.28	31.32	32.89
Figure 16	97.18	100.19	39.65	45.39	44.09	44.59
Figure 17	139.83	151.26	21.40	25.55	33.25	33.30
Figure 18	57.36	42.74	31.79	28.19	22.93	22.48

Table 19: Errors of the algorithms MATODS, FastICA and SW with the mixture matrix as in (70) in terms of PSNR.

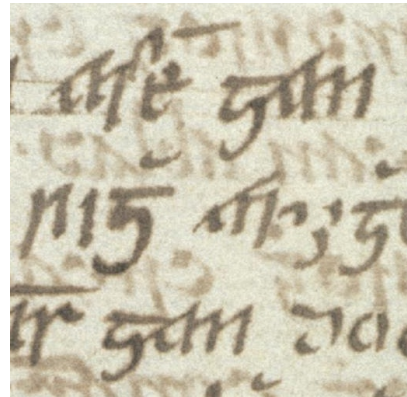
Document	MATODS	FastICA	SW
Figure 12	$6.23 \cdot 10^{-15}$	0.0029	0.0022
Figure 13	$2.21 \cdot 10^{-13}$	0.0059	0.0025
Figure 14	$3.33 \cdot 10^{-11}$	0.032	0.0026
Figure 15	$1.21 \cdot 10^{-4}$	0.0056	0.0026
Figure 16	$1.44 \cdot 10^{-9}$	0.0026	0.0020
Figure 17	$2.21 \cdot 10^{-14}$	0.016	0.0058
Figure 18	$1.36 \cdot 10^{-4}$	0.0041	0.0035

Table 20: Errors of the estimated mixing matrices by the algorithms MATODS, FastICA and SW with the mixture matrix as in (70) in terms of MSE.

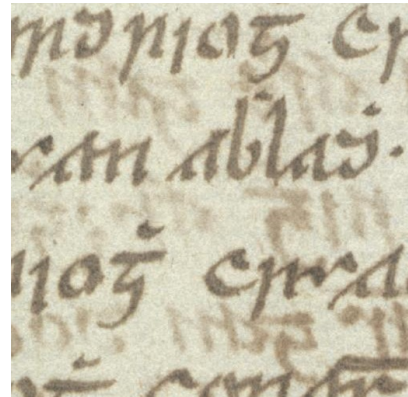
Observe that, in general, even considering the overlapping matrices, the results obtained by means of the SW and FastICA are very similar. This confirms the results obtained in [53] using covariance matrices. Moreover, note that the estimation of the source overlapping level is very useful for a correct reconstruction of the original sources. Indeed, the MATODS algorithm obtaines always the best results.

Now we see how the NIT-MATODS algorithm restores real ancient documents. In this case, we take some practical measures. Namely, we compare the maximum of the light intensity of the recto and of the verso corresponding to our data. If the two values do not coincide, then we add a constant to the light intensity of the darker image, in order to make its background similar to that of the brighter image. This is justified by the fact that the color of the paper has to be the same both in the recto and in the verso. Since images of real documents present a noise degradation phenomena, in general the brightest value does not coincide with that of the background. So, for all three components red, green and blue, instead of estimating the maximum value of the light intensity, we compute the statistical mode of the recto and the verso. We assume that the determinant of the overlapping matrix of the observed data  $C_R$  ( $C_G$ , or  $C_B$ ), corresponding to each channel of each involved subimage, is zero when  $\det(C_R)/\|C_R\|_\infty \leq \bar{\varepsilon}$  (resp.  $\det(C_G)/\|C_G\|_\infty \leq \bar{\varepsilon}$  or  $\det(C_B)/\|C_B\|_\infty \leq \bar{\varepsilon}$ ), where  $\bar{\varepsilon}$  is a prefixed threshold and  $\|C_B\|_\infty$  is the infinity norm. In the following experiments we set the subwindow size as  $\bar{n} = 128$ , and this subwindow is shifted during the execution of the algorithm by  $\nu = 16$  pixels. In this setting, the NIT-MATODS algorithm, dealing with  $512 \times 512$  documents, has an average computation time of 59.72 seconds.

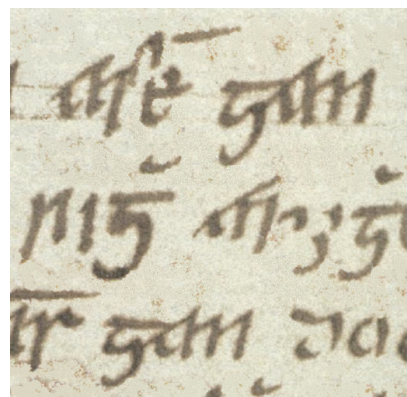
The data document in Figures 30 and 33–36 (a) and (b) are taken by the database created by the project *Irish Script on Screen* (ISOS) of the School of Celtic Studies, Dublin Institute for Advances Studies, in conjunction with the SIGMEDIA group of the Department of Electrical and Electronic Engineering at the Trinity College in Dublin (see [33]). This database contains ancient documents affected by bleed-through. In Figures 30–32 we present some results obtained by NIT-MATODS, restoring the document in Figures 30 (a) and (b), with different parameters  $\bar{n}$  and  $\nu$ , in order to show how NIT-MATODS works using non-optimal parameters. The reconstruction obtained by NIT-MATODS of the other ISOS document, with  $\bar{n} = 128$  and  $\nu = 16$ , are presented in Figures 33–36 (c) and (d).



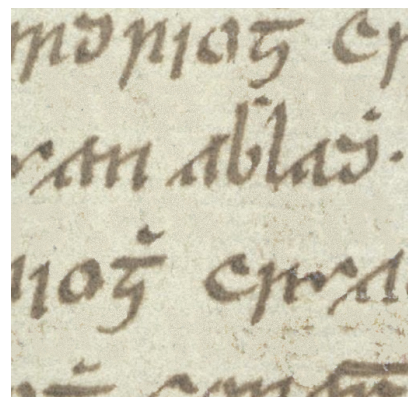
(a) Data document recto.



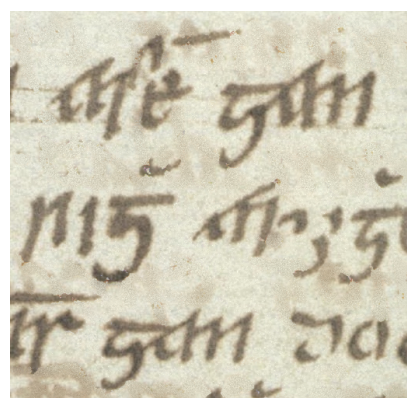
(b) Data document verso.



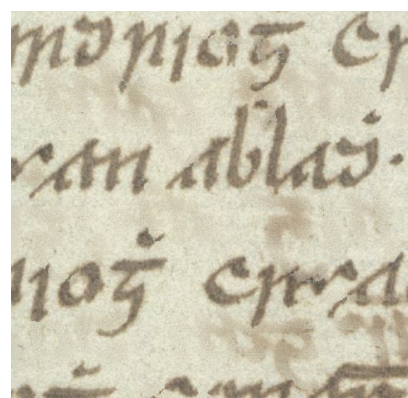
(c) NIT-MATODS estimated recto  
( $\bar{n} = 128, \nu = 16$ ).



(d) NIT-MATODS estimated  
verso( $\bar{n} = 128, \nu = 16$ ).

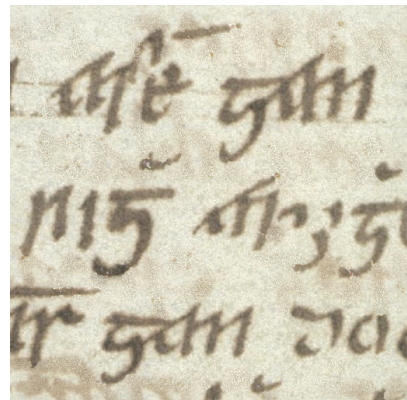


(e) NIT-MATODS estimated recto  
( $\bar{n} = 32, \nu = 4$ ).



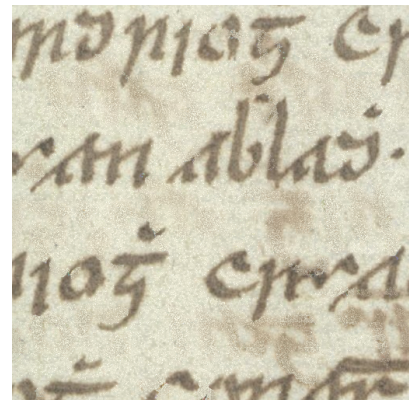
(f) NIT-MATODS estimated verso  
( $\bar{n} = 32, \nu = 4$ ).

Figure 30: First considered  $512 \times 512$  ISOS document.



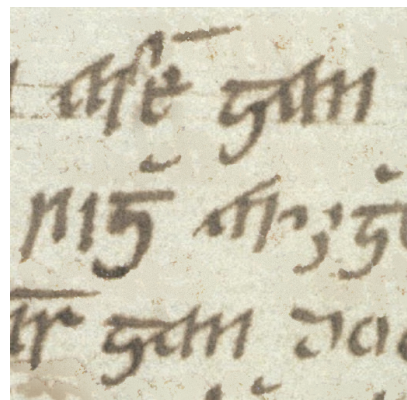
me gam  
nig m̄i  
tr gam da

(a) NIT-MATODS estimated recto  
( $\bar{n} = 32, \nu = 8$ ).



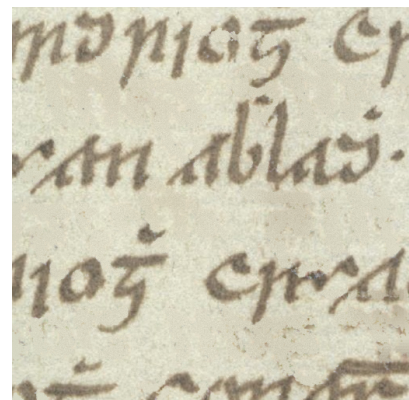
monias et  
can ablaci.  
noz cren  
et cantri

(b) NIT-MATODS estimated verso  
( $\bar{n} = 32, \nu = 8$ ).



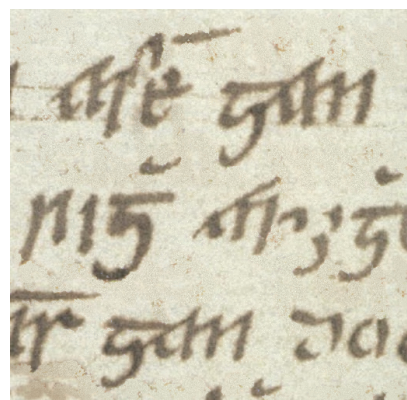
me gam  
nig m̄i  
tr gam da

(c) NIT-MATODS estimated recto  
( $\bar{n} = 64, \nu = 4$ ).



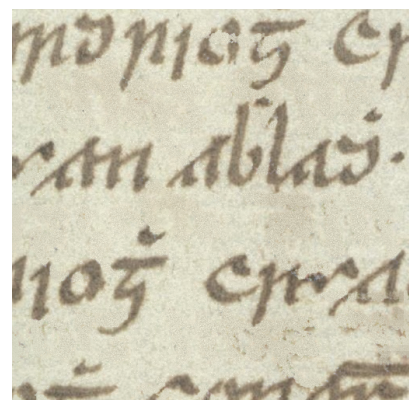
monias et  
can ablaci.  
noz cren  
et cantri

(d) NIT-MATODS estimated verso  
( $\bar{n} = 64, \nu = 4$ ).



me gam  
nig m̄i  
tr gam da

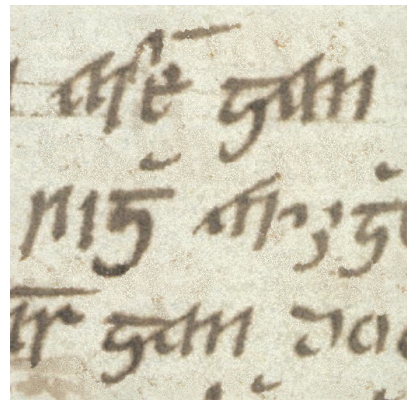
(e) NIT-MATODS estimated recto  
( $\bar{n} = 64, \nu = 8$ ).



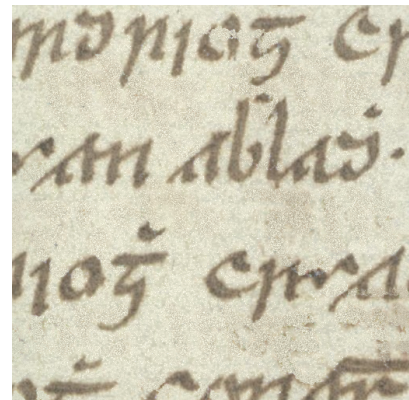
monias et  
can ablaci.  
noz cren  
et cantri

(f) NIT-MATODS estimated verso  
( $\bar{n} = 64, \nu = 8$ ).

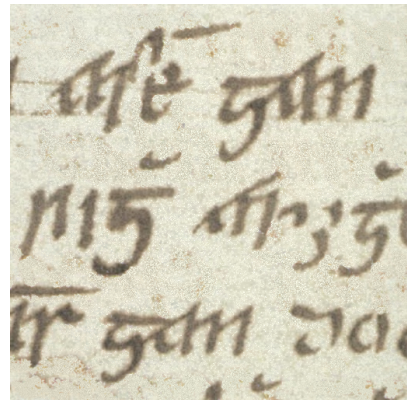
Figure 31: First considered  $512 \times 512$  ISOS document.



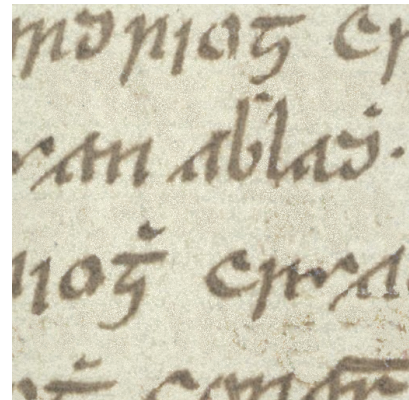
(a) NIT-MATODS estimated recto  
( $\bar{n} = 64$ ,  $\nu = 16$ ).



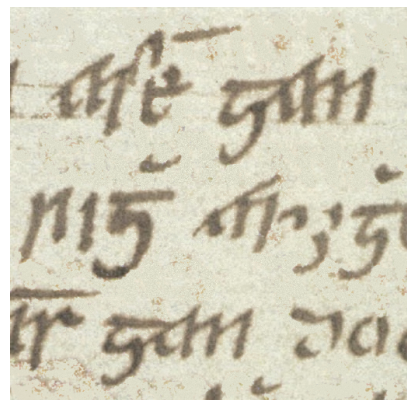
(b) NIT-MATODS estimated verso  
( $\bar{n} = 64$ ,  $\nu = 16$ ).



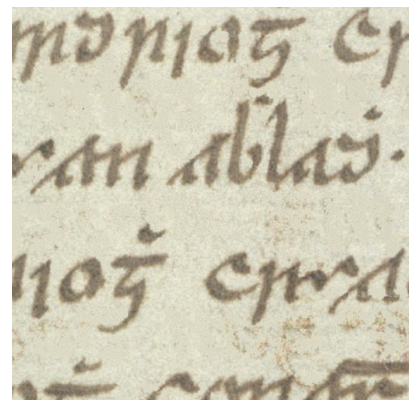
(c) NIT-MATODS estimated recto  
( $\bar{n} = 128$ ,  $\nu = 32$ ).



(d) NIT-MATODS estimated verso  
( $\bar{n} = 128$ ,  $\nu = 32$ ).

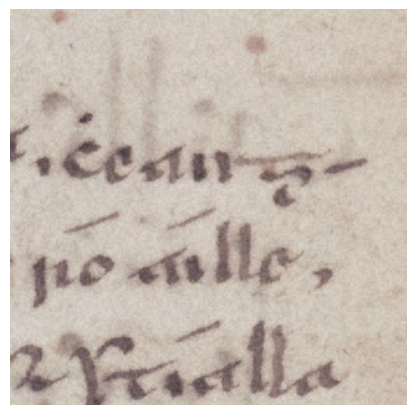


(e) NIT-MATODS estimated recto  
( $\bar{n} = 256$ ,  $\nu = 32$ ).



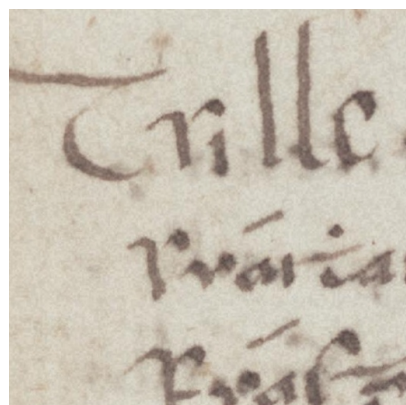
(f) NIT-MATODS estimated verso  
( $\bar{n} = 256$ ,  $\nu = 32$ ).

Figure 32: First considered  $512 \times 512$  ISOS document.



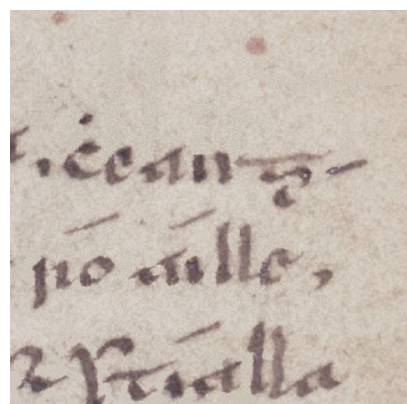
l. écau-  
no uille,  
et vialla

(a) Data document recto.



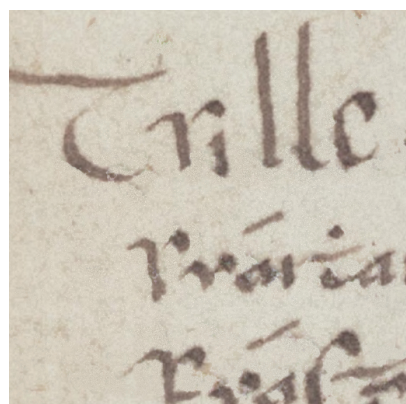
Trille  
Prácia  
Prácia

(b) Data document verso.



l. écau-  
no uille,  
et vialla

(c) NIT-MATODS estimated recto.



Trille  
Prácia  
Prácia

(d) NIT-MATODS estimated verso.

Figure 33: Second considered 512 × 512 ISOS document.

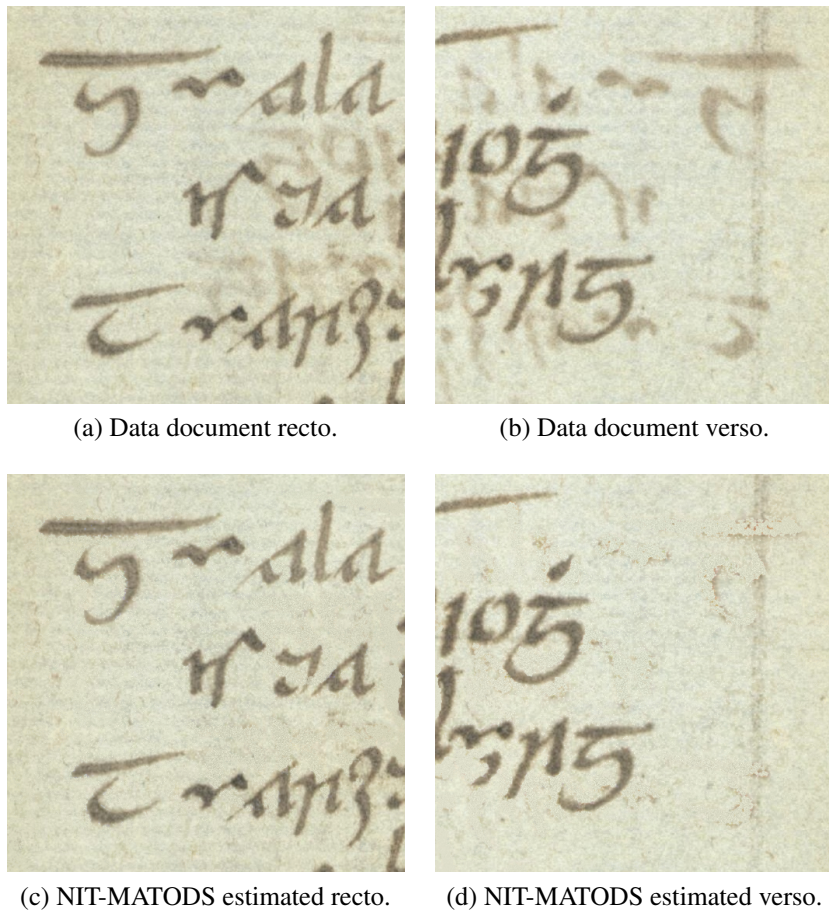


Figure 34: Third considered  $512 \times 512$  ISOS document.

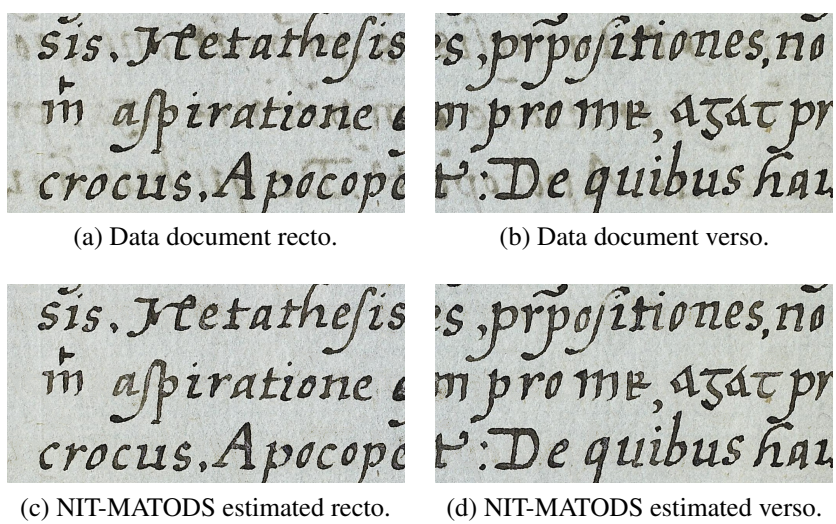
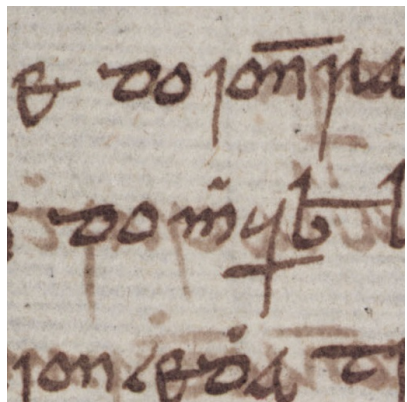
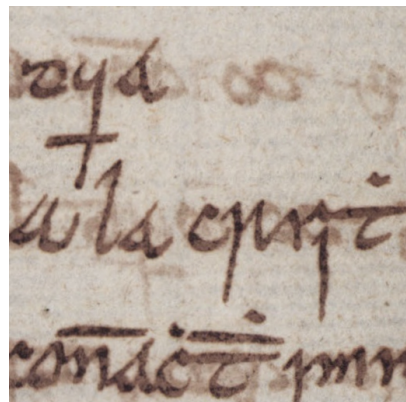


Figure 35: Fourth  $1024 \times 512$  ISOS document.



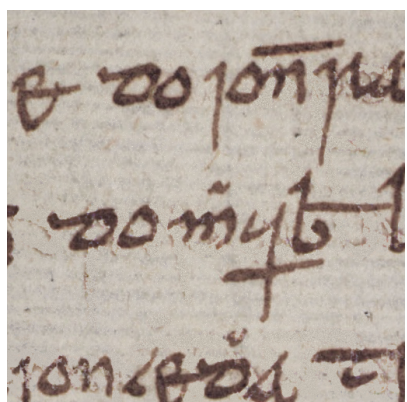
B do lōnīra  
is domyf  
monies

(a) Data document recto.



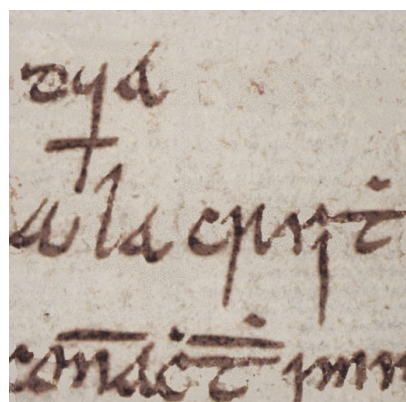
zyd oo o  
ula cpriz  
conicē pnr

(b) Data document verso.



B do lōnīra  
is domyf  
monies

(c) NIT-MATODS estimated recto.



zyd  
ula cpriz  
conicē pnr

(d) NIT-MATODS estimated verso.

Figure 36: Fifth 512 × 512 ISOS document.

## 7 Appendix

In this appendix, we study the periodicity of the objective function  $f^{(l)}(\theta, \iota, C_R)$  defined in (47), with respect to  $\theta$ . Let  $\iota = 1, -1$ ,  $\theta \in \mathbb{R}$ ,  $Q_\iota$  be as in (18),

$$C_R^{1/2} = \begin{bmatrix} \bar{c}_{11}^R & \bar{c}_{12}^R \\ \bar{c}_{21}^R & \bar{c}_{22}^R \end{bmatrix}$$

be as in (29),

$$Z_{R,\iota}(\theta) = C_R^{1/2} Q_\iota(\theta) = \begin{bmatrix} z_{11}^{R,\iota}(\theta) & z_{12}^{R,\iota}(\theta) \\ z_{21}^{R,\iota}(\theta) & z_{22}^{R,\iota}(\theta) \end{bmatrix}$$

be as in (19),

$$W_{R,\iota}^{(l)}(\theta) = \begin{bmatrix} w_{11}^{R,\iota,(l)}(\theta) & w_{12}^{R,\iota,(l)}(\theta) \\ w_{21}^{R,\iota,(l)}(\theta) & w_{22}^{R,\iota,(l)}(\theta) \end{bmatrix}$$

be as in (22), where  $w_{i,j}^{R,\iota,(l)}(\theta)$ ,  $i, j = 1, 2$ , are in (26). Let

$$\tilde{A}_{R,\iota}^{(l)}(\theta) = Z_{R,\iota}(\theta) (W_{R,\iota}^{(l)}(\theta))^{-1},$$

where

$$\tilde{A}_{R,\iota}^{(l)}(\theta) = \begin{bmatrix} a_{11}^{R,\iota,(l)}(\theta) & a_{12}^{R,\iota,(l)}(\theta) \\ a_{21}^{R,\iota,(l)}(\theta) & a_{22}^{R,\iota,(l)}(\theta) \end{bmatrix}$$

is as in (24). We get

$$\begin{aligned} Z_{R,1}(\theta) &= \begin{bmatrix} z_{11}^{R,1}(\theta) & z_{12}^{R,1}(\theta) \\ z_{21}^{R,1}(\theta) & z_{22}^{R,1}(\theta) \end{bmatrix} = C_R^{1/2} Q_1(\theta) = \\ &= \begin{bmatrix} \bar{c}_{11}^R & \bar{c}_{12}^R \\ \bar{c}_{21}^R & \bar{c}_{22}^R \end{bmatrix} \begin{bmatrix} \sin \theta & -\cos \theta \\ \cos \theta & \sin \theta \end{bmatrix} = \\ &= \begin{bmatrix} \bar{c}_{11}^R \sin \theta + \bar{c}_{12}^R \cos \theta & -\bar{c}_{11}^R \cos \theta + \bar{c}_{12}^R \sin \theta \\ \bar{c}_{21}^R \sin \theta + \bar{c}_{22}^R \cos \theta & -\bar{c}_{21}^R \cos \theta + \bar{c}_{22}^R \sin \theta \end{bmatrix}; \end{aligned}$$

$$\begin{aligned} Z_{R,-1}(\theta) &= \begin{bmatrix} z_{11}^{R,-1}(\theta) & z_{12}^{R,-1}(\theta) \\ z_{21}^{R,-1}(\theta) & z_{22}^{R,-1}(\theta) \end{bmatrix} = C_R^{1/2} Q_{-1}(\theta) = \\ &= \begin{bmatrix} \bar{c}_{11}^R & \bar{c}_{12}^R \\ \bar{c}_{21}^R & \bar{c}_{22}^R \end{bmatrix} \begin{bmatrix} \sin \theta & \cos \theta \\ \cos \theta & -\sin \theta \end{bmatrix} = \\ &= \begin{bmatrix} \bar{c}_{11}^R \sin \theta + \bar{c}_{12}^R \cos \theta & \bar{c}_{11}^R \cos \theta - \bar{c}_{12}^R \sin \theta \\ \bar{c}_{21}^R \sin \theta + \bar{c}_{22}^R \cos \theta & \bar{c}_{21}^R \cos \theta - \bar{c}_{22}^R \sin \theta \end{bmatrix} = \\ &= \begin{bmatrix} z_{11}^{R,1}(\theta) & -z_{12}^{R,1}(\theta) \\ z_{21}^{R,1}(\theta) & -z_{22}^{R,1}(\theta) \end{bmatrix}; \end{aligned}$$

$$\det(Z_{R,-1}(\theta)) = -\det(Z_{R,1}(\theta)).$$

Therefore, we have

$$\begin{aligned}
w_{11}^{R,-1,(l)}(\theta) &= \frac{\det(C_R) - k_R^{(l)}(z_{11}^{R,-1}(\theta) - z_{21}^{R,-1}(\theta))^2}{(-z_{22}^{R,-1}(\theta) + z_{12}^{R,-1}(\theta))(-\det(Z_{R,-1}(\theta)))} = w_{11}^{R,1,(l)}(\theta); \\
w_{12}^{R,-1,(l)}(\theta) &= -k_R^{(l)} \frac{z_{11}^{R,-1}(\theta) - z_{21}^{R,-1}(\theta)}{\det(Z_{R,-1}(\theta))} = -w_{12}^{R,1,(l)}(\theta); \\
w_{21}^{R,-1,(l)}(\theta) &= 0 = w_{21}^{R,-1,(l)}(\theta), \\
w_{22}^{R,-1,(l)}(\theta) &= -\frac{\det(Z_{R,-1}(\theta))}{z_{11}^{R,-1}(\theta) - z_{21}^{R,-1}(\theta)} = -w_{22}^{R,1,(l)}(\theta)
\end{aligned}.$$

Since

$$\tilde{A}_{R,-1}^{(l)}(\theta) = Z_{R,-1}(\theta) (W_{R,-1}^{(l)}(\theta))^{-1},$$

it is

$$\begin{aligned}
a_{11}^{R,-1,(l)}(\theta) &= -\frac{-z_{11}^{R,-1}(\theta)w_{22}^{R,-1,(l)}(\theta) + z_{12}^{R,-1}(\theta)w_{21}^{R,-1,(l)}(\theta)}{\det(W_{R,-1}^{(l)}(\theta))} = a_{11}^{R,1,(l)}(\theta); \\
a_{12}^{R,-1,(l)}(\theta) &= -\frac{-z_{12}^{R,-1}(\theta)w_{11}^{R,-1,(l)}(\theta) + z_{11}^{R,-1}(\theta)w_{12}^{R,-1,(l)}(\theta)}{\det(W_{R,-1}^{(l)}(\theta))} = a_{12}^{R,1,(l)}(\theta); \\
a_{21}^{R,-1,(l)}(\theta) &= -\frac{-z_{21}^{R,-1}(\theta)w_{22}^{R,-1,(l)}(\theta) + z_{22}^{R,-1}(\theta)w_{21}^{R,-1,(l)}(\theta)}{\det(W_{R,-1}^{(l)}(\theta))} = a_{21}^{R,1,(l)}(\theta); \\
a_{22}^{R,-1,(l)}(\theta) &= -\frac{-z_{22}^{R,-1}(\theta)w_{11}^{R,-1,(l)}(\theta) + z_{21}^{R,-1}(\theta)w_{12}^{R,-1,(l)}(\theta)}{\det(W_{R,-1}^{(l)}(\theta))} = a_{22}^{R,1,(l)}(\theta),
\end{aligned}$$

namely

$$\tilde{A}_{R,-1}^{(l)}(\theta) = \tilde{A}_{R,1}^{(l)}(\theta). \quad (71)$$

Set now  $\theta^* = \theta + \pi$ ,  $\theta \in \mathbb{R}$ . We have

$$\begin{aligned}
Z_{R,1}(\theta^*) &= \begin{bmatrix} z_{11}^{R,1}(\theta^*) & z_{12}^{R,1}(\theta^*) \\ z_{21}^{R,1}(\theta^*) & z_{22}^{R,1}(\theta^*) \end{bmatrix} = \\
&= \begin{bmatrix} \bar{c}_{11}^R & \bar{c}_{12}^R \\ \bar{c}_{21}^R & \bar{c}_{22}^R \end{bmatrix} \begin{bmatrix} \sin(\theta + \pi) & -\cos(\theta + \pi) \\ \cos(\theta + \pi) & \sin(\theta + \pi) \end{bmatrix} = \\
&= \begin{bmatrix} \bar{c}_{11}^R & \bar{c}_{12}^R \\ \bar{c}_{21}^R & \bar{c}_{22}^R \end{bmatrix} \begin{bmatrix} -\sin\theta & \cos\theta \\ -\cos\theta & -\sin\theta \end{bmatrix} = -Z_{R,1}(\theta);
\end{aligned}$$

$$\det(Z_{R,1}(\theta^*)) = \det(Z_{R,1}(\theta)).$$

Thus, we get

$$\begin{aligned}
w_{11}^{R,1,(l)}(\theta^*) &= \frac{\det(C_R) - k_R^{(l)}(-z_{11}^{R,1}(\theta) + z_{21}^{R,1}(\theta))^2}{(z_{22}^{R,1}(\theta) - z_{12}^{R,1}(\theta))(\det(Z_{R,1}(\theta)))} = -w_{11}^{R,1,(l)}(\theta); \\
w_{12}^{R,1,(l)}(\theta^*) &= k_R^{(l)} \frac{-z_{11}^{R,1}(\theta) + z_{21}^{R,1}(\theta)}{\det(Z_{R,1}(\theta))} = -w_{12}^{R,1,(l)}(\theta); \\
w_{21}^{R,1,(l)}(\theta^*) &= 0 = -w_{21}^{R,1,(l)}(\theta); \\
w_{22}^{R,1,(l)}(\theta^*) &= \frac{\det(Z_{R,1}(\theta))}{z_{11}^{R,1}(\theta) - z_{21}^{R,1}(\theta)} = -w_{22}^{R,1,(l)}(\theta).
\end{aligned}$$

Therefore,

$$\begin{aligned}
\tilde{A}_{R,1}^{(l)}(\theta^*) &= Z_{R,1}(\theta^*) (W_{R,1}^{(l)}(\theta^*))^{-1} = \\
&= (-Z_{R,1}(\theta)) (-W_{R,1}^{(l)}(\theta))^{-1} = \tilde{A}_{R,1}^{(l)}(\theta).
\end{aligned}$$

From this, it is not difficult to deduce that  $f^{(l)}(\theta, \iota, C_R)$  has period (at most)  $\pi$ , with respect to  $\theta$ .

Now, set  $\theta^{**} = \theta + \pi/2$ ,  $\theta \in \mathbb{R}$ . We have

$$\begin{aligned}
Z_{R,1}(\theta^{**}) &= \begin{bmatrix} z_{11}^{R,1}(\theta^{**}) & z_{12}^{R,1}(\theta^{**}) \\ z_{21}^{R,1}(\theta^{**}) & z_{22}^{R,1}(\theta^{**}) \end{bmatrix} = \\
&= \begin{bmatrix} \bar{c}_{11}^R & \bar{c}_{12}^R \\ \bar{c}_{21}^R & \bar{c}_{22}^R \end{bmatrix} \begin{bmatrix} \sin(\theta + \pi/2) & -\cos(\theta + \pi/2) \\ \cos(\theta + \pi/2) & \sin(\theta + \pi/2) \end{bmatrix} = \\
&= \begin{bmatrix} \bar{c}_{11}^R & \bar{c}_{12}^R \\ \bar{c}_{21}^R & \bar{c}_{22}^R \end{bmatrix} \begin{bmatrix} \cos \theta & \sin \theta \\ -\sin \theta & \cos \theta \end{bmatrix} = \\
&= \begin{bmatrix} -z_{12}^{R,1}(\theta) & z_{11}^{R,1}(\theta) \\ -z_{22}^{R,1}(\theta) & z_{21}^{R,1}(\theta) \end{bmatrix}; \tag{72}
\end{aligned}$$

$$\det(Z_{R,1}(\theta^{**})) = \det(Z_{R,1}(\theta)).$$

It is readily seen experimentally by the related graphs that, in general,  $f^{(l)}(\theta, \iota, C_R)$  does not have period  $\pi/2$  with respect to  $\theta$ .

If  $\theta = \varphi_R^{(1)}$ , where  $\varphi_R^{(1)}$  is as in (39), then  $z_{11}^{R,1}(\varphi_R^{(1)}) = z_{21}^{R,1}(\varphi_R^{(1)})$ . By (72), we get

$$z_{12}^{R,1}(\varphi_R^{(1)} + \pi/2) = z_{11}^{R,1}(\varphi_R^{(1)}) = z_{21}^{R,1}(\varphi_R^{(1)}) = z_{22}^{R,1}(\varphi_R^{(1)} + \pi/2).$$

We recall that the points of discontinuity of the function  $f$  when  $z_{12}^{R,1}(\theta) = z_{22}^{R,1}(\theta)$  are given by the values of  $\theta$  of type  $\varphi_R^{(5)} + k\pi$ , where  $k \in \mathbb{Z}$  and  $\varphi_R^{(5)}$  is as (41). Hence, there exists a  $k \in \mathbb{Z}$  such that

$$\varphi_R^{(1)} + \frac{\pi}{2} = \varphi_R^{(5)} + k\pi.$$

On the other hand, the points of discontinuity of the function  $f$ , when  $z_{11}^{R,1}(\theta) = z_{21}^{R,1}(\theta)$ , are given by the values of  $\theta$  of type  $\varphi_R^{(1)} + k\pi$ , where  $k \in \mathbb{Z}$  and  $\varphi_R^{(1)}$  is as (39). Therefore, the equation (26) is not well-defined only in the points of type  $\varphi_R^{(1)} + k\frac{\pi}{2}$ , where  $k \in \mathbb{Z}$ .

When  $k^{(l)} = 0$ , it is

$$w_{11}^{R,1,(l)}(\theta^{**}) = \frac{\det(Z_{R,1}(\theta))}{z_{22}^{R,1}(\theta) - z_{12}^{R,1}(\theta)} = -w_{11}^{R,1,(l)}(\theta);$$

$$w_{12}^{R,1,(l)}(\theta^{**}) = 0 = -w_{12}^{R,1,(l)}(\theta);$$

$$w_{21}^{R,1,(l)}(\theta^{**}) = 0 = -w_{21}^{R,1,(l)}(\theta);$$

$$w_{22}^{R,1,(l)}(\theta^{**}) = \frac{\det(Z_{R,1}(\theta))}{z_{11}^{R,1}(\theta) - z_{21}^{R,1}(\theta)} = -w_{22}^{R,1,(l)}(\theta).$$

Therefore,

$$\begin{aligned} \tilde{A}_{R,1}^{(l)}(\theta^{**}) &= Z_{R,1}(\theta^*) (W_{R,1}^{(l)}(\theta^*))^{-1} = \\ &= \frac{1}{\det(Z_{R,1}(\theta))} \begin{bmatrix} -z_{12}^{R,1}(\theta) & z_{11}^{R,1}(\theta) \\ -z_{22}^{R,1}(\theta) & z_{21}^{R,1}(\theta) \end{bmatrix} \begin{bmatrix} z_{21}^{R,1}(\theta) - z_{11}^{R,1}(\theta) & 0 \\ 0 & z_{22}^{R,1}(\theta) - z_{12}^{R,1}(\theta) \end{bmatrix} = \\ &= \frac{1}{\det(Z_{R,1}(\theta))} \begin{bmatrix} -z_{12}^{R,1}(\theta)(z_{21}^{R,1}(\theta) - z_{11}^{R,1}(\theta)) & z_{11}^{R,1}(\theta)(z_{22}^{R,1}(\theta) - z_{12}^{R,1}(\theta)) \\ -z_{22}^{R,1}(\theta)(z_{21}^{R,1}(\theta) - z_{11}^{R,1}(\theta)) & z_{21}^{R,1}(\theta)(z_{22}^{R,1}(\theta) - z_{12}^{R,1}(\theta)) \end{bmatrix} = \\ &= \begin{bmatrix} a_{12}^{R,1,(l)}(\theta) & a_{11}^{R,1,(l)}(\theta) \\ a_{22}^{R,1,(l)}(\theta) & a_{21}^{R,1,(l)}(\theta) \end{bmatrix} = \begin{bmatrix} a_{11}^{R,1,(l)}(\theta) & a_{12}^{R,1,(l)}(\theta) \\ a_{21}^{R,1,(l)}(\theta) & a_{22}^{R,1,(l)}(\theta) \end{bmatrix} \begin{bmatrix} 0 & 1 \\ 1 & 0 \end{bmatrix} = \\ &= \tilde{A}_{R,1}^{(l)}(\theta) \begin{bmatrix} 0 & 1 \\ 1 & 0 \end{bmatrix}. \end{aligned}$$

From this, since  $\begin{bmatrix} 0 & 1 \\ 1 & 0 \end{bmatrix}^2 = \begin{bmatrix} 1 & 0 \\ 0 & 1 \end{bmatrix}$ , we deduce

$$(\tilde{A}_{R,1}^{(l)}(\theta^{**}))^{-1} = \begin{bmatrix} 0 & 1 \\ 1 & 0 \end{bmatrix} (\tilde{A}_{R,1}^{(l)}(\theta))^{-1}. \quad (73)$$

From (73) we obtain

$$\begin{aligned} \begin{bmatrix} \tilde{s}_{rR}^T(\theta^{**}) \\ \tilde{s}_{vR}^T(\theta^{**}) \end{bmatrix} &= \tilde{s}_R^T(\theta^{**}) = (\tilde{A}_{R,1}^{(l)}(\theta^{**}))^{-1} x_R^T = \\ &= \begin{bmatrix} 0 & 1 \\ 1 & 0 \end{bmatrix} (\tilde{A}_{R,1}^{(l)}(\theta))^{-1} x_R^T = \\ &= \begin{bmatrix} 0 & 1 \\ 1 & 0 \end{bmatrix} \begin{bmatrix} \tilde{s}_{rR}^T(\theta) \\ \tilde{s}_{vR}^T(\theta) \end{bmatrix} = \begin{bmatrix} \tilde{s}_{vR}^T(\theta) \\ \tilde{s}_{rR}^T(\theta) \end{bmatrix}. \end{aligned}$$

Hence, we get

$$\begin{aligned} f^{(l)}(\theta^{**}, 1, C_R) &= (\tau(\tilde{s}_{r,R,1}^{(l)}(\theta^{**})))^T \cdot \tau(\tilde{s}_{v,R,1}^{(l)}(\theta^{**})) = \\ &= (\tau(\tilde{s}_{v,R,1}^{(l)}(\theta)))^T \cdot \tau(\tilde{s}_{r,R,1}^{(l)}(\theta)) = f^{(l)}(\theta^{**}, 1, C_R). \end{aligned}$$

Thus, when  $k^{(l)} = 0$ ,  $f^{(l)}(\theta, \iota, C_R)$  has period  $\pi/2$  (with respect to  $\theta$ ).

## Conclusions

In this article, we dealt with a Blind Source Separation problem in the particular case of document restoration. We proposed a Correlated Component Analysis technique that gives as a solution a Nonnegative Factorization of the observed data. We initially analyzed a linear invariant for translation model, and we developed a fixed point algorithm that iteratively estimates the overlapping level of the recto and the verso of the document to be restored. From the estimated overlapping level we compute the estimation of the ideal sources and of the mixture matrix. The given algorithm was called *Minimum Amount of Text Overlapping in Document Separation* (MATODS). The MATODS algorithm is a fast and unsupervised method. Then we proposed a translation not invariant and local linear model in order to deal with real ancient documents. The algorithm related to this model was called *Not Invariant for Translation MATODS* (NIT-MATODS). The experimental results confirmed that MATODS works better than some classical fast and unsupervised developed algorithms for a linear and translation invariant model, while the NIT-MATODS algorithm gives qualitatively good results in reconstructing ancient documents degraded by a bleed-through effect.

**Acknowledgments:** We thank Bruno Iannazzo for his helpful suggestion about the minimization over unitary matrices.

## References

- [1] E. AARTS, J. KORST, *Simulated Annealing and Boltzmann Machines*. John Wiley & Sons, New York, 1989.
- [2] S. AMARI AND A. CICHOCKI, *Adaptive Blind Signal Processing-Neural Network Approaches*, Proceedings IEEE, 86 (10) (1998), pp. 2026–2048.
- [3] L. ARMIJO, *Minimization of Functions having Lipschitz Continuous First Partial Derivatives*, Pacific J. Math., 16 (1) (1966), pp. 1–3.
- [4] G. ANESCU *A Heuristic Fast Gradient Descent Method for Unimodal Optimization*, Journal of Advances in Mathematics and Computer Science, 26 (5) (2018), pp. 1–20.
- [5] H. I. AVI-ITZHAK, T. A. DIEP, AND H. GARLAND, *High Accuracy Optical Character Recognition using Neural Networks with Centroid Dithering*, IEEE Trans. Patt. Anal. Mach. Intell. 17 (1995), pp. 218–224.
- [6] A. K. BARROS, *The Independence Assumption: Dependent Component Analysis*, In: M. Girolami (ed.), *Advances in Independent Component Analysis*, Springer, Berlin Heidelberg New York (2000), pp. 63–71.
- [7] X. BENLIN, L. FANGFANG, M. XINGLIANG, AND J. HUAZHONG, *Study on Independent Component Analysis Application in Classification and Change Detection of Multispectral Images*, The International Archives of the Photogrammetry, Remote Sensing and Spatial Information Sciences, 37 (2008), pp. 871–876.

- [8] A. BOCCUTO, I. GERACE, AND F. MARTINELLI, *Half-Quadratic Image Restoration with a Non-Parallelism Constraint*, J. Math. Imaging Vis., 59 (2) (2017), pp. 270-295.
- [9] R. BRENT, *Algorithms for Minimization without Derivatives*, Prentice-Hall, Inc., Englewood Cliffs, New Jersey, 1973.
- [10] H. BUNKE AND P. S. P. WANG (EDS.), *Handbook of Character Recognition and Document Image Analysis*, World Scientific, Singapore, 1997.
- [11] T.-H. CHAN, W.-K. MA, C.-Y. CHI, AND Y. WANG, *A Convex Analysis Framework for Blind Separation of Non-Negative Sources*, IEEE Trans. Signal Process., 56 (10) (2008), pp. 5120–5134.
- [12] A. CICHOCKI AND S.-I. AMARI, *Adaptive Blind Signal and Image Processing*, John Wiley & Sons, Chichester, 2002.
- [13] A. CICHOCKI, R. ZDUNEK, AND S.-I. AMARI, *New Algorithms for Non-Negative Matrix Factorization in Applications to Blind Source Separation*, In: Proceedings of the 2006 IEEE International Conference Acoustics, Speech and Signal Processing, Toulouse, France (2006), pp. 1–4.
- [14] F. CLUNI, D. COSTARELLI, A. M. MINOTTI, AND G. VINTI, *Applications of Sampling Kantorovich Operators to Thermographic Images for Seismic Engineering*, J. Comput. Anal. Appl., 19 (4) (2015), pp. 602–617.
- [15] F. CLUNI, D. COSTARELLI, A. M. MINOTTI, AND G. VINTI, *Enhancement of Thermographic Images as Tool for Structural Analysis in Earthquake Engineering*, NTD & E International, 70 (2015), pp. 60–72.
- [16] F. CLUNI, D. COSTARELLI, A. M. MINOTTI, AND G. VINTI, *Applications of Approximation Theory to Thermographic Images in Earthquake Engineering*, Proc. Appl. Math. Mech., 15 (2015), pp. 663–664.
- [17] P. COMON, *Independent Component Analysis, A New Concept?* Signal Processing, 36 (1994), pp. 287–314.
- [18] P. COMON AND C. JUTTEN, *Handbook of Blind Source Separation*. Academic Press, New York, 2010.
- [19] Y. C. ELDAR AND A. V. OPPENHEIM, *MMSE Whitening and Subspace Whitening*, IEEE Trans. Information Theory, 7 (49) (2003), pp. 1846–1851.
- [20] L. FEDELI, I. GERACE, AND F. MARTINELLI, *Unsupervised Blind Separation and Deblurring of Mixtures of Sources*, Proceedings of Knowledge-Based Intelligent Information and Engineering Systems, Vietri sul Mare, Italy, Lecture Notes Computer Sciences 4694 (2007), pp. 25–32.
- [21] S. GEMAN AND D. GEMAN, *Stochastic Relaxation, Gibbs Distributions, and the Bayesian Restoration of Images*. IEEE Trans. Pattern Anal. Machine Intell., 6 (1984), pp. 721–740.

- [22] N. GILLIS, *Successive Nonnegative Projection Algorithm for Robust Nonnegative Blind Source Separation*, SIAM J. Imaging Sci., 7 (2) (2014), pp. 1420–1450.
- [23] N. GILLIS, *Sparse and unique nonnegative matrix factorization through data pre-processing*, J. Machine Learning Research, 13 (2012), pp. 3349–3386.
- [24] J. HADAMARD, *Lectures on Cauchy’s Problem in Linear Partial Differential Equations*, New Haven, Yale Univ. Press, Yale, 1923.
- [25] A. HYVÄRINEN, *New Approximations of Differential Entropy for Independent Component Analysis and Projection Pursuit*, In: Advances in Neural Information Processing Systems, 10 (1998), pp. 273–279.
- [26] A. HYVÄRINEN, *Gaussian Moments for Noisy Independent Component Analysis*. IEEE Signal Process. Letters, 6 (1999), pp. 145–147.
- [27] A. HYVÄRINEN, *Fast and Robust Fixed-Point Algorithms for Independent Component Analysis*, IEEE Trans. Neural Networks, 10 (3) (1999), pp. 626–634.
- [28] A. HYVÄRINEN, *The Fixed-Point Algorithm and Maximum Likelihood Estimation for Independent Component Analysis*, Neural Process. Letters 10, (1) (1999), pp. 1–5.
- [29] A. HYVÄRINEN, *Survey on Independent Component Analysis*, Neural Computing Surveys, 2 (1999), pp. 94–128.
- [30] A. HYVÄRINEN, J. KARHUNEN, AND E. OJA, *Independent Component Analysis*. John Wiley & Sons, New York, 2001.
- [31] A. HYVÄRINEN AND E. OJA, *A Fast Fixed-Point Algorithm for Independent Component Analysis*, Neural Computation 9 (7) (1997), pp. 1483–1492.
- [32] A. HYVÄRINEN AND E. OJA, *Independent Component Analysis: Algorithms and Applications*, Neural Networks 13 (4–5) (2000), pp. 411–430.
- [33] *Irish Script on Screen Bleed-Through Database*: <https://www.isos.dias.ie/master.html?https://www.isos.dias.ie/libraries/Sigmedia/BleedThrough/irish/index.html>
- [34] P. JARRATT, *An iterative method for locating turning points*, the Computer Journal, 10 (1) 1967, pp. 82–84.
- [35] H. KANEMITSU, M. MIYAKOSHI, AND M. SHIMBO *Properties of Unimodal and multimodal Functions Defined by the Use of Local Minimal Value Set* Electronics and Communications in Japan (Part III Fundamental Electronic Science) 81 (1) 1998, pp. 42–51.
- [36] R. K. KARSH, R. H. LASKAR, AND S. ROY, *Modified FastICA Algorithm for Separation of Mixed Images*, In: Proceedings of the 5th International Conference on Computer and Communication Technology (ICCCT), Allahabad, India (2014), pp. 381–385.

- [37] A. KHAPARDE, M. MADHAVILATHA, M. B. L. MANASA, AND S. PRADEEP KUMAR, *FastICA Algorithm for the Separation of Mixed Images*. WSEAS Transactions on Signal Process., 4 (5) (2008), pp. 271–278.
- [38] J. KIEFER, *Sequential Minimax Search for a Maximum*. In Proceedings of the American Mathematical Society, 4 (1953), pp. 502–506.
- [39] E. KURUOGLU, L. BEDINI, M. T. PARATORE, E. SALERNO, AND A. TONAZZINI, *Source Separation in Astrophysical Maps Using Independent Factor Analysis*, Neural Networks 16, 3–4 (2003), pp. 479–491.
- [40] G. LEEDHAM, S. VARMA, A. PATANKAR, AND V. GOVINDARAJU, *Separating Text and Background in Degraded Document Images – a Comparison of Global Thresholding Techniques for Multi-Stage Thresholding*, In: Proceedings of the 8th International Workshop on Frontiers in Handwriting Recognition, Niagara on the Lake, Canada (2002), pp 244–249.
- [41] R. K. MALIK AND K. SOLANKI, *FastICA Based Blind Source Separation for CT Imaging Under Noise Conditions*, Int. J. Advances in Engineering and Technology, 5 (1) (2012), pp. 47–55.
- [42] R. MARTÍN-CLEMENTE AND S. HORNILLO-MELLADO, *Image Processing using ICA: a New Perspective*, In: Proceedings of the IEEE MELECON 2006, Benalmádena (Málaga), Spain (2006), pp. 1–4.
- [43] F. MERRIKH-BAYAT, M. BABAIE-ZADEH, AND C. JUTTEN, *Using Non-Negative Matrix Factorization for Removing Show-Through*, Proc. LVA/ICA, (2010), pp. 482–489.
- [44] N. METROPOLIS, A. W. ROSENBLUTH, M. N. ROSENBLUTH, AND E. TELLER *Equations of State Calculations by Fast Computing Machines*. J. Chem. Phys. 21 (1953), pp 1087–1092.
- [45] W. S. B. OUEDRAOGO, A. SOULOUMIAC, M. JAIDANE, AND C. JUTTEN, *Non-Negative Blind Source Separation Algorithm Based on Minimum Aperture Simplicial Cone*, IEEE Transactions on Signal Processing, 62 (2) (2014), pp. 376–389.
- [46] S. RICCIARDI, A. BONALDI, P. NATOLI, G. POLENTA, C. BACCIGALUPI, E. SALERNO, K. KAYABOL, L. BEDINI, AND G. DE ZOTTI, *Correlated Component Analysis for Diffuse Component Separation with Error Estimation on Simulated Plank Polarization Data*, Mon. Not. R. Astron. Soc., 406 (2010), pp. 1644–1658.
- [47] S. V. RICE, G. NAGY, AND T. A. NARTKER, *Optical Character Recognition: An Illustrated Guide to the Frontier*, The Springer International Series in Engineering and Computer Science, Springer US, New York, 1999.
- [48] J. V. STONE, *Independent Component Analysis: an introduction*. Trends in Cognitive Sciences, 6 (2) (2002), 59–64.

- [49] P. TICHAWSKY, Z. KOLDOVSKY, AND E. OJA, *Performance Analysis of the FastICA Algorithm and Cramér-Rao Bounds for Linear Independent Component Analysis*, IEEE Trans. Signal Process., 54 (4) (2006), pp. 1–14. (2006).
- [50] A. TONAZZINI AND L. BEDINI, *Restoration of Recto-Verso Colour Documents using Correlated Component Analysis*, EURASIP Journal on Advances in Signal Processing, 58 (2013), pp.1–10.
- [51] A. TONAZZINI, L. BEDINI, E. E. KURUOGLU, AND E. SALERNO, *Blind Separation of Auto-Correlated Images from Noisy Mixtures using MRF Models*, In: Proceedings of the 4th International Symposium on Independent Component Analysis and Blind Source Separation, Nara, Japan (2003), pp. 675–680.
- [52] A. TONAZZINI, I. GERACE, AND F. MARTINELLI, *Document Image Restoration and Analysis as Separation of Mixtures of Patterns: From Linear to Nonlinear Models*, In: B. K. Gunturk and X. Li (Eds.), *Image Restoration - Fundamentals and Advances*, CRC Press, Taylor & Francis, Boca Raton (2013), pp. 285–310.
- [53] A. TONAZZINI, E. SALERNO, AND L. BEDINI, *Fast Correction of Bleed-Through Distortion in Greyscale Documents by a Blind Source Separation Technique*, Int. J. Document Analysis 10 (1) (2007), pp. 17–25.
- [54] A. TONAZZINI, E. SALERNO, M. MOCHI, AND L. BEDINI, *Bleed-Through Removal from Degraded Documents Using a Color Decorrelation Method*, In: S. Marinai, A. R. Dengel (eds.) *Document Analysis Systems VI*. DAS 2004, Lecture Notes in Computer Science, 3163, Springer, Berlin-Heidelberg, 2004.
- [55] L. TONG, R. W. LIU, V. C. SOON, AND Y.-F. HUANG, *Indeterminacy and Identifiability of Blind Identification*, IEEE Trans. Circuits Sys., 38 (1991), pp. 499–509.
- [56] S. VASEGHI AND H. JETELOVA, *Principal and Independent Component Analysis in Image Processing*, In: Proceedings of the 14th ACM International Conference on Mobile Computing and Networking (MOBICOM ’06), San Francisco, Calif., USA (2006), pp. 1–5.
- [57] S. VAVASIS, *On the Complexity of Nonnegative Matrix Factorization*, SIAM J. Optimization, 20 (3) (2009), pp. 1364–1377.
- [58] G. WINKLER, *Image Analysis, Random Fields and Dynamic Monte Carlo Methods-A Mathematical Introduction*, Springer-Verlag, Berlin-Heidelberg, 1995.